ORNL/TM-2010/286

OAK RIDGE
NATIONAL LABORATORY
MANAGED BY UT-BATTELLE
FOR THE DEPARTMENT OF ENERGY

# SCALE 5 Analysis of BWR Spent Nuclear Fuel Isotopic Compositions for Safety Studies

## December 2010

**Prepared by**
**U. Mertyurek**
**M. W. Francis**
**I. C. Gauld**

UT-BATTELLE
ORNL-27 (4-00)

**DOCUMENT AVAILABILITY**

**Reports produced after January 1, 1996, are generally available free via the U.S. Department of Energy (DOE) Information Bridge:**

**Web site: http://www.osti.gov/bridge**

**Reports produced before January 1, 1996, may be purchased by members of the public from the following source:**

**National Technical Information Service**
**5285 Port Royal Road**
**Springfield, VA 22161**
**Telephone: 703-605-6000 (1-800-553-6847)**
**TDD: 703-487-4639**
**Fax: 703-605-6900**
**E-mail: info@ntis.fedworld.gov**
**Web site: http://www.ntis.gov/support/ordernowabout.htm**

**Reports are available to DOE employees, DOE contractors, Energy Technology Data Exchange (ETDE) representatives, and International Nuclear Information System (INIS) representatives from the following source:**

**Office of Scientific and Technical Information**
**P.O. Box 62**
**Oak Ridge, TN 37831**
**Telephone: 865-576-8401**
**Fax: 865-576-5728**
**E-mail: reports@adonis.osti.gov**
**Web site: http://www.osti.gov/contact.html**

This report was prepared as an account of work sponsored by an agency of the United States Government. Neither the United States government nor any agency thereof, nor any of their employees, makes any warranty, express or implied, or assumes any legal liability or responsibility for the accuracy, completeness, or usefulness of any information, apparatus, product, or process disclosed, or represents that its use would not infringe privately owned rights. Reference herein to any specific commercial product, process, or service by trade name, trademark, manufacturer, or otherwise, does not necessarily constitute or imply its endorsement, recommendation, or favoring by the United States Government or any agency thereof. The views and opinions of authors expressed herein do not necessarily state or reflect those of the United States Government or any agency thereof.

ORNL/TM-2010/286

Reactor and Nuclear Systems Division

# SCALE 5 Analysis of BWR Spent Nuclear Fuel Isotopic Compositions for Safety Studies

U. Mertyurek
M. W. Francis
I. C. Gauld

Date Published: December 2010

Prepared by
OAK RIDGE NATIONAL LABORATORY
P.O. Box 2008
Oak Ridge, Tennessee 37831-6283
managed by
UT-BATTELLE, LLC
for the
U.S. DEPARTMENT OF ENERGY
under contract DE-AC05-00OR22725

**CONTENTS**

**Page**

**CONTENTS (continued)**

**Page**



..

## LIST OF FIGURES

## LIST OF FIGURES (continued)

**Page**



## APPENDIX FIGURES

## LIST OF TABLES

**Page**



## APPENDIX TABLE

## ACRONYMS

| | |
|---|---|
| 2-D | two-dimensional |
| BWR | boiling water reactor |
| C/E | calculated to measured isotopic concentration (ratio) |
| CENTRM | Continuous ENergy TRansport Module |
| DOE | US Department of Energy |
| dps | disintegrations per second |
| ENDF | Evaluated Nuclear Data File |
| FP | fission product |
| GE | General Electric |
| GWd | gigawatt-day |
| JAERI | Japan Atomic Energy Research Institute |
| KRB | Kernkraftwerk RWE-Bayernwerk GmbH |
| LWR | light water reactor |
| MCC | Materials Characterization Center |
| MTU | metric ton of uranium |
| NEWT | NEW Transport algorithm |
| NITAWL | Nordheim Integral Treatment And Working Library production |
| OCRWM | Office of Civilian Radioactive Waste Management |
| ORIGEN | Oak Ridge Isotope Generation and Depletion Code |
| ORNL | Oak Ridge National Laboratory |
| PNNL | Pacific Northwest National Laboratory |
| SCALE | Standardized Computer Analysis for Licensing Evaluation |
| TEPCO | Tokyo Electric Power Company |
| TIHM | ton of initial heavy metal |
| TRITON | Transport Rigor Implemented with Time-dependent Operation for Neutronic depletion |

## ACKNOWLEDGMENTS

This work was performed under contract with the US Department of Energy Office of Civilian Radioactive Waste Management Lead Laboratory for Repository Systems. The authors would like to thank Georgeta Radulescu and John Scaglione for their review and valuable comments.

# 1. INTRODUCTION

This report documents validation of calculated isotopic concentrations for boiling water reactor (BWR) fuel using the Standardized Computer Analysis for Licensing Evaluation version 5.1 (SCALE 5.1) code system.[1] The calculation methodology employs the TRITON depletion sequence using the NEWT (NEW Transport algorithm) two-dimensional (2-D) transport code and ORIGEN-S code for isotope depletion calculations and the 44-neutron-group ENDF/B-V cross-section library.

The validation study involved comparison of isotopic contents calculated using SCALE 5.1 depletion simulations with measured isotopic data for 32 spent BWR fuel samples obtained from fuel assemblies of the Fukushima Daini Unit 2 (Fukushima Daini-2), Cooper, and Gundremmingen-A reactors. The initial fuel enrichments for the samples varied from 2.53 to 3.91 wt % $^{235}$U, and burnup values ranged from 14.39 to 43.99 GWd/MTU. Measurements for 40 isotopes were evaluated in this study. Table 1 presents a summary of the experimental programs and the evaluated isotopic data.

Modern BWR fuel assemblies make heavy use of burnable absorbers, have heterogeneous time-dependent moderator densities, and employ control blades during normal operation. In many cases, details of the operating history of the benchmark samples are considered commercial proprietary information and are not well documented in public sources. The lack of adequate documentation for modern BWR assembly designs and operational void, control blade, and fuel temperature histories for the spent fuel assemblies has been a major impediment to the availability of quality benchmark data for code validation. Important operating history data such as axial void fraction profile history, fuel temperature history, and control blade insertion history are not available for any samples evaluated in this report. Missing operations data, and in some cases physical design dimensions, were obtained from publicly available generic plant data and assumed to be constant throughout the irradiation history of the samples. Two axial void fraction profile correlations are developed in Appendix A to calculate the missing average void fraction data for some samples. The impact of modeling uncertainties due to application of approximate operational data is evaluated in this report.

This report describes the assembly models developed and the results obtained from comparisons of the experimental and calculated isotopic concentrations. The experimental program, the nuclide measurement techniques, and the reported uncertainties are also summarized.

**Table 1. Sample identification table**

| Sample number | Axial position[a] (mm) | Burnup (GWd/MTU) | Fuel rod | Enrichment ($^{235}$U wt %) | Fuel assembly | Reactor |
|---|---|---|---|---|---|---|
| 1 | 423 | 36.94 | SF98 | 3.91 | 2F2DN23 | Fukushima Daini-2 |
| 2 | 692 | 42.35 | SF98 | 3.91 | 2F2DN23 | Fukushima Daini-2 |
| 3 | 1214 | 43.99 | SF98 | 3.91 | 2F2DN23 | Fukushima Daini-2 |
| 4 | 2050 | 39.92 | SF98 | 3.91 | 2F2DN23 | Fukushima Daini-2 |
| 5 | 2757 | 39.41 | SF98 | 3.91 | 2F2DN23 | Fukushima Daini-2 |
| 6 | 3397 | 27.18 | SF98 | 3.91 | 2F2DN23 | Fukushima Daini-2 |
| 7 | 286 | 22.63 | SF99 | 3.41 | 2F2DN23 | Fukushima Daini-2 |
| 8 | 502 | 32.44 | SF99 | 3.41 | 2F2DN23 | Fukushima Daini-2 |
| 9 | 686 | 35.42 | SF99 | 3.41 | 2F2DN23 | Fukushima Daini-2 |
| 10 | 1189 | 37.41 | SF99 | 3.41 | 2F2DN23 | Fukushima Daini-2 |
| 11 | 2061 | 32.36 | SF99 | 3.41 | 2F2DN23 | Fukushima Daini-2 |
| 12 | 2744 | 32.13 | SF99 | 3.41 | 2F2DN23 | Fukushima Daini-2 |
| 13 | 3388 | 21.83 | SF99 | 3.41 | 2F2DN23 | Fukushima Daini-2 |
| 14 | 3540 | 16.65 | SF99 | 3.41 | 2F2DN23 | Fukushima Daini-2 |
| 15 | 1310 | 33.94 | ADD2966 | 2.93 | CZ346 | Cooper |
| 16 | 1869 | 33.07 | ADD2966 | 2.93 | CZ346 | Cooper |
| 17 | 3517 | 18.96 | ADD2966 | 2.93 | CZ346 | Cooper |
| 18 | 1147 | 31.04 | ADD2974 | 2.93 | CZ346 | Cooper |
| 19 | 2907 | 29.23 | ADD2974 | 2.93 | CZ346 | Cooper |
| 20 | 3501 | 17.84 | ADD2974 | 2.93 | CZ346 | Cooper |
| 21 | 440 | 25.73 | A1 | 2.53 | B23 | Gundremmingen-A |
| 22 | 2680 | 27.40 | A1 | 2.53 | B23 | Gundremmingen-A |
| 23 | 2680 | 21.47 | B3 | 2.53 | B23 | Gundremmingen-A |
| 24 | 2680 | 22.25 | B4 | 2.53 | B23 | Gundremmingen-A |
| 25 | 2680 | 22.97 | C5 | 2.53 | B23 | Gundremmingen-A |
| 26 | 2680 | 23.51 | E3 | 2.53 | B23 | Gundremmingen-A |
| 27 | 2680 | 25.29 | E5 | 2.53 | B23 | Gundremmingen-A |
| 28 | 440 | 20.30 | A1 | 2.53 | C16 | Gundremmingen-A |
| 29 | 2680 | 19.85 | A1 | 2.53 | C16 | Gundremmingen-A |
| 30 | 2680 | 14.39 | B3 | 2.53 | C16 | Gundremmingen-A |
| 31 | 2680 | 15.84 | C5 | 2.53 | C16 | Gundremmingen-A |
| 32 | 2680 | 17.49 | E5 | 2.53 | C16 | Gundremmingen-A |

[a]From the bottom of the active fuel.

## 2. QUALITY ASSURANCE REQUIREMENTS

This document was developed and is controlled in accordance with Oak Ridge National Laboratory (ORNL)–US Department of Energy (DOE) Office of Civilian Radioactive Waste Management (OCRWM) quality assurance procedures. Unqualified external source data were used as direct inputs to the calculations performed for this report. Hence, unless noted otherwise, information must be evaluated for adequacy relative to its specific use if relied upon to support designs or decisions important to safety or waste isolation. Development of this report followed the plan described in *Test Plan for: Isotopic Validation for Postclosure Criticality of Commercial Spent Nuclear Fuel*.[2] The test plan identifies procedures applicable to the development, documentation, and electronic management of the data for this report.

The development of the calculation and analysis documentation was performed in accordance with ORNL-OCRW-19.1, *Calculation Packages*.[3] The test plan for the development of the report was prepared in accordance with ORNL-OCRW-21.0, *Scientific Investigations*.[4] The control of electronic data was performed in accordance with ORNL-OCRW-23.0, *Control of the Electronic Management of Data.*[5] The computer codes used in this calculation have been qualified per ORNL-OCRW-19.0, *Software Control*.[6]

# 3. USE OF SOFTWARE

## 3.1 SCALE

The SCALE code system was used to perform transport, depletion, and decay calculations. The SCALE 5.1 code system[1] used herein has been qualified per ORNL-OCRW-19.0, *Software Control*.[6]

- Software Title: SCALE
- Version/Revision Number: Version 5.1
- Status/Operating System: Qualified/Linux 2.6.9-42.0.2 ELsmp #1, x86_64 GNU/Linux[7]
- Computer Type: CPILE2 Linux cluster of the Nuclear Systems Analysis, Design, and Safety organization, Nuclear Science and Technology Division, ORNL

The input and output files for the SCALE depletion calculations are located on a CD that accompanies this report (refer to Appendix B for the contents of the CD) so that an independent repetition of the calculations may be performed.

## 3.2 EXCEL

The commercial off-the-shelf software Microsoft Office Excel 2008 (copyright Microsoft Corporation) was used in calculations to manipulate the inputs and tabulate and chart results using standard mathematical expressions and operations. Excel was used only as a worksheet and not as a software routine. Therefore, Excel is exempt from the requirements of ORNL-OCRW-19.0, *Software Control*.[6] All necessary information for reproducing the operations performed is provided on the CD that accompanies this report.

# 4. ISOTOPIC MEASUREMENTS

## 4.1 FUKUSHIMA DAINI UNIT 2

The Fukushima Daini Nuclear Power Station, operated by Tokyo Electric Power Company (TEPCO), used Hitachi BWR fuel bundles with an 8 × 8 pin lattice for the fuel cycles analyzed in this report. A nuclide composition benchmark data set was generated by the Japan Atomic Energy Research Institute (JAERI) as part of a burnup credit research project titled "The Technical Development on Criticality Safety Management of Spent LWR Fuels".[8] This project was supported by the Science and Technology Agency of Japan, in cooperation with TEPCO. In the analysis, 18 samples were examined from two rods from Fukushima Daini-2 with initial $^{235}$U enrichments of 3.41 and 3.91 wt % and burnups ranging from 4.15 to 43.99 GWd/MTU. Two rods, SF98 and SF99, from assembly 2F2DN23 were irradiated for a total of 1,174 days during the period from January 14, 1989, to November 16, 1992.

### 4.1.1 Measurements and Uncertainties

Destructive and nondestructive analyses were carried out from 1995 through 1997. Destructive analyses are conducted to determine nuclide compositions. Nondestructive gamma scans are performed for axial burnup distributions. For destructive analyses, the samples were collected by cutting 0.5 mm thick slices axially at different locations as shown in Fig. 1[9] and Fig. 2[9] for fuel rods SF98 and SF99, respectively. Each cutting, corresponding to ~ 300 mg of specimen[10] (also reported as ~ 1 g U in Ref. 8), was dissolved in 15 mL of 7 M nitric acid by heating to 100°C. The solution was fed through an ion exchange separation process to get fractions of the fission products (FPs), Pu, Np, and U. A second ion exchange column was used on the FP mixture to separate further fractions of Cs, Sr, Gd, Cm/Sr, Am, and Nd. Isotopic compositions of U, Pu, Am, and Nd were then measured by isotopic dilution mass spectroscopy using $^{150}$Nd, $^{233}$U, and $^{242}$ Pu. Alpha spectroscopy was used to measure ratios of $^{234}$U, $^{237}$Np, $^{238}$Pu, $^{241}$Am, $^{243}$Am, $^{242}$Cm, and $^{244}$Cm to uranium. γ-spectroscopy was used to measure the ratios of $^{134}$Cs, $^{137}$Cs, $^{154}$Eu, and $^{144}$Ce with high resolution gamma detectors.

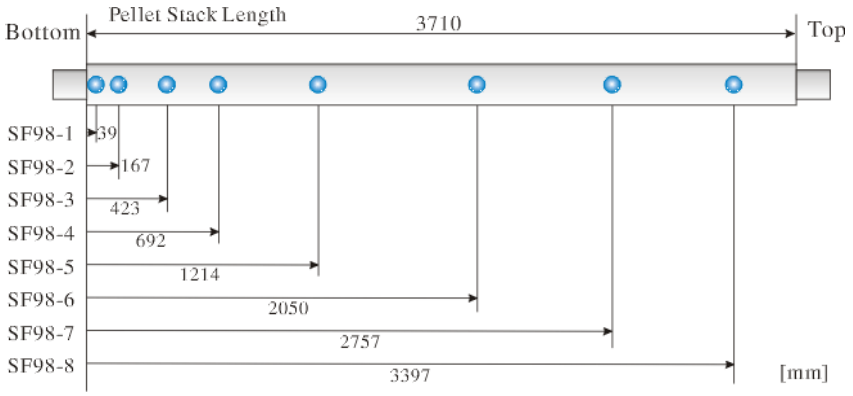


**Fig. 1. Rod measurement positions for rod SF98.**

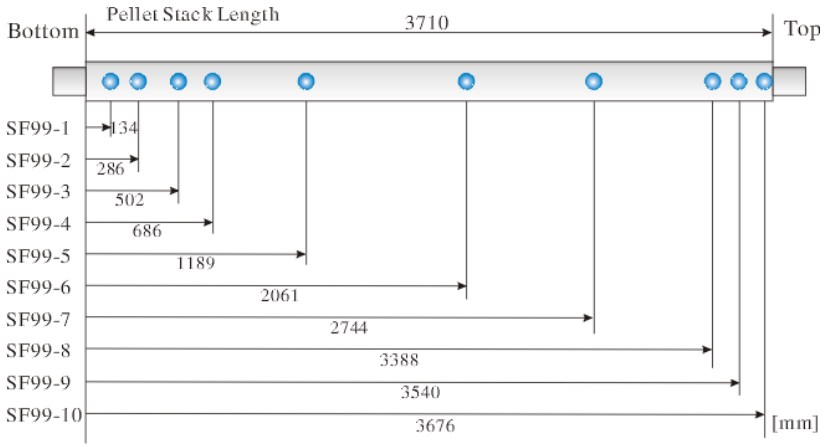


**Fig. 2. Rod measurement positions for rod SF99.**

The measured isotopic concentrations for each sample are listed in Table 2 and Table 3. All results were normalized to the reactor discharge date except the samarium isotopes. The reported burnups for each sample were calculated by JAEA[10] using the $^{148}$Nd method.[11] A conversion factor of 9.6 was used to convert burnups calculated in atomic percent fission to gigawatt-day per ton. The uncertainty in burnup rate with this method is less than 3%.

The reported measurement uncertainties for the isotopes are as follows.

1. Isotope-dilution-mass spectrometry: Less than 0.1% for $^{235}$U, $^{238}$U, Nd, and Sm isotopes; less than 1% for $^{234}$U; less than 2% for $^{236}$U; less than 0.3% for $^{239}$Pu, $^{240}$Pu, $^{241}$Pu, and $^{242}$ Pu; and less than 0.5% for $^{238}$Pu.
2. α-ray spectrum measurements: Less than 2% for $^{241}$Am, $^{243}$Cm, $^{244}$Cm, and $^{245}$Cm; less than 5% for $^{243}$Am, and $^{246}$Cm; and less than 10% for $^{242m}$ Am, $^{242}$Cm, and $^{247}$Cm.
3. γ-ray spectrum measurements: Less than 3% for $^{134}$Cs, $^{137}$Cs, and $^{154}$Eu; less than 5% for $^{106}$Ru; and less than 10% for $^{125}$Sb and $^{144}$Ce.
4. Less than 0.1% in Gd isotopic ratios and less than 10% in $^{237}$Np quantification.

**Table 2. Measurement results of SF98 samples**

| Sample | SF98-1[a] | SF98-2[a] | SF98-3[a] | SF98-4[a] | SF98-5[b] | SF98-6[c] | SF98-7[b] | SF98-8[b] |
|---|---|---|---|---|---|---|---|---|
| **Burnup (GWd/MTU)** | 4.15 | 26.51 | 36.94 | 42.35 | 43.99 | 39.92 | 39.41 | 27.18 |
| **Cutting position from bottom of active length (mm)** | 39 | 167 | 423 | 692 | 1214 | 2050 | 2757 | 3397 |
| **Nuclide** | **(g/ton of initial heavy metal)** | | | | | | | |
| $^{234}$U | 4.880E+01 | 2.677E+02 | 2.178E+02 | 1.976E+02 | 1.903E+02 | 1.860E+02 | 1.962E+02 | 2.354E+02 |
| $^{235}$U | 4.128E+03 | 1.743E+04 | 8.142E+03 | 5.966E+03 | 6.315E+03 | 9.062E+03 | 9.357E+03 | 1.545E+04 |
| $^{236}$U | 4.858E+02 | 3.551E+03 | 4.994E+03 | 5.284E+03 | 5.307E+03 | 5.140E+03 | 5.140E+03 | 4.291E+03 |
| $^{238}$U | 9.884E+05 | 9.460E+05 | 9.406E+05 | 9.358E+05 | 9.328E+05 | 9.334E+05 | 9.332E+05 | 9.431E+05 |
| $^{237}$Np | 2.379E+01 | 1.479E+02 | 3.346E+02 | 4.318E+02 | 3.862E+02 | 5.157E+02 | 4.573E+02 | 2.918E+02 |
| $^{238}$Pu | 3.135E+00 | 2.827E+01 | 1.167E+02 | 1.678E+02 | 1.936E+02 | 1.692E+02 | 2.083E+02 | 9.544E+01 |
| $^{239}$Pu | 2.297E+03 | 3.372E+03 | 3.694E+03 | 3.792E+03 | 4.265E+03 | 5.305E+03 | 5.628E+03 | 5.341E+03 |
| $^{240}$Pu | 5.474E+02 | 1.121E+03 | 2.135E+03 | 2.458E+03 | 2.613E+03 | 2.630E+03 | 2.668E+03 | 1.816E+03 |
| $^{241}$Pu | 1.332E+02 | 4.308E+02 | 8.949E+02 | 1.032E+03 | 1.172E+03 | 1.292E+03 | 1.355E+03 | 9.079E+02 |
| $^{242}$Pu | 1.688E+01 | 9.292E+01 | 4.623E+02 | 6.622E+02 | 6.939E+02 | 5.431E+02 | 5.439E+02 | 2.220E+02 |
| $^{241}$Am | 1.028E+01 | 2.300E+01 | 3.271E+01 | 3.417E+01 | 3.734E+01 | 4.091E+01 | 4.388E+01 | 3.295E+01 |
| $^{242m}$ Am | 7.984E-02 | 2.967E-01 | 4.999E-01 | 5.298E-01 | 6.417E-01 | 8.623E-01 | 8.975E-01 | 7.074E-01 |
| $^{243}$Am | 5.839E-01 | 6.991E+00 | 6.678E+01 | 1.138E+02 | 1.273E+02 | 1.116E+02 | 1.087E+02 | 3.259E+01 |
| $^{242}$Cm | 5.309E-01 | 3.581E+00 | 1.696E+01 | 2.263E+01 | 3.460E+01 | 5.925E+01 | 2.892E+01 | 1.153E+01 |
| $^{243}$Cm | No Data | 3.710E-02 | 3.135E-01 | 4.247E-01 | 4.946E-01 | 5.347E-01 | 5.932E-01 | 2.073E-01 |
| $^{244}$Cm | 3.094E-02 | 8.003E-01 | 1.696E+01 | 3.635E+01 | 4.999E+01 | 4.299E+01 | 4.484E+01 | 8.687E+00 |
| $^{245}$Cm | No Data | 1.646E-02 | 5.485E-01 | 1.338E+00 | 2.322E+00 | 2.480E+00 | 2.734E+00 | 3.928E-01 |
| $^{246}$Cm | No Data | No Data | 7.666E-02 | 2.311E-01 | 3.850E-01 | 2.935E-01 | 3.007E-01 | 1.635E-02 |
| $^{247}$Cm | No Data | No Data | No Data | No Data | No Data | No Data | No Data | No Data |
| $^{143}$Nd | 1.208E+02 | 7.567E+02 | 8.234E+02 | 8.486E+02 | 9.039E+02 | 9.199E+02 | 9.183E+02 | 7.358E+02 |
| $^{144}$Nd | 1.153E+02 | 8.511E+02 | 1.275E+03 | 1.492E+03 | 1.476E+03 | 1.284E+03 | 1.207E+03 | 7.478E+02 |
| $^{145}$Nd | 9.192E+01 | 5.974E+02 | 7.648E+02 | 8.423E+02 | 8.667E+02 | 7.950E+02 | 7.845E+02 | 5.770E+02 |
| $^{146}$Nd | 7.769E+01 | 5.278E+02 | 7.629E+02 | 8.916E+02 | 9.320E+02 | 8.427E+02 | 8.330E+02 | 5.550E+02 |
| $^{148}$Nd | 4.560E+01 | 2.905E+02 | 4.058E+02 | 4.662E+02 | 4.850E+02 | 4.407E+02 | 4.356E+02 | 2.997E+02 |
| $^{150}$Nd | 2.187E+01 | 1.279E+02 | 1.867E+02 | 2.193E+02 | 2.294E+02 | 2.098E+02 | 2.080E+02 | 1.389E+02 |
| $^{137}$Cs | 1.634E+02 | 8.286E+02 | 1.329E+03 | 1.577E+03 | 1.588E+03 | 1.508E+03 | 1.559E+03 | 9.494E+02 |
| $^{134}$Cs | 3.579E+00 | 3.214E+01 | 1.010E+02 | 1.407E+02 | 1.553E+02 | 1.514E+02 | 1.621E+02 | 6.979E+01 |
| $^{154}$Eu | 8.151E-01 | 6.857E+00 | 1.818E+01 | 2.413E+01 | 2.601E+01 | 2.931E+01 | 2.924E+01 | 1.708E+01 |
| $^{144}$Ce | 2.782E+01 | 1.833E+02 | 2.996E+02 | 3.538E+02 | 4.107E+02 | 3.520E+02 | 3.786E+02 | 2.867E+02 |
| $^{125}$Sb | No Data | No Data | No Data | No Data | No Data | 5.223E+00 | No Data | No Data |
| $^{106}$Ru | 1.749E+01 | 4.985E+01 | 1.091E+02 | 1.237E+02 | 1.326E+02 | 1.113E+02 | 1.309E+02 | 7.522E+01 |
| $^{147}$Sm | 4.777E+01 | 2.303E+02 | 3.091E+02 | 3.207E+02 | 3.025E+02 | 2.891E+02 | 2.800E+02 | 2.454E+02 |
| $^{148}$Sm | 5.983E+00 | 5.771E+01 | 1.531E+02 | 1.971E+02 | 2.022E+02 | 1.855E+02 | 1.852E+02 | 1.079E+02 |
| $^{149}$Sm | 6.367E-01 | 2.201E+00 | 2.553E+00 | 2.502E+00 | 3.701E+00 | 3.374E+00 | 4.199E+00 | 4.082E+00 |
| $^{150}$Sm | 3.343E+01 | 1.790E+02 | 3.309E+02 | 3.865E+02 | 3.808E+02 | 3.536E+02 | 3.505E+02 | 2.408E+02 |
| $^{151}$Sm | 2.554E+00 | 8.203E+00 | 9.192E+00 | 9.738E+00 | 1.039E+01 | 1.272E+01 | 1.310E+01 | 1.245E+01 |
| $^{152}$Sm | 2.230E+01 | 9.016E+01 | 1.425E+02 | 1.555E+02 | 1.432E+02 | 1.233E+02 | 1.222E+02 | 9.771E+01 |
| $^{154}$Sm | 4.561E+00 | 1.874E+01 | 3.950E+01 | 4.828E+01 | 4.912E+01 | 4.377E+01 | 4.472E+01 | 2.933E+01 |

Source: Ref. 12, Tables A.3.30 and A.2.19.

[a]Decay corrected for zero day cooling except Sm isotopes, which were reported at a cooling time of 5.5 years.

[b]Decay corrected for zero day cooling except Sm isotopes, which were reported at a cooling time of 5.9 years.

[c]Decay corrected for zero day cooling except Sm isotopes, which were reported at a cooling time of 6.2 years.

**Table 3. Measurement results of SF99 samples**

| Sample | SF99-1 | SF99-2[a] | SF99-3[b] | SF99-4[a] | SF99-5[b] | SF99-6[a] | SF99-7[b] | SF99-8[c] | SF99-9[b] | SF99-10[a] |
|---|---|---|---|---|---|---|---|---|---|---|
| **Burnup (GWd/MTU)** | 7.53 | 22.63 | 32.44 | 35.42 | 37.41 | 32.36 | 32.13 | 21.83 | 16.65 | 7.19 |
| **Cutting position from bottom of active length (mm)** | 134 | 286 | 502 | 686 | 1189 | 2061 | 2744 | 3388 | 3540 | 3676 |
| **Nuclide** | **(g/ton of initial heavy metal)** | | | | | | | | | |
| $^{234}$U | 3.898E+01 | 2.006E+02 | 1.782E+02 | 1.666E+02 | 1.602E+02 | 1.649E+02 | 1.643E+02 | 1.960E+02 | 2.184E+02 | 4.094E+01 |
| $^{235}$U | 2.913E+03 | 1.398E+04 | 8.657E+03 | 6.981E+03 | 7.381E+03 | 1.046E+04 | 1.092E+04 | 1.575E+04 | 1.906E+04 | 3.041E+03 |
| $^{236}$U | 6.868E+02 | 3.467E+03 | 4.251E+03 | 4.480E+03 | 4.522E+03 | 4.295E+03 | 4.251E+03 | 3.458E+03 | 2.833E+03 | 6.743E+02 |
| $^{238}$U | 9.839E+05 | 9.522E+05 | 9.452E+05 | 9.432E+05 | 9.394E+05 | 9.409E+05 | 9.403E+05 | 9.493E+05 | 9.538E+05 | 9.841E+05 |
| $^{237}$Np | 5.674E+01 | 2.177E+02 | 3.632E+02 | 3.666E+02 | 4.617E+02 | 4.146E+02 | 4.464E+02 | 2.758E+02 | 1.975E+02 | 5.493E+01 |
| $^{238}$Pu | 1.130E+01 | 3.961E+01 | 9.696E+01 | 1.145E+02 | 1.234E+02 | 1.374E+02 | 1.377E+02 | 6.476E+01 | 3.427E+01 | 1.098E+01 |
| $^{239}$Pu | 3.010E+03 | 3.907E+03 | 3.980E+03 | 3.865E+03 | 4.549E+03 | 5.633E+03 | 6.036E+03 | 5.448E+03 | 4.731E+03 | 3.011E+03 |
| $^{240}$Pu | 1.064E+03 | 1.519E+03 | 2.131E+03 | 2.293E+03 | 2.535E+03 | 2.445E+03 | 2.487E+03 | 1.647E+03 | 1.182E+03 | 1.052E+03 |
| $^{241}$Pu | 3.598E+02 | 6.763E+02 | 9.452E+02 | 1.010E+03 | 1.196E+03 | 1.263E+03 | 1.313E+03 | 8.332E+02 | 5.372E+02 | 3.359E+02 |
| $^{242}$Pu | 8.237E+01 | 1.896E+02 | 4.374E+02 | 5.573E+02 | 6.073E+02 | 4.334E+02 | 4.215E+02 | 1.723E+02 | 8.334E+01 | 7.328E+01 |
| $^{241}$Am | 2.698E+01 | 2.110E+01 | 3.950E+01 | 3.410E+01[d] | 4.363E+01 | 4.558E+01 | 4.848E+01 | 3.619E+01 | 2.885E+01 | 1.612E+01 |
| $^{242m}$ Am | 2.469E−01 | 4.239E-01 | 5.444E-01 | 5.418E-01[d] | 6.917E-01 | 9.306E-01 | 9.240E-01 | 6.812E-01 | 4.078E-01 | 2.138E−01 |
| $^{243}$Am | 5.786E+00 | 1.895E+01 | 6.496E+01 | 9.037E+01 | 1.128E+02 | 8.514E+01 | 8.453E+01 | 2.574E+01 | 9.255E+00 | 5.620E+00 |
| $^{242}$Cm | 2.848E+00 | 1.624E+01 | 2.270E+01 | 3.477E+01 | 6.130E+01 | 3.844E+01 | 4.067E+01 | 1.593E+01 | 5.534E+00 | 3.583E+00 |
| $^{243}$Cm | 2.999E−02 | 9.310E-02 | 2.759E-01 | 3.692E-01 | 4.750E-01 | 4.413E-01 | 4.762E-01 | 1.629E-01 | 7.257E-02 | 3.279E−02 |
| $^{244}$Cm | 5.891E−01 | 3.180E+00 | 1.645E+01 | 2.692E+01 | 3.871E+01 | 3.008E+01 | 3.000E+01 | 6.152E+00 | 1.515E+00 | 6.833E−01 |
| $^{245}$Cm | 1.006E−02 | 8.762E-02 | 5.695E-01 | 1.014E+00 | 1.767E+00 | 1.735E+00 | 1.793E+00 | 2.702E-01 | 8.185E-02 | 1.319E−02 |
| $^{246}$Cm | 9.574E−04 | No Data | 6.949E-02 | 1.495E-01 | 2.412E-01 | 1.603E-01 | 1.561E-01 | 1.441E-02 | 1.217E-02 | No Data |
| $^{247}$Cm | 3.945E−04 | No Data | 1.427E−03 | No Data | 2.809E−03 | No Data | 3.881E−03 | No Data | 1.224E−02 | No Data |
| $^{143}$Nd | 1.948E+02 | 6.136E+02 | 7.627E+02 | 7.808E+02 | 8.397E+02 | 7.984E+02 | 8.089E+02 | 6.143E+02 | 5.007E+02 | 1.895E+02 |
| $^{144}$Nd | 2.629E+02 | 6.537E+02 | 1.321E+03 | 1.203E+03 | 1.166E+03 | 9.321E+02 | 8.171E+02 | 5.531E+02 | 4.406E+02 | 2.509E+02 |
| $^{145}$Nd | 1.579E+02 | 4.917E+02 | 6.728E+02 | 7.198E+02 | 7.511E+02 | 6.519E+02 | 6.509E+02 | 4.671E+02 | 3.705E+02 | 1.517E+02 |
| $^{146}$Nd | 1.410E+02 | 4.476E+02 | 6.610E+02 | 7.314E+02 | 7.774E+02 | 6.671E+02 | 6.645E+02 | 4.397E+02 | 3.307E+02 | 1.366E+02 |
| $^{148}$Nd | 8.284E+01 | 2.486E+02 | 3.570E+02 | 3.903E+02 | 4.130E+02 | 3.575E+02 | 3.556E+02 | 2.411E+02 | 1.837E+02 | 7.970E+01 |
| $^{150}$Nd | 4.177E+01 | 1.142E+02 | 1.674E+02 | 1.844E+02 | 1.979E+02 | 1.735E+02 | 1.724E+02 | 1.136E+02 | 8.436E+01 | 4.040E+01 |
| $^{137}$Cs | 2.859E+02 | 8.515E+02 | 1.231E+03 | 1.346E+03 | 1.427E+03 | 1.249E+03 | 1.266E+03 | 8.343E+02 | 6.329E+02 | 2.772E+02 |
| $^{134}$Cs | 1.041E+01 | 4.643E+01 | 9.117E+01 | 1.126E+02 | 1.306E+02 | 1.137E+02 | 1.193E+02 | 5.684E+01 | 3.213E+01 | 1.091E+01 |
| $^{154}$Eu | 2.664E+00 | 1.022E+01 | 1.792E+01 | 1.992E+01 | 2.465E+01 | 2.549E+01 | 2.659E+01 | 1.404E+01 | 8.215E+00 | 2.755E+00 |
| $^{144}$Ce | No Data | 2.153E+02 | No Data | 2.915E+02 | 3.847E+02 | 3.169E+02 | 4.240E+02 | 2.540E+02 | 1.657E+02 | No Data |

**Table 3 (continued)**

| Sample | SF99-1 | SF99-2[a] | SF99-3[b] | SF99-4[a] | SF99-5[b] | SF99-6[a] | SF99-7[b] | SF99-8[c] | SF99-9[b] | SF99-10[a] |
|---|---|---|---|---|---|---|---|---|---|---|
| **Burnup (GWd/MTU)** | 7.53 | 22.63 | 32.44 | 35.42 | 37.41 | 32.36 | 32.13 | 21.83 | 16.65 | 7.19 |
| **Cutting position from bottom of active length (mm)** | 134 | 286 | 502 | 686 | 1189 | 2061 | 2744 | 3388 | 3540 | 3676 |
| **Nuclide** | **(g/ton of initial heavy metal)** | | | | | | | | | |
| $^{125}$Sb | 9.655E−01 | 3.674E+00 | 4.205E+00 | 4.588E+00 | 4.667E+00 | 5.071E+00 | 3.837E+00 | 2.430E+00 | 1.234E+00 | 8.973E−01 |
| $^{106}$Ru | 2.661E+01 | 3.280E+01 | 8.056E+01 | 7.833E+01 | 6.988E+01 | 6.899E+01 | 4.985E+01 | 4.366E+01 | 5.029E+01 | 3.862E+01 |
| $^{147}$Sm | 7.780E+01 | No Data | 2.609E+02 | No Data | 2.770E+02 | No Data | 2.436E+02 | 1.965E+02 | 1.633E+02 | No Data |
| $^{148}$Sm | 1.649E+01 | No Data | 1.167E+02 | No Data | 1.579E+02 | No Data | 1.343E+02 | 7.545E+01 | 4.483E+01 | No Data |
| $^{149}$Sm | 8.841E−01 | No Data | 2.469E+00 | No Data | 2.723E+00 | No Data | 3.426E+00 | 2.959E+00 | 2.600E+00 | No Data |
| $^{150}$Sm | 6.174E+01 | No Data | 2.676E+02 | No Data | 3.246E+02 | No Data | 2.778E+02 | 1.830E+02 | 1.313E+02 | No Data |
| $^{151}$Sm | 3.408E+00 | No Data | 8.490E+00 | No Data | 1.025E+01 | No Data | 1.294E+01 | 1.155E+01 | 9.999E+00 | No Data |
| $^{152}$Sm | 3.946E+01 | No Data | 1.179E+02 | No Data | 1.272E+02 | No Data | 1.024E+02 | 7.730E+01 | 6.172E+01 | No Data |
| $^{154}$Sm | 9.380E+00 | No Data | 3.353E+01 | No Data | 4.215E+01 | No Data | 3.579E+01 | 2.211E+01 | 1.540E+01 | No Data |

Source: Ref. 12, Table A.3.31.

[a]Decay corrected for zero day cooling.

[b]Decay corrected for zero day cooling except Sm isotopes, which were reported at a cooling time of 6.7 years.

[c]Decay corrected for zero day cooling except Sm isotopes, which were reported at a cooling time of 6.5 years.

[d]These values are misreported in Refs. 10 and 13.

## 4.2 COOPER

As a part of the DOE OCRWM program, fuel samples from two spent fuel assemblies were measured from the Cooper Nuclear Power Plant, operated by the Nebraska Public Power District, after five cycles for investigation of nuclear waste forms. The 7 × 7 fuel type assemblies were manufactured by General Electric (GE).

The fuel samples were analyzed and nuclide composition data were generated at Pacific Northwest National Laboratory (PNNL) by the Materials Characterization Center (MCC). The report prepared by MCC, *Characterization of Spent Fuel Approved Testing Material-ATM-105*,[14] provides isotopic data for six samples from fuel rods ADD2966 and ADD2974 from fuel assembly CZ346. Both fuel rods had an initial $^{235}$U enrichment of 2.939 wt % and were irradiated for a total of 1,941 days[15] during the period from July 4, 1974, to May 21, 1982. The six fuel samples had burnups ranging from 17.84 to 33.94 GWd/t.

### 4.2.1 Measurements and Uncertainties

Samples ranging from 1.21 cm to 2.5 cm were taken for the destructive analysis of fuel assembly CZ346. Cuttings 1.23–1.24 cm in length were used for burnup and isotopic analyses of the fuel rods.

Of the six samples taken for isotopic analyses, three samples came from rod ADD2966 and three samples from ADD2974. The axial locations of the samples are documented differently in the references. The OECD/NE SFCOMPO[9] isotopic database web site illustrates the sample locations as shown in Fig. 3 and Fig. 4 for rods ADD2966 and ADD2974, respectively.

The original PNNL report[14] gives the sample locations with respect to the top of the fuel rod in Table D.1 and Table D.2.[14] The sample locations only become consistent with Fig. 3 and Fig. 4 if the top of the fuel is considered to be at the active fuel length of 371 cm. However, the last cutting was reported to be taken from between 330.045 cm and 416.20 cm from the top of the fuel rod ADD2966. The location of the last cutting suggests that the sample locations were measured from the top of the actual fuel rod length not from the top of the active fuel section. Therefore, assuming the active fuel section is located in the middle of the fuel rod, there is a 22.5 cm difference in the axial sample locations reported in the SFCOMPO and PNNL references.[9,10] The sample locations are only used to calculate moderator densities at the sample locations; therefore, the sample locations with respect to the bottom of the active fuel need to be known. Unfortunately, the detailed dimensions of the analyzed fuel rods were not provided in the related reports. However, Ref. 16 documents the distance between the top of the fuel rod and the top of the active fuel length as 35 cm in a fresh 9 × 9 BWR assembly. Assuming the same gap holds for the ADD2974 and ADD2966 fuel rods and the measurements are taken from the bottom of the end plug, the beginning of the active fuel is calculated to be 406 cm from the top of the fuel rod. The sample locations were calculated with respect to the bottom of the active fuel length in Table 4.

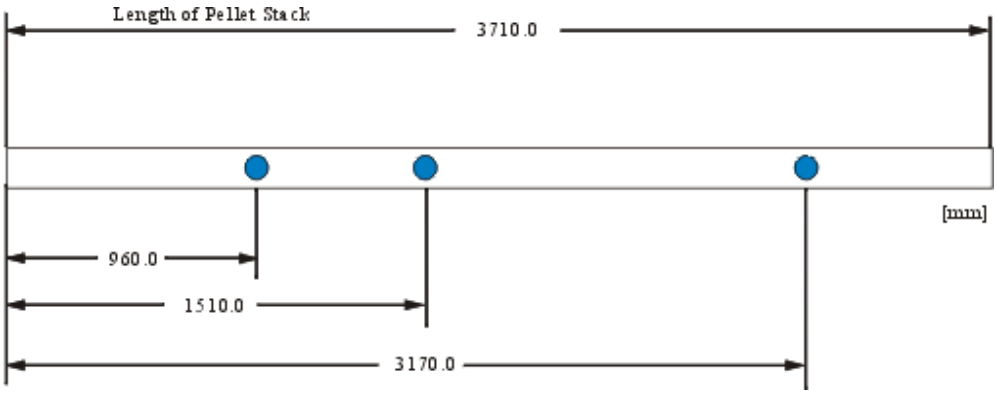


**Fig. 3. Rod measurement positions for rod ADD2966.** (Note: Measurement positions are as described by Ref 9.)

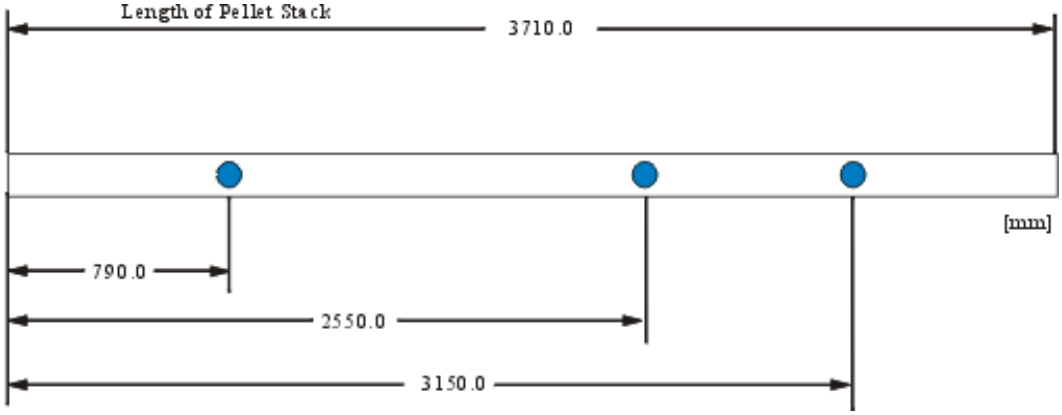


**Fig. 4. Rod measurement positions for rod ADD2974.** (Note: Measurement positions are as described by Ref 9.)

The samples were dissolved in heated 12 M nitric acid, and the fuel was separated from cladding. The concentrations in the solution were determined by mass spectroscopy. First, Nd was chemically separated from the solution using $^{150}$Nd as a diluent; then a calibrated triple spike of $^{150}$Nd, $^{233}$U, and $^{242}$Pu used to determine Nd, U, and Pu isotopes. For $^{79}$Se nuclide measurements, $^{79}$Se was separated from the solution by passing the solution through a cation plus anion exchange column and dissolving $^{79}$Se in nitric acid. The $^{79}$Se concentration was later determined by liquid scintillation. $^{90}$Sr was similarly extracted from the solution by selective elution through a cation exchange resin and was measured by beta counting of $^{90}$Y and calculating the growth of the $^{90}$Y daughter over a measured period of time. Another beta counting was performed to measure $^{99}$Tc concentration after other species were absorbed to a cation exchange resin. $^{126}$Sn and $^{137}$Cs concentrations were both determined by gamma spectroscopy on diluted solutions separated by different processes. The abundance of $^{135}$Cs was measured by mass spectroscopy after separating Cs from other elements by chromatographic elution from a cation exchange column. Actinides $^{241}$Am and $^{243}$Cm + $^{244}$Cm concentrations were determined by alpha spectroscopy after a cation anion exchange column. Finally $^{237}$Np concentrations were measured by alpha counting after a series of extraction-dilution processes and adding a $^{239}$Np tracer to determine the recovery factor.

The reported burnup rate for each sample was calculated using the Nd-148 method.[11] The mentioned measurement uncertainties were as follows.

1. Mass spectroscopy for Pu and U isotopes less than 1.6%, and up to 14% for $^{135}$Cs.
2. Liquid scintillation counting less than 4.9% for $^{79}$Se.
3. Beta counting: less than 5.7% for $^{90}$Sr and less than 3.5% for $^{99}$Tc.
4. Gamma spectroscopy: less than 10.2% for $^{126}$Sn and less than 3.5% for $^{137}$Cs.
5. Alpha and gamma counting: less than 1.9% for $^{237}$Np.
6. Alpha spectroscopy: less than 4.9% for $^{241}$Am and less than 4.1% for $^{243}$Cm+$^{244}$Cm concentration.

In addition to the listed uncertainties above, a 1% uncertainty in the preparation of the original nitric acid solution was also reported in the PNNL report.[14]

The measured concentrations of the nuclides in the spent fuel samples per gram of $UO_2$ fuel were listed in Table 4.17 of Reference 14. For consistency, each concentration is renormalized with respect to the initial uranium content by multiplying with the atomic weight ratios of $UO_2$ to U ($\frac{M_{UO_2}}{M_U} = 1.1346\ 10^6$) in Table 4.

**Table 4. Measurement results of ADD2966 and ADD2974 samples**

| Sample | ADD2966 (Cut T)[a] | ADD2966 (Cut K)[a] | ADD2966 (Cut B)[a] | ADD2974 (Cut U)[b] | ADD2974 (Cut J)[b] | ADD2974 (Cut B)[b] |
|---|---|---|---|---|---|---|
| **Burnup (GWd/MTU)** | 33.94 | 33.07 | 18.96 | 31.04 | 29.23 | 17.84 |
| **Cutting position from Bottom of Active Length (mm)** | 1310 | 1869 | 3517 | 1147 | 2907 | 3501 |
| **Nuclide** | **(g/ton of initial heavy metal)** | | | | | |
| $^{234}$U | 1.633E+02 | 1.531E+02 | 1.928E+02 | 1.75E+02 | 1.66E+02 | 1.97E+02 |
| $^{235}$U | 5.477E+03 | 6.056E+03 | 1.351E+04 | 7.12E+03 | 8.80E+03 | 1.47E+04 |
| $^{236}$U | 4.105E+03 | 4.003E+03 | 2.983E+03 | 3.95E+03 | 3.81E+03 | 2.81E+03 |
| $^{238}$U | 9.516E+05 | 9.465E+05 | 9.568E+05 | 9.59E+05 | 9.63E+05 | 9.69E+05 |
| $^{238}$Pu | 1.935E+02 | 1.977E+02 | 6.067E+01 | 1.58E+02 | 1.86E+02 | 5.91E+01 |
| $^{239}$Pu | 3.783E+03 | 4.059E+03 | 4.239E+03 | 4.16E+03 | 5.13E+03 | 4.60E+03 |
| $^{240}$Pu | 2.484E+03 | 2.513E+03 | 1.384E+03 | 2.36E+03 | 2.45E+03 | 1.34E+03 |
| $^{241}$Pu | 7.032E+02 | 7.247E+02 | 3.859E+02 | 6.96E+02 | 7.54E+02 | 3.87E+02 |
| $^{242}$Pu | 5.372E+02 | 4.998E+02 | 1.122E+02 | 4.34E+02 | 3.68E+02 | 9.91E+01 |
| **Nuclide** | **(Ci/ton of initial heavy metal)** | | | | | |
| $^{237}$Np | 2.790E-01 | 2.880E-01 | 1.259E-01 | 2.68E-01 | 2.66E-01 | 1.24E-01 |
| $^{241}$Am | 9.503E+02 | 9.957E+02 | 5.874E+02 | 9.85E+02 | 1.07E+03 | 5.93E+02 |
| $^{243}$Cm+$^{244}$Cm | 1.701E+03 | 1.644E+03 | 1.247E+02 | 1.21E+03 | 1.25E+03 | 1.29E+02 |
| $^{79}$Se | 5.625E-02 | 5.205E-02 | 3.141E-02 | 5.10E-02 | 4.83E-02 | 3.06E-02 |
| $^{90}$Sr | 5.772E+04 | 5.511E+04 | 3.640E+04 | 5.47E+04 | 4.97E+04 | 3.31E+04 |
| $^{99}$Tc | 1.202E+01 | 1.168E+01 | 7.514E+00 | 1.13E+01 | 1.12E+01 | 7.00E+00 |
| $^{126}$Sn | 1.814E-01 | 1.724E-01 | 8.834E-02 | 1.66E-01 | 1.60E-01 | 8.32E-02 |
| $^{135}$Cs | 4.865E-01 | 5.058E-01 | 4.241E-01 | 4.89E-01 | 5.93E-01 | 4.34E-01 |
| $^{137}$Cs | 8.732E+04 | 8.483E+04 | 4.842E+04 | 7.77E+04 | 8.22E+04 | 4.59E+04 |

Source: Reference 14, Table 4.17.

[a]Reported at a cooling time of 5.35 years.

[b]Reported at a cooling time of 5.28 years.

## 4.3 GUNDREMMINGEN-A

The Gundremmingen-A Nuclear Power Plant, operated by Kernkraftwerk RWE-Bayernwerk GmbH (KRB), was a dual cycle 250 MW(e) BWR. The reactor started commercial operation in 1967 and was permanently shut down in 1977. The reactor core operated with 6 × 6 fuel assemblies and cruciform $B_4C$ control blades. As a part of the cooperation agreement among the European Communities, KRB, and Kraftwerk Union AG Frankfurt, two fuel assemblies, B23 and C16, were unloaded at the end of the fifth irradiation cycle for a post-irradiation analysis program.[17] The main objective of the program was to provide burnup-dependent isotopic data for nuclear code benchmarking. The analyses were carried out in the European Commission Joint Research Center laboratories at Ispra and Karlsruhe.

Fuel assembly B23 was irradiated from August 25, 1969, to March 5, 1973, for four cycles, reaching an average burnup of 22.600 GWd/MTU. The other fuel assembly, C16, was irradiated from July 25, 1970, to March 5, 1973, for three cycles, reaching an average burnup of 17.100 GWd/MTU. Both assemblies were composed of 29 rods with initial enrichment of 2.53 wt % $^{235}U$ and 7 rods with an initial enrichment of 1.87 wt % $^{235}U$. A total of 10 fuel rods were selected for the analysis.

### 4.3.1 Measurements and Uncertainties

A total of 12 samples from 10 fuel rods in fuel assemblies C16 and B23 were selected for the measurements. Fuel samples 10 mm thick were cut at 2,680 mm from the bottom of all sampled fuel rods. Two additional samples were cut at 440 mm from the bottom of A-1 rods in the B23 and C16 assemblies. The sample axial locations are illustrated in Fig. 5 (Ref. 18).

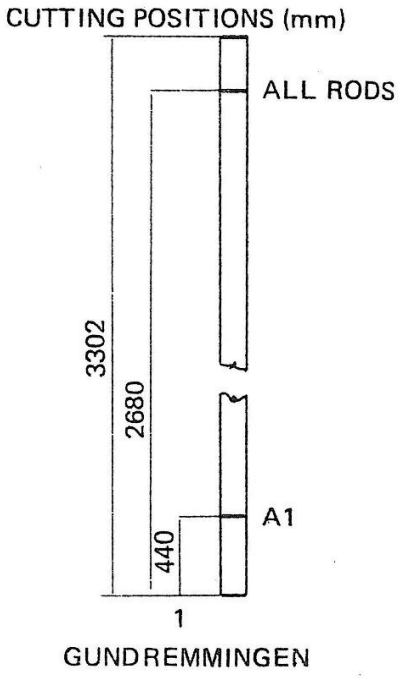


**Fig. 5. Rod measurement positions for B23 and C16 assemblies.**

Isotopic measurements of 10 samples were performed at the Ispra laboratories. In addition to the remaining two samples, four samples were also analyzed at the Karlsruhe site to cross-check the measurements.

The fuel samples were dissolved in nitric acid in hot cells. Small aliquots of the dissolved solution were transferred to glove boxes for radiochemical processing. The radioactive FPs were determined by gamma spectrometry. Plutonium, uranium, and $^{148}$Nd isotope concentrations were determined by isotopic dilution and mass spectrometry using $^{233}$U, $^{242}$Pu, and $^{150}$Nd spiking isotopes for calibration. $^{236}$Pu, $^{238}$Pu, $^{241}$Am, $^{242}$Cm, and $^{244}$Cm were determined by alpha spectroscopy.

The measured isotopic concentrations were reported with respect to either final total uranium or final $^{238}$U atom concentration as shown in Table 5 and Table 6. The burnup rates of the all-fuel samples presented in the tables were calculated by the Nd-148 method[11] for all Karlsruhe samples, whereas the burnup rates of the three Ispra samples were calculated using $^{137}$Cs activity. In this report, the isotopic atomic ratios reported by the two laboratories were averaged and converted to weights with respect to the initial uranium weight for consistency. The results are presented in Table 7 and Table 8 for assemblies B23 and C16, respectively.

The total uncertainty for isotope dilution and mass spectroscopy was reported as 0.5% for uranium and plutonium isotopes. The total error in determination of the $^{148}$Nd concentration was about 1%, again for the same measurement procedure. The standard deviation of the destructive and the nondestructive gamma spectrum measurements were reported as 1.5% for $^{134}$Cs and $^{137}$Cs isotopes and 5% for $^{154}$Eu.

Typical global uncertainties for all isotopic measurements performed under the post-irradiation analyses program at the Karlsruhe and Ispra sites were also calculated to include contributions from sample cutting to chemical treatments of the samples. These uncertainties are presented in Table 9 (Ref. 18) at 24.637 GWd/MTU. In addition to the reported uncertainties, Karlsruhe and Ispra measurements for the cross-checked samples are compared in Fig. 6. As seen from the figure, this comparison reveals large discrepancies in $^{241}$Am measurements. The differences in $^{244}$Cm and $^{137}$Cs measurements are also much higher than the reported uncertainties for the same samples.

**Table 5. Measured isotopic concentrations of B23 samples**

| **Laboratory** | | Ispra | Ispra | Ispra | Karlsruhe | Ispra | Karlsruhe | Ispra | Ispra | Karlsruhe |
|---|---|---|---|---|---|---|---|---|---|---|
| **Sample** | | A1-1 | A1-2 | B3 | B3 | B4 | C5 | E3 | E5 | E5 |
| **Burnup (GWd/MTU)** | | 25.73 | 27.40 | 21.69 | 21.24 | 22.25 | 22.97 | 23.51 | 25.38[a] | 25.19 |
| **Nuclide** | **Units** | | | | | | | | | |
| $^{137}$Cs | dps[b]/g final U ($10^{9}$) | 3.66 | 2.89 | 2.61 | 2.67 | 2.7 | 3.07 | 2.75 | 3.08 | 3.24 |
| $^{134}$Cs | dps/g final U ($10^{9}$) | 3.49 | 3.28 | 2.57 | — | 2.94 | — | 3 | 3.25 | — |
| $^{154}$Eu | dps/g final U ($10^{8}$) | 1.79 | 1.80 | 1.55 | — | 1.49 | — | 1.53 | 1.61 | — |
| $^{235}$U Depletion | atom/atom final U ($10^{-2}$) | 1.923 | 1.879 | 1.577 | 1.557 | 1.656 | 1.695 | 1.689 | 1.886 | 1.869 |
| $^{236}$U Production | atom/atom final U ($10^{-2}$) | 0.329 | 0.329 | 0.297 | 0.298 | 0.302 | 0.318 | 0.316 | 0.328 | 0.336 |
| $^{238}$U Depletion | atom/atom final U ($10^{-2}$) | 1.828 | 2.241 | 1.808 | 1.889 | 1.839 | 1.924 | 1.969 | 1.992 | 2.057 |
| $^{236}$Pu | atom/atom final U ($10^{-7}$) | 10.67 | 15.61 | 12.34 | — | — | — | — | 7.34 | — |
| $^{238}$Pu | atom/atom final U ($10^{-10}$) | 0.068 | 0.108 | 0.080 | 0.086 | 0.092 | 0.089 | 0.084 | 0.097 | 0.099 |
| $^{239}$Pu | atom/atom final U ($10^{-3}$) | 3.72 | 4.78 | 5.29 | 5.41 | 5.01 | 4.91 | 4.80 | 4.52 | 4.45 |
| $^{240}$Pu | atom/atom final U ($10^{-3}$) | 1.80 | 2.15 | 1.81 | 1.87 | 1.84 | 1.95 | 1.83 | 2.09 | 2.08 |
| $^{241}$Pu | atom/atom final U ($10^{-3}$) | 0.782 | 1.128 | 0.857 | 0.884 | 0.859 | 0.879 | 0.844 | 0.898 | 0.892 |
| $^{242}$Pu | atom/atom final U ($10^{-6}$) | 0.325 | 0.442 | 0.215 | 0.224 | 0.232 | 0.263 | 0.242 | 0.331 | 0.333 |
| $^{241}$Am | atom/atom final U ($10^{-4}$) | 3.73 | 6.55 | 3.10 | — | — | 1.04 | 2.19 | 2.12 | 1.14 |
| $^{242}$Cm | atom/atom final U ($10^{-6}$) | 9.92 | 14.32 | 9.37 | 9.22 | 9.17 | 9.90 | 9.46 | 11.29 | 10.26 |
| $^{244}$Cm | atom/atom final U ($10^{-6}$) | 8.65 | 19.28 | 8.46 | 8.36 | 9.16 | 10.58 | 8.95 | 15.24 | 14.14 |
| $^{148}$Nd | atom/atom final $^{238}$U ($10^{-4}$) | 4.88 | 5.22 | — | 4.03 | 4.22 | 4.36 | 4.58 | — | 4.92 |
| $^{137}$Cs | atom/atom final $^{238}$U ($10^{-3}$) | 2.12 | 1.67 | 1.52 | 1.55 | 1.57 | 1.78 | 1.59 | 1.78 | 1.87 |

Source: Reference 17.

All reported values were normalized to the reactor shutdown date.

[a] $^{137}$Cs activity was used for the burnup calculation.

[b] dps = disintegrations per second.

**Table 6. Measured isotopic concentrations of C16 samples**

| **Laboratory** | | Ispra | Ispra | Ispra | Karlsruhe | Ispra | Karlsruhe | Ispra |
|---|---|---|---|---|---|---|---|---|
| **Sample** | | A1-1 | A1-2 | B3 | B3 | C5 | E5 | E5 |
| **Burnup (GWd/MTU)** | | 20.30 | 19.85 | 15.22[a] | 14.39 | 15.84 | 17.49 | 15.97[a] |
| **Nuclide** | **Units** | | | | | | | |
| $^{137}$Cs | dps[b]/g final U ($10^{9}$) | 2.55 | 2.69 | 1.83 | 1.91 | 2.2 | 1.92 | 2.32 |
| $^{134}$Cs | dps/g final U ($10^{9}$) | 2.26 | 2.85 | 1.45 | — | — | 1.63 | — |
| $^{154}$Eu | dps/g final U ($10^{8}$) | 0.89 | 1.09 | 0.75 | — | — | 0.84 | — |
| $^{235}$U Depletion | atom/atom final U ($10^{-2}$) | 1.692 | 1.569 | 1.238 | 1.230 | 1.305 | 1.516 | 1.492 |
| $^{236}$U Production | atom/atom final U ($10^{-2}$) | 0.308 | 0.291 | 0.246 | 0.248 | 0.252 | 0.273 | 0.279 |
| $^{238}$U Depletion | atom/atom final U ($10^{-2}$) | 1.363 | 1.523 | 1.196 | 1.249 | 1.289 | 1.274 | 1.346 |
| $^{236}$Pu | atom/atom final U ($10^{-10}$) | — | — | 3.77 | — | — | 4.16 | — |
| $^{238}$Pu | atom/atom final U ($10^{-3}$) | 0.036 | 0.048 | 0.033 | 0.033 | 0.035 | 0.041 | 0.041 |
| $^{239}$Pu | atom/atom final U ($10^{-3}$) | 3.62 | 4.40 | 4.66 | 4.69 | 4.42 | 4.15 | 4.13 |
| $^{240}$Pu | atom/atom final U ($10^{-3}$) | 1.46 | 1.52 | 1.15 | 1.17 | 1.23 | 1.43 | 1.43 |
| $^{241}$Pu | atom/atom final U ($10^{-3}$) | 0.604 | 0.756 | 0.536 | 0.542 | 0.537 | 0.596 | 0.59 |
| $^{242}$Pu | atom/atom final U ($10^{-3}$) | 0.179 | 0.198 | 0.087 | 0.088 | 0.098 | 0.151 | 0.144 |
| $^{241}$Am | atom/atom final U ($10^{-2}$) | 2.77 | 2.64 | 1.00 | 0.94 | 0.32 | 1.43 | 1.02 |
| $^{242}$Cm | atom/atom final U ($10^{-4}$) | 5.17 | 6.76 | 3.68 | 3.80 | 3.76 | 5.09 | 4.82 |
| $^{244}$Cm | atom/atom final U ($10^{-6}$) | 2.55 | 4.37 | 1.44 | 1.62 | 1.89 | 2.46 | 2.99 |
| $^{148}$Nd | atom/atom final $^{238}$U ($10^{-4}$) | 3.30 | 3.72 | — | 2.73 | 2.96 | — | 3.33 |
| $^{137}$Cs | atom/atom final $^{238}$U ($10^{-3}$) | 1.46 | 1.54 | 1.05 | 1.10 | 1.26 | 1.10 | 1.33 |

Source: Reference 17.

All reported values were normalized to the reactor shutdown date.

[a] $^{137}$Cs activity was used for the burnup calculation.

[b] dps= disintegrations per second.

**Table 7. Measured isotopic concentrations of B23 samples after conversion**

| Sample | A1-1 | A1-2 | B3 | B4 | C5 | E3 | E5 |
|---|---|---|---|---|---|---|---|
| **Burnup (GWd/MTU)** | 25.73 | 27.4 | 21.47 | 22.25 | 22.97 | 23.51 | 25.29 |
| **Cutting position from bottom of active length (mm)** | 440 | 2680 | 2680 | 2680 | 2680 | 2680 | 2680 |
| **Nuclide** | **g/ton of initial heavy metal** | | | | | | |
| $^{137}$Cs | 1.098 | 0.863 | 0.794 | 0.812 | 0.922 | 0.825 | 0.946 |
| $^{134}$Cs | 0.0704 | 0.0659 | 0.0520 | 0.0594 | No Data | 0.0605 | 0.0654 |
| $^{154}$Eu | 0.0173 | 0.0173 | 0.0150 | 0.0144 | No Data | 0.0148 | 0.0155 |
| $^{235}$U | 6.3068 | 6.7414 | 9.8230 | 8.9439 | 8.5587 | 8.6180 | 6.7562 |
| $^{236}$U | 3.263 | 3.263 | 2.951 | 2.996 | 3.154 | 3.134 | 3.293 |
| $^{238}$U | 956.41 | 952.28 | 956.21 | 956.30 | 955.45 | 955.00 | 954.45 |
| $^{236}$Pu | 1.058E-06 | 1.548E-06 | 1.224E-06 | No Data | No Data | No Data | 7.281E-07 |
| $^{238}$Pu | 0.068 | 0.108 | 0.083 | 0.092 | 0.089 | 0.084 | 0.098 |
| $^{239}$Pu | 3.737 | 4.802 | 5.374 | 5.033 | 4.932 | 4.822 | 4.505 |
| $^{240}$Pu | 1.816 | 2.169 | 1.856 | 1.856 | 1.967 | 1.846 | 2.103 |
| $^{241}$Pu | 0.792 | 1.143 | 0.882 | 0.870 | 0.890 | 0.855 | 0.907 |
| $^{242}$Pu | 0.331 | 0.450 | 0.223 | 0.236 | 0.268 | 0.246 | 0.338 |
| $^{241}$Am | 0.378 | 0.663 | 0.314 | No Data | 0.105 | 0.222 | 0.165 |
| $^{242}$Cm | 0.0101 | 0.0146 | 0.0095 | 0.0093 | 0.0101 | 0.0096 | 0.0110 |
| $^{244}$Cm | 0.0089 | 0.0198 | 0.0086 | 0.0094 | 0.0109 | 0.0092 | 0.0151 |
| $^{148}$Nd | 0.290 | 0.309 | 0.239 | 0.251 | 0.259 | 0.272 | 0.292 |

Source: Gundremmingen_Experimental_Data.xls.

**Table 8. Measured isotopic concentrations of C16 samples after conversion**

| Sample | A1-1 | A1-2 | B3 | C5 | E5 |
|---|---|---|---|---|---|
| **Burnup (GWd/MTU)** | 20.30 | 19.85 | 14.39 | 15.84 | 17.49 |
| **Cutting position from bottom of active length (mm)** | 440 | 2680 | 2680 | 2680 | 2680 |
| **Nuclide** | **g/ton of initial heavy metal** | | | | |
| $^{137}$Cs | 0.770 | 0.812 | 0.568 | 0.667 | 0.642 |
| $^{134}$Cs | 0.0459 | 0.0578 | 0.0296 | No Data | 0.0332 |
| $^{154}$Eu | 0.0087 | 0.0106 | 0.0073 | No Data | 0.0082 |
| $^{235}$U | 8.5884 | 9.8032 | 13.1120 | 12.4107 | 10.4452 |
| $^{236}$U | 3.055 | 2.886 | 2.450 | 2.500 | 2.738 |
| $^{238}$U | 961.07 | 959.47 | 962.47 | 961.81 | 961.60 |
| $^{236}$Pu | No Data | No Data | 3.739E-07 | No Data | 4.126E-07 |
| $^{238}$Pu | 0.036 | 0.048 | 0.033 | 0.035 | 0.041 |
| $^{239}$Pu | 3.636 | 4.420 | 4.696 | 4.440 | 4.159 |
| $^{240}$Pu | 1.473 | 1.533 | 1.170 | 1.241 | 1.442 |
| $^{241}$Pu | 0.612 | 0.766 | 0.546 | 0.544 | 0.601 |
| $^{242}$Pu | 0.182 | 0.201 | 0.089 | 0.100 | 0.150 |
| $^{241}$Am | 0.281 | 0.267 | 0.098 | 0.032 | 0.124 |
| $^{242}$Cm | 0.0053 | 0.0069 | 0.0038 | 0.0038 | 0.0050 |
| $^{244}$Cm | 0.0026 | 0.0045 | 0.0016 | 0.0019 | 0.0028 |
| $^{148}$Nd | 0.227 | 0.222 | 0.163 | 0.177 | 0.199 |

Source: Gundremmingen_Experimental_Data.xls.

**Table 9. Typical global percent uncertainties at 24.637 GWd/MTU**

| Parameter | Analytical uncertainty (%) | Global uncertainty (%) (central pin region) |
|---|---|---|
| $^{148}$Nd Burnup | 1.43 | 1.43 |
| $^{235}$U Depletion | 1.03 | 1.03 |
| $^{236}$U Buildup | 1.24 | 1.24 |
| $^{238}$Pu Buildup | 1.99 | 2.05 |
| $^{239}$Pu Buildup | 0.88 | 1.01 |
| $^{240}$Pu Buildup | 0.99 | 1.11 |
| $^{241}$Pu Buildup | 1.15 | 1.25 |
| $^{242}$Pu Buildup | 1.10 | 1.21 |
| $^{241}$Am Buildup | 20.00 | 20.00 |
| $^{242}$Cm Buildup | 4.21 | 4.21 |
| $^{244}$Cm Buildup | 2.75 | 2.72 |

Source: Reference 18.

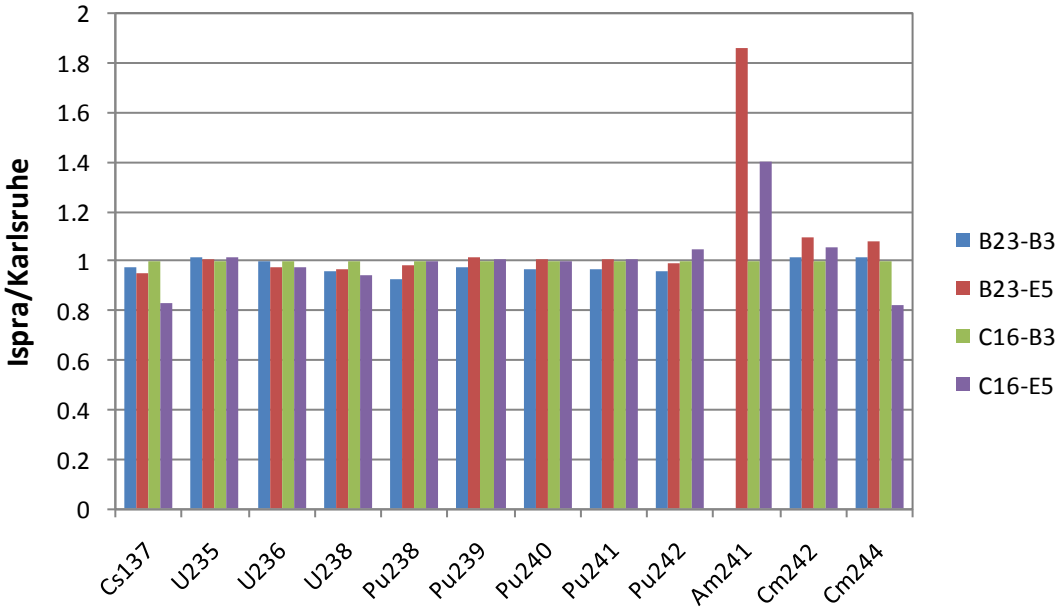


**Fig. 6. Comparison of Ispra and Karlsruhe measurements.**

# 5. ASSEMBLY DESIGN AND OPERATING HISTORY

## 5.1 FUKUSHIMA DAINI UNIT 2

The reactor core operation parameters and the physical dimensions and characteristics of the fuel assemblies and fuel rods are given in Table 10. Most of the reactor operation data and the assembly/fuel rod design parameters were obtained from Nakahara et al.[10] based on the related JAERI report[8] for the Fukushima Daini-2 measurements. As the measured Fukushima fuel assembly 2F2DN23 is classified as an 8 × 8-2 lattice type,[19] the channel and water rod data were obtained from the reported Tsuruga 8 × 8-2 lattice dimensions in a recent Japan Nuclear Energy Safety Organization report on BWR isotopics measurement.[16]

**Table 10. Fukushima Daini-2 nuclear power station reactor and assembly parameters**

| Parameter | Data |
|---|---|
| Assembly and reactor data | |
| Nominal thermal power (MW)[10] | 3,293 |
| Lattice type[10] | 8 × 8-2 |
| Number of fuel rods[10] | 62 |
| Number of water rods[10] | 2 |
| Active core height (m)[10] | 3.71 |
| Assembly pitch (cm)[16] | 15.2 |
| Coolant mass flow (kg/s)[10] | $1.3417 \times 10^4$ |
| Fuel rod data | |
| Fuel material[10] | $UO_2$, $UO_2$-$Gd_2O_3$ |
| Fuel pellet density (g/cm$^3$) [10,12] | 10.412 (~95% theoretical) |
| Smeared fuel pellet density (g/cm$^3$)[a] | 9.943 |
| Fuel pellet diameter (cm)[10] | 1.03 |
| Pellet-clad gap clearance (cm)[10b] | 0.024 |
| Clad material[10] | Zircaloy-2 |
| Clad thickness (cm)[10] | 0.086 |
| Clad outer diameter (cm)[10] | 1.23 |
| Number of gadolinium rods[10] | 8 |
| Rod pitch (cm)[10] | 1.63 |
| Fuel temperature (K)[19] | 900 |
| Moderator data | |
| Nominal pressure (Pa)[10] | $6.93 \times 10^6$ |
| Nominal inlet subcooling (kcal/kg)[10] | 11.4 |
| Nominal outlet temperature (K)[10] | 559 |
| Water rod data | |
| Water rod material[10] | Zircaloy |
| Water rod inner diameter (cm)[13] | 1.35 |
| Water rod outer diameter (cm)[10,13,16] | 1.50 |
| Channel box data | |
| Channel box inner width (cm) [13,16] | 13.4 |
| Channel box thickness (cm) [13] | 0.203 |

[a]Based on fresh fuel diameter + gap distance.
[b]Diametral gap thickness.

Fig. 7 shows the layout of assembly 2F2DN23 and the axially averaged enrichment distribution (Ref. 9). Rod SF98 corresponds to position B-2 within the assembly. Of the 18 samples taken from assembly 2F2DN23, 8 samples came from rod SF98 and 10 samples from SF99. The second rod, SF99, corresponds to position C-2 and contains gadolinium as a burnable poison. Type 1 and type G rods contain a natural uranium blanket segment at the upper and lower tips of the rods as seen in Fig. 8 (Ref. 8). Except for these two rod types, the axial enrichment distribution for the assembly was not provided.[8,9,10] Therefore, the axial enrichments for the remaining rods were calculated from the axially averaged enrichments in Fig. 7 assuming the same natural uranium blankets exists in all fuel rods.

Based on the similarity between the reported assembly dimensions of 8 × 8-2 and the GE 8 × 8 fuel assembly dimensions shown in Fig. 9 (Ref. 13), the missing design information such as the channel thickness was assumed to be the same for both fuel assembly types.

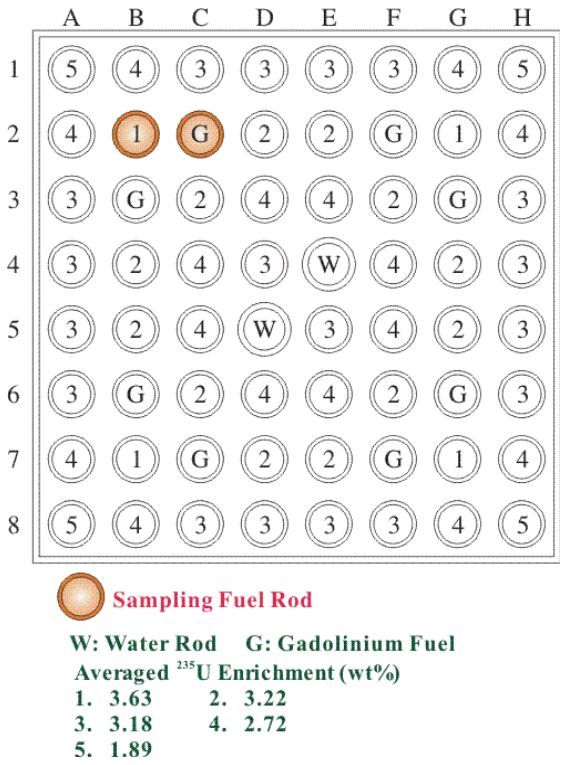


**Fig. 7. Radial loading diagram of assembly 2F2DN23.**

The irradiation histories of each sample taken from the SF98 and SF99 fuel rods were reported in the original JAERI report[8] and are presented in Table 11 and Table 12. These tabulated values were directly used in the depletion simulations. Time averaged axial void fraction profiles for the samples from the two assemblies were also provided in the JAERI report. However, the reported values in Table 13 were gathered from the Fukushima Daini-2 power plant modification permit application,[10] and it is not clear whether these void profiles are actually assembly specific, cycle averaged or core averaged, cycle generic void fraction profiles.

For validation of the developed void fraction profile models in Appendix A, a core average, axial void profile was also calculated using the core average, cycle generic Fukushima Daini-2 thermal hydraulic parameters.[10] As seen in Fig. 10, the profile fit model shows a good agreement with the documented void fraction distribution.

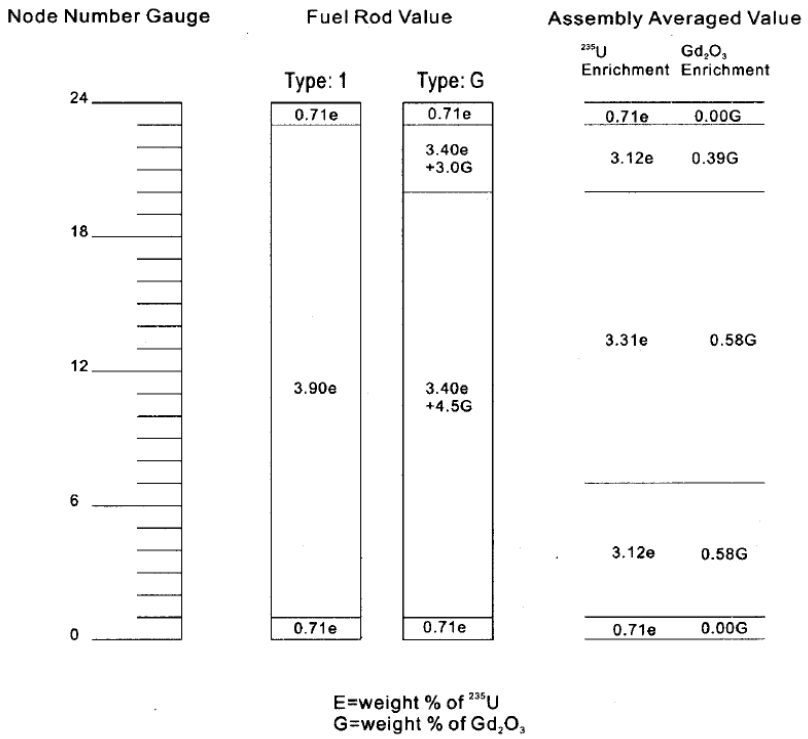


**Fig. 8. Axial distribution diagram for rods SF98 and SF99.**

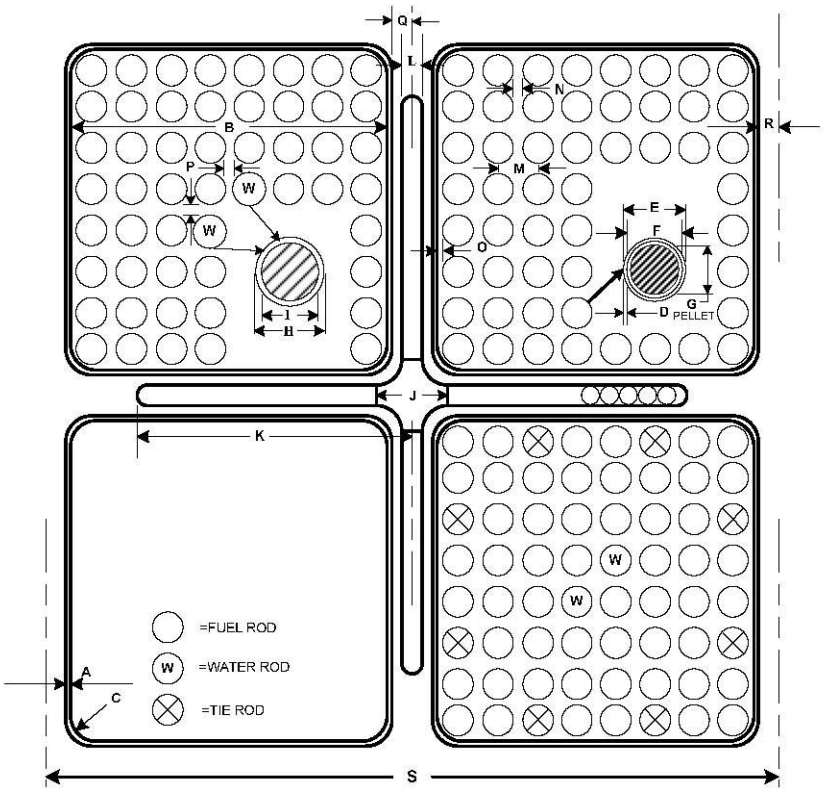


| | Length (cm) |
|---|---|
| **A** | 0.2032 |
| **B** | 13.40612 |
| **C** | 0.9652 |
| **D** | 0.08128 |
| **E** | 1.22682 |
| **F** | 1.06426 |
| **G** | 1.0414 |
| **H** | 1.50114 |
| **I** | 1.34874 |
| **J** | 4.0132 |
| **K** | 12.3825 |
| **L** | 0.6604 |
| **M** | 1.6256 |
| **N** | 0.39878 |
| **O** | 0.40132 |
| **P** | 0.26162 |
| **Q** | 0.71374 |
| **R** | 0.71374 |
| **S** | 30.48 |
| **T** | 2.8575 |

**Fig. 9. Dimensions for 8 × 8 BWR fuel assembly.**

**Table 11. Irradiation histories of SF98 samples**

| Days | Power (MW/MTU) | | | | | | | |
|---|---|---|---|---|---|---|---|---|
| | SF98-1 | SF98-2 | SF98-3 | SF98-4 | SF98-5 | SF98-6 | SF98-7 | SF98-8 |
| 6 | 1.27 | 8.10 | 11.29 | 12.95 | 13.45 | 12.21 | 12.05 | 8.31 |
| 3 | 3.20 | 20.46 | 28.50 | 32.68 | 33.95 | 30.81 | 30.41 | 20.98 |
| 132 | 3.95 | 25.22 | 35.14 | 40.29 | 41.84 | 37.98 | 37.49 | 25.86 |
| 21 | 0.00 | 0.00 | 0.00 | 0.00 | 0.00 | 0.00 | 0.00 | 0.00 |
| 5 | 1.43 | 9.13 | 12.73 | 14.59 | 15.16 | 13.76 | 13.58 | 9.37 |
| 244 | 3.44 | 22.00 | 30.65 | 35.15 | 36.51 | 33.13 | 32.70 | 22.56 |
| 8 | 3.99 | 25.47 | 35.49 | 40.70 | 42.27 | 38.36 | 37.87 | 26.12 |
| 117 | 0.00 | 0.00 | 0.00 | 0.00 | 0.00 | 0.00 | 0.00 | 0.00 |
| 5 | 1.43 | 9.13 | 12.73 | 14.59 | 15.16 | 13.76 | 13.58 | 9.37 |
| 317 | 3.44 | 22.00 | 30.65 | 35.15 | 36.51 | 33.13 | 32.70 | 22.56 |
| 9 | 0.00 | 0.00 | 0.00 | 0.00 | 0.00 | 0.00 | 0.00 | 0.00 |
| 4 | 1.49 | 9.52 | 13.27 | 15.21 | 15.80 | 14.34 | 14.15 | 9.76 |
| 72 | 3.50 | 22.38 | 31.19 | 35.76 | 37.15 | 33.71 | 33.28 | 22.95 |
| 10 | 3.95 | 25.22 | 35.14 | 40.29 | 41.84 | 37.98 | 37.49 | 25.86 |
| 81 | 0.00 | 0.00 | 0.00 | 0.00 | 0.00 | 0.00 | 0.00 | 0.00 |
| 3 | 1.63 | 10.42 | 14.52 | 16.65 | 17.29 | 15.69 | 15.49 | 10.69 |
| 365 | 3.65 | 23.29 | 32.45 | 37.20 | 38.64 | 35.07 | 34.62 | 23.88 |

Source: Reference 8.

**Table 12. Irradiation histories of SF99 samples**

| Days | Power (MW/MTU) | | | | | | | | | |
|---|---|---|---|---|---|---|---|---|---|---|
| | SF99-1 | SF99-2 | SF99-3 | SF99-4 | SF99-5 | SF99-6 | SF99-7 | SF99-8 | SF99-9 | SF99-10 |
| 6 | 2.30 | 6.92 | 9.92 | 10.83 | 11.44 | 9.89 | 9.82 | 6.67 | 5.09 | 2.20 |
| 3 | 5.81 | 17.46 | 25.03 | 27.33 | 28.87 | 24.97 | 24.79 | 16.84 | 12.85 | 5.55 |
| 132 | 7.16 | 21.53 | 30.86 | 33.69 | 35.58 | 30.78 | 30.56 | 20.76 | 15.84 | 6.84 |
| 21 | 0.00 | 0.00 | 0.00 | 0.00 | 0.00 | 0.00 | 0.00 | 0.00 | 0.00 | 0.00 |
| 5 | 2.59 | 7.80 | 11.18 | 12.21 | 12.89 | 11.15 | 11.07 | 7.52 | 5.74 | 2.48 |
| 244 | 6.25 | 18.78 | 26.92 | 29.40 | 31.05 | 26.85 | 26.66 | 18.12 | 13.82 | 5.97 |
| 8 | 7.23 | 21.75 | 31.17 | 34.04 | 35.95 | 31.09 | 30.87 | 20.98 | 16.00 | 6.91 |
| 117 | 0.00 | 0.00 | 0.00 | 0.00 | 0.00 | 0.00 | 0.00 | 0.00 | 0.00 | 0.00 |
| 5 | 2.59 | 7.80 | 11.18 | 12.21 | 12.89 | 11.15 | 11.07 | 7.52 | 5.74 | 2.48 |
| 317 | 6.25 | 18.78 | 26.92 | 29.40 | 31.05 | 26.85 | 26.66 | 18.12 | 13.82 | 5.97 |
| 9 | 0.00 | 0.00 | 0.00 | 0.00 | 0.00 | 0.00 | 0.00 | 0.00 | 0.00 | 0.00 |
| 4 | 2.70 | 8.13 | 11.65 | 12.72 | 13.44 | 11.62 | 11.54 | 7.84 | 5.98 | 2.58 |
| 72 | 6.35 | 19.11 | 27.39 | 29.91 | 31.59 | 27.33 | 27.13 | 18.43 | 14.06 | 6.08 |
| 10 | 21.53 | 30.86 | 33.69 | 35.58 | 30.78 | 30.56 | 20.76 | 15.84 | 10 | 21.53 |
| 81 | 0.00 | 0.00 | 0.00 | 0.00 | 0.00 | 0.00 | 0.00 | 0.00 | 0.00 | 0.00 |
| 3 | 2.96 | 8.90 | 12.75 | 13.92 | 14.71 | 12.72 | 12.63 | 8.58 | 6.54 | 2.83 |
| 365 | 6.61 | 19.88 | 28.50 | 31.11 | 32.86 | 28.42 | 28.22 | 19.17 | 14.62 | 6.32 |

Source: Reference 8.

**Table 13. Fukushima Daini-2 nuclear power station samples void ratios**

| Sample | Void ratio %[a] | Density[b] ($kg/m^3$) | Sample | Void ratio %[a] | Density ($kg/m^3$)[b] |
|---|---|---|---|---|---|
| SF98-1 | 0.0 | 740.19 | SF99-1 | 0.0 | 740.19 |
| SF98-2 | 0.0 | 740.19 | SF99-2 | 1.4 | 730.34 |
| SF98-3 | 3.0 | 719.08 | SF99-3 | 5.8 | 699.38 |
| SF98-4 | 11.0 | 662.79 | SF99-4 | 10.8 | 664.20 |
| SF98-5 | 32.0 | 515.02 | SF99-5 | 27.7 | 545.28 |
| SF98-6 | 54.5 | 356.70 | SF99-6 | 54.7 | 355.29 |
| SF98-7 | 68.0 | 261.71 | SF99-7 | 66.5 | 272.26 |
| SF98-8 | 73.0 | 226.52 | SF99-8 | 71.7 | 235.67 |
| | | | SF99-9 | 72.9 | 227.23 |
| | | | SF99-10 | 74.3 | 217.38 |

[a]Source: Reference 8.
[b]Source: FukushimaDaini2 Void Calculation_V2.xlsx.

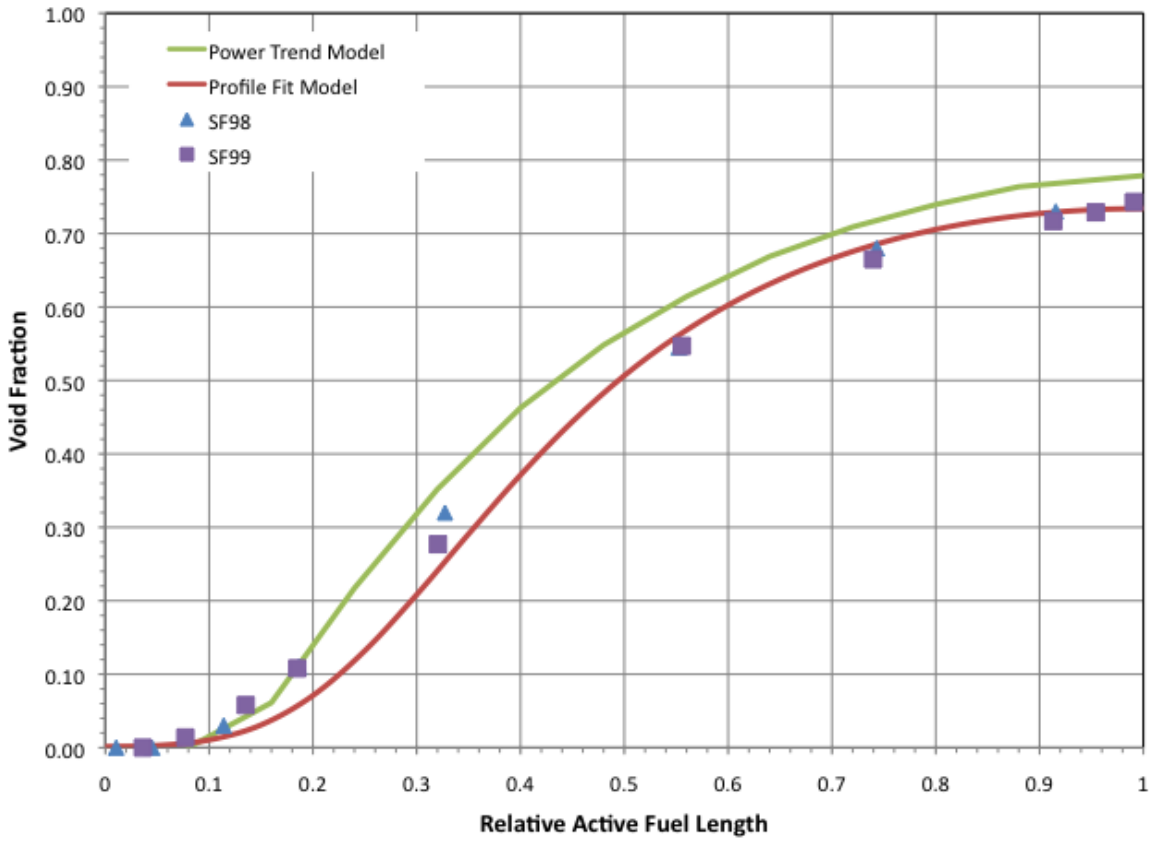


**Fig. 10. Fukushima Daini-2 void profile model comparisons.** Source: FukushimaDaini2 Void Calculation_V2.xlsx.

Table 14 shows the reported[10] fresh fuel isotopic compositions of the SF98 and SF99 rods. When the reported concentrations are compared with the isotopic ratios from Table 15, it can be seen that the reported single digit $^{234}U$ concentration is an approximate rounded value. Because the final $^{234}U$ concentration is strongly sensitive to the initial concentration, rounding the concentration up or down can lead to a 70% deviation in the final concentration. Therefore, based on the comparison with Table 15 Table values, it is postulated that the original $^{234}U$ concentration of the SF98 rod was equal to or slightly above 0.035% and it was rounded up to 0.04% in the JAERI report.[8] A similar analysis for the SF99 rod shows that the $^{234}U$ concentration was most likely rounded from 0.0303% to 0.03%. Therefore the reported concentrations were not changed in modeling the fuel isotopes as shown in Table 16. The isotopic ratios from Table 15 were used in modeling the remaining fuel pins.

**Table 14. Reported initial isotopic compositions of SF98 and SF99 rods**

| Isotope | SF98 (wt %) | SF99 (wt %) |
|---|---|---|
| $^{234}U$ | 0.04 | 0.03 |
| $^{235}U$ | 3.91 | 3.41 |
| $^{238}U$ | 96.05 | 96.56 |

Source: Reference 10.

**Table 15. Uranium isotope dependence on *X* weight percent $^{235}U$ enrichment**

| Isotope | Assay, wt % |
|---|---|
| $^{234}U$ | 0.0089 *X* |
| $^{235}U$ | 1.0000 *X* |
| $^{236}U$ | 0.0046 *X* |
| $^{238}U$ | 100-1.0135 *X* |

Source: Reference 22, Table 3.12.

**Table 16. Modeled initial isotopic compositions of SF98 and SF99 rods**

| Isotopes | SF98 (wt %) | SF99 (wt %) |
|---|---|---|
| $^{234}U$ | 0.035 | 0.03 |
| $^{235}U$ | 3.91 | 3.41 |
| $^{238}U$ | 96.055 | 96.56 |

Source: Reference 8.

## 5.2 COOPER

The reactor core operation parameters and the physical dimensions and characteristics of the fuel assemblies and the fuel rods for the Cooper reactor are given in Table 17. The original report on Cooper

spent fuel measurements[14] only provided detailed dimensions and isotopic contents for the fuel rods. The basic fuel assembly dimensions are approximated in Fig. 11. Important bundle geometry data such as channel thickness and bundle pitch were not reported in the references reviewed. The description of the wide-wide corner (i.e., away from the control blade) in Fig. 12 suggests nonuniform gaps (i.e., two different assembly pitches). The report on the neutronic benchmark of the Quad Cities-1 mixed oxide assembly[20] documents the detailed geometry of another GE 7 × 7 fuel assembly (GEB161), shown in Fig. 13. Based on the agreement between the reported GE-3b[15] (Cooper assembly) and GEB161 dimensions in Fig. 11 and Fig. 13, it is assumed that the dimensions for the two assemblies are identical. Therefore, missing assembly geometry information and the fuel temperature used for modeling the Cooper samples were taken from Reference 20.

**Table 17. Cooper nuclear power station reactor and assembly parameters**

| Parameter | Data |
|---|---|
| Assembly and reactor data | |
| Nominal thermal power (MW)[15] | 2,381 |
| Lattice type[15] | 7 × 7 GE-3b |
| Number of fuel rods[14] | 49 |
| Active core height (m)[14] | 3.71 |
| Assembly pitch, wide-wide (cm)[20] | 15.718 |
| Assembly pitch, narrow-narrow (cm)[20] | 14.763 |
| Coolant mass flow (metric ton/h)[23a] | 33800 |
| Fuel rod data | |
| Fuel material[14] | $UO_2$, $UO_2$-$Gd_2O_3$ |
| Fresh fuel pellet density (g/cm$^3$)[14] | 10.32 |
| Smeared fuel pellet density (g/cm$^3$)[b] | 9.795 |
| Fuel pellet diameter (cm)[14] | 1.21 |
| Rod pitch (cm)[14] | 1.875 |
| Fuel temperature (K)[20] | 833 |
| Clad material | Zircaloy-2 |
| Clad thickness (cm)[14] | 0.094 |
| Clad outer diameter (cm)[14] | 1.43 |
| Clad inner/hot pellet diameter (cm) | 1.242 |
| Number of gadolinia rods[14] | 5 |
| Moderator data | |
| Nominal pressure (Pa)[21] | $6.91 \times 10^6$ |
| Nominal outlet temperature (K)[23] | 558 |
| Channel box data | |
| Channel box outside width (cm)[20] | 13.813 |
| Channel box thickness (cm)[20] | 0.203 |

[a]The total core flow rate reported in Reference 21 is about half of the value reported in Reference 23, and it is believed to be an error because that it is too low for the reported core power level.

[b]Based on clad inner diameter.

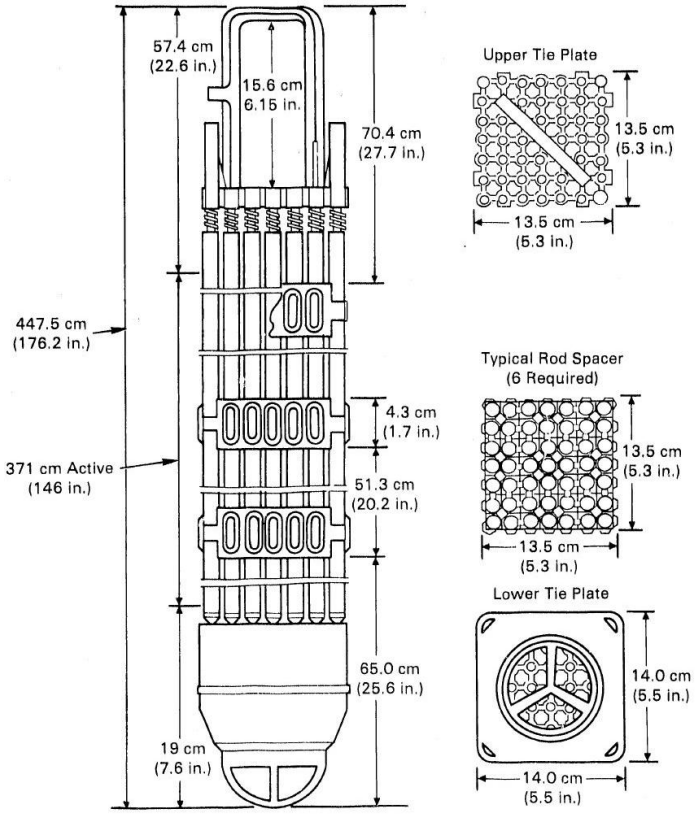


**Fig. 11. General Electric 7 × 7 fuel assembly.**

The layout of the measured fuel assembly CZ346 can be seen in Fig. 12. The analyzed fuel rods ADD2966 and ADD2974 correspond to position B-3 (second column, third row) and C-3 (third column, third row), respectively.

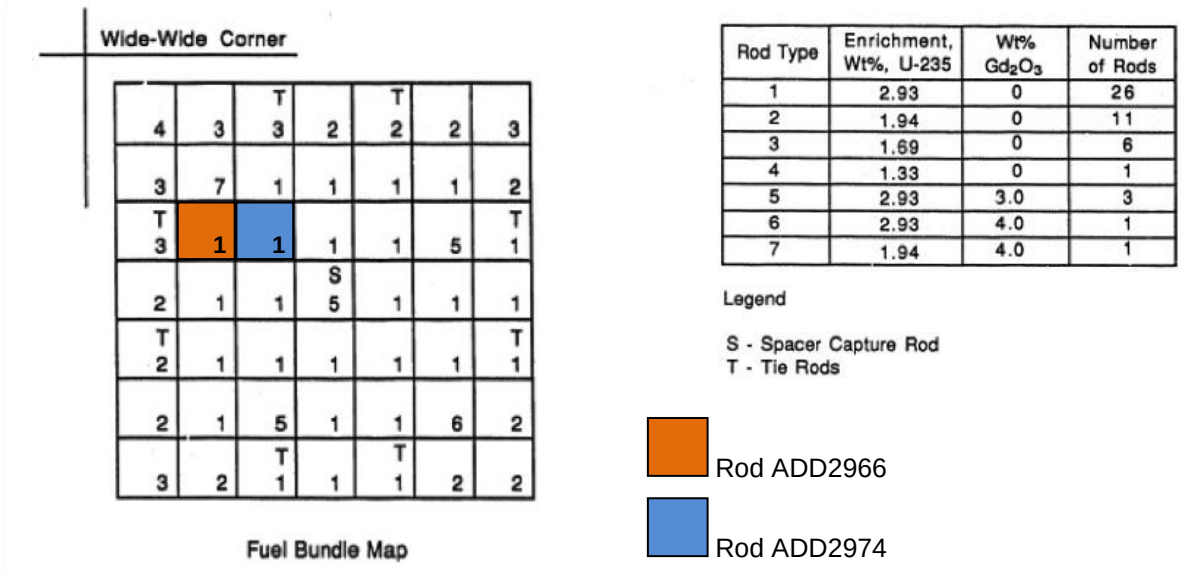


**Fig. 12. Radial loading diagram of assembly CZ346.** Source: Reference 14.

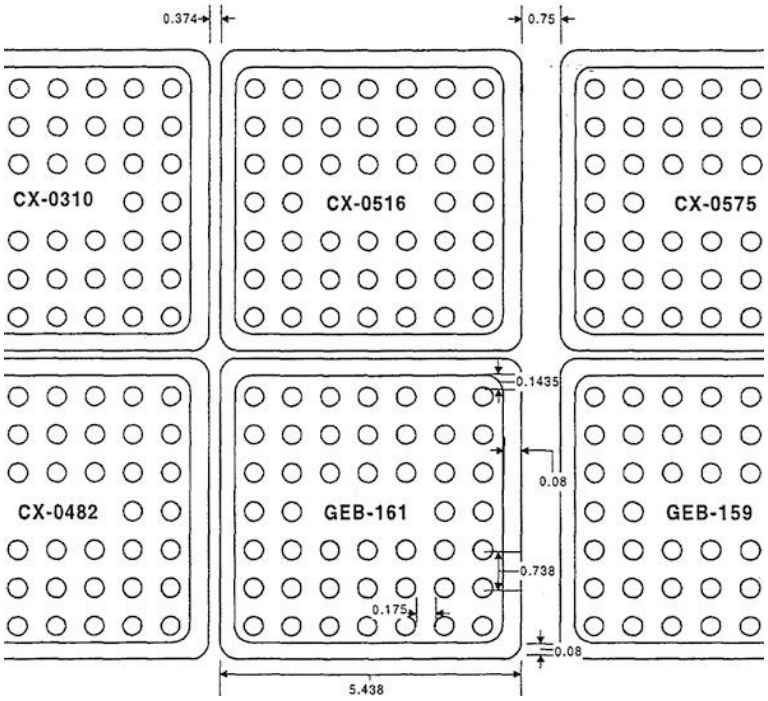


**Note: Dimensions shown in inches**

**Fig. 13. General Electric 7 × 7 GEB-161 fuel assembly.**

The power history of the fuel assembly CZ346 is given in Table 18. Assuming the ratio of the sample to the assembly average burnup is constant during irradiation, the sample burnup for each cycle inside the core can be calculated from the following equation:

$$e_c = E_c \frac{e_7}{E_7}, \quad \text{where cycle} = 1,2,3,6,7 \ , \tag{5.1}$$

where $e$ and $E$ are the burnup values for the sample and the assembly, respectively. The calculated sample power histories are presented in Table 19 and Table 20.

**Table 18. Irradiation history of CZ346 assembly**

| Cycle | Start-up | Shutdown | Assembly burnup (GWd/MTU) (Cumulative) |
|---|---|---|---|
| 1 | 07/04/74 | 09/17/76 | 13.90 |
| 2 | 11/16/76 | 09/17/77 | 19.14 |
| 3 | 10/18/77 | 03/31/78 | 21.92 |
| 6 | 06/08/80 | 04/20/81 | 25.20 |
| 7 | 06/08/81 | 05/21/82 | 28.05 |

Source: Reference 15.

**Table 19. Irradiation histories for the measured ADD2966 samples**

| Days | Power (MW/MTU) | | |
|---|---|---|---|
| | Cut T | Cut K | Cut B |
| 0 | 0.00 | 0.00 | 0.00 |
| 807 | 20.87 | 20.33 | 11.66 |
| 59 | 0.00 | 0.00 | 0.00 |
| 306 | 20.72 | 20.19 | 11.58 |
| 31 | 0.00 | 0.00 | 0.00 |
| 164 | 20.39 | 19.86 | 11.39 |
| 799 | 0.00 | 0.00 | 0.00 |
| 317 | 12.52 | 12.20 | 6.99 |
| 48 | 0.00 | 0.00 | 0.00 |
| 348 | 9.94 | 9.68 | 5.55 |

Source: Reference 15.

**Table 20. Irradiation histories for the measured ADD2974 samples**

| Days | Power (MW/MTU) | | |
|---|---|---|---|
| | Cut U | Cut J | Cut B |
| 0 | 0.00 | 0.00 | 0.00 |
| 807 | 19.08 | 17.97 | 10.97 |
| 59 | 0.00 | 0.00 | 0.00 |
| 306 | 18.95 | 17.84 | 10.89 |
| 31 | 0.00 | 0.00 | 0.00 |
| 164 | 18.64 | 17.56 | 10.72 |
| 799 | 0.00 | 0.00 | 0.00 |
| 317 | 11.45 | 10.78 | 6.58 |
| 48 | 0.00 | 0.00 | 0.00 |
| 348 | 9.09 | 8.56 | 5.22 |

Source: Reference 15.

Because no void fraction information was reported for the measured samples, the moderator densities for each sample were calculated using the void profile fit model developed in Appendix A. The thermal hydraulic parameters for the void calculations were obtained from publicly available power plant directories.[21,22,23] For validation, the void fraction profile was also calculated using the semiempirical power trend model, and the results are compared in Fig. 14. As seen in the figure, there is a 5% to 10% difference between the models caused by a deficiency of the power trend model to predict the void fractions for fuel assemblies operating below or above the core average power. Fuel assembly CZ346 power is below the core average value; therefore, the power trend model overpredicts the void fraction. When core average power is used, both models agree well, as seen in Fig. 15. The void fraction values used for modeling the samples were calculated from the profile fit model and are listed in Table 21.

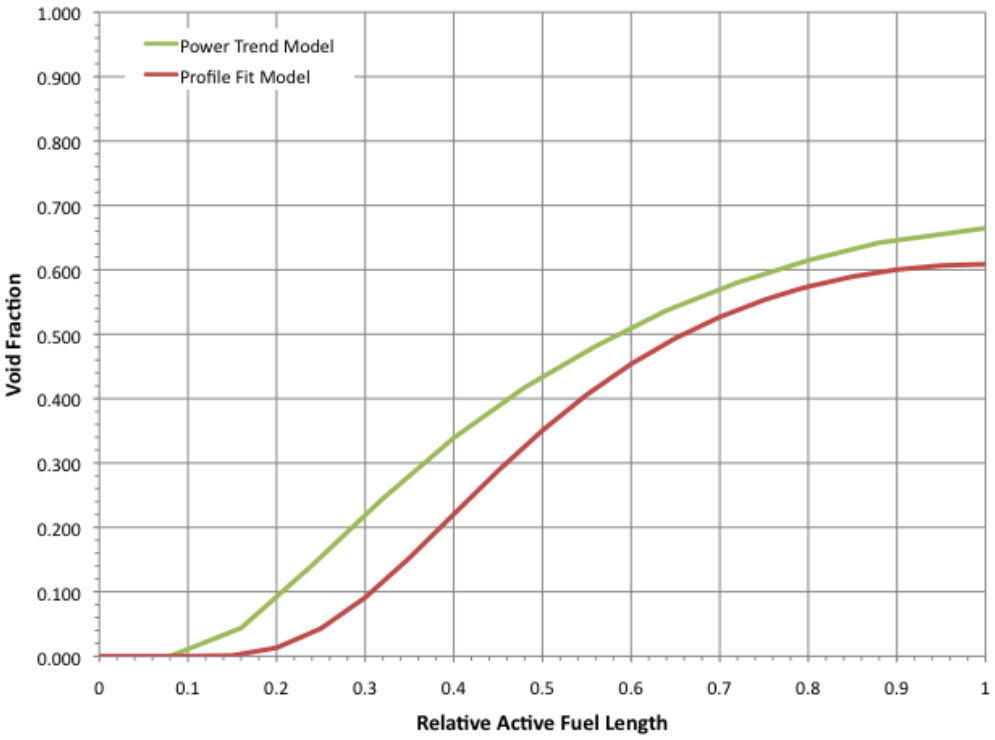


**Fig. 14. Void profile comparisons for fuel assembly CZ346.** Source: Cooper Void Calculation_Version2.xlsx.

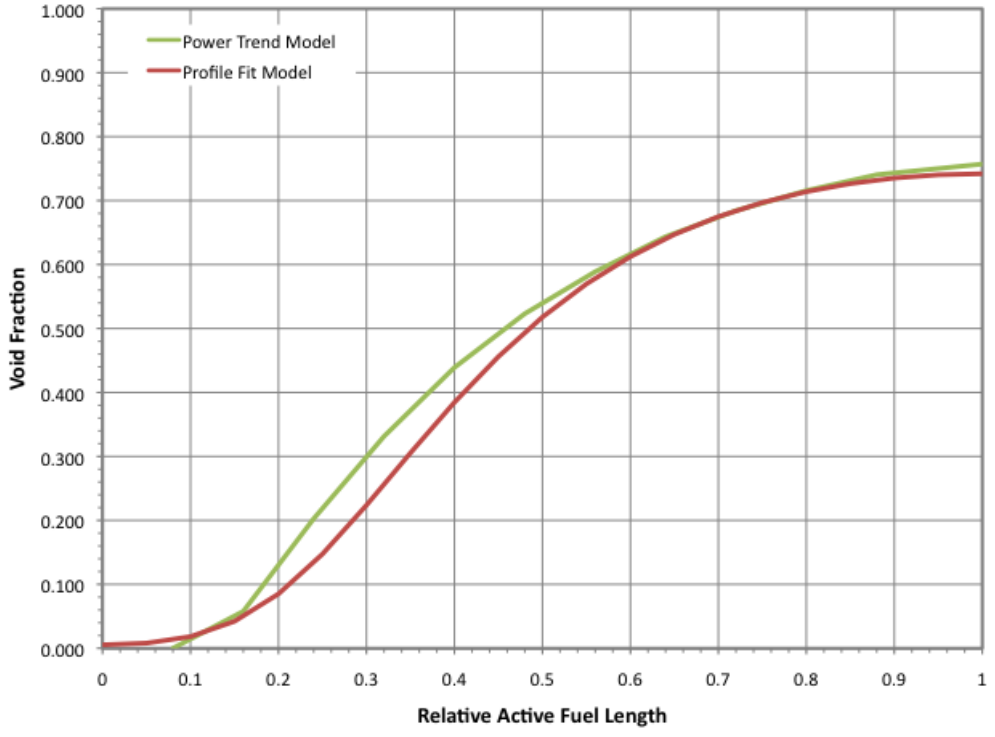


**Fig. 15. Void profile comparisons for an average power Cooper fuel assembly.** Source: Cooper Void Calculation_average_channelV1.xlsx.

**Table 21. Calculated void fractions and moderator densities for Cooper samples**

| Bundle | Sample | Void fraction % | Density ($kg/m^3$) |
|---|---|---|---|
| ADD2966 | Cut T | 12.5 | 652 |
| ADD2966 | Cut K | 32.8 | 509 |
| ADD2966 | Cut B | 59.6 | 320 |
| ADD2974 | Cut U | 6.6 | 693 |
| ADD2974 | Cut J | 55.6 | 349 |
| ADD2974 | Cut B | 59.6 | 320 |

Source: Cooper Void Calculation_Version2.xlsx.

## 5.3 GUNDREMMINGEN-A

The reactor core operating parameters and physical dimensions and characteristics of the fuel assemblies and the fuel rods for the Gundremmingen-A reactor are given in Table 22. Most of the design information was obtained from two reports on the spent fuel measurements at the European Commission Joint Research Center.[17,18] A detailed drawing of the fuel assembly is provided in Fig. 16 (Ref. 18). Gundremmingen-A power plant was one of the first commercial BWRs, and like other early versions of BWRs, it used the early designs of burnable poisons, so called poison curtains, in the reactor core. The poison curtains were boron loaded stainless steel plates located along the narrow gap edges.[24]

**Table 22. Gundremmingen-A nuclear power station reactor and assembly parameters**

| Parameter | Data |
|---|---|
| Assembly and reactor data | |
| Nominal thermal power (MW)[21] | 801 |
| Lattice type[17] | 6 × 6 |
| Number of fuel rods[17] | 36 |
| Number of water rods[17] | 0 |
| Active core height (m)[17] | 3.302 |
| Assembly pitch, wide-wide (cm)[18] | 13.098 |
| Assembly pitch, narrow-narrow (cm)[24] | 12.303 |
| Coolant mass flow (ton/h)[21] | 12300 |
| Fuel rod data | |
| Fuel material[17] | $UO_2$ |
| Fresh fuel pellet density ($g/cm^3$)[17] | 10.5 |
| Smeared fuel pellet density (g/cm)[a] | 10.07 |
| Fuel pellet diameter (cm)[17] | 1.224 |
| Rod pitch (cm)[18] | 1.78 |
| Fuel temperature (K)[17] | 923 |
| Clad material[17] | Zircaloy-2 |
| Pellet-cladding gap (cm)[17] | 0.01375 |
| Clad thickness (cm)[17] | 0.0889 |
| Clad inner diameter (cm)[17] | 1.25 |

**Table 22 (continued)**

| Moderator data | |
|---|---|
| Nominal pressure (bar)[17] | 69 |
| Nominal outlet temperature (K)[17] | 559 |
| **Parameter** | **Data** |
| Channel box data | |
| Channel box outside width (cm)[17] | 11.352 |
| Channel box thickness (cm)[18] | 0.15 |
| Channel box material[17] | Zircolay-4 |

[a]Based on clad inner diameter.

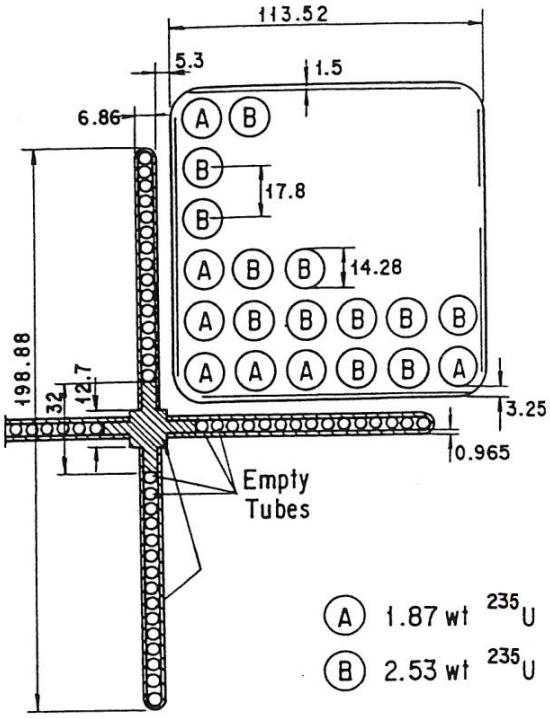


**Fig. 16. Gundremmingen-A fuel assembly.**
Source: Reference 17.

The two major reports on the Gundremmingen-A measurements do not provide information regarding the poison curtains and the narrow assembly gap distance. A drawing of the Gundremmingen-A reactor core was obtained from a BWR patent[24] from 1975. Using the control blade pitch in the figure, the narrow gap distance was calculated as 0.475 cm.

The assembly configuration and the analyzed fuel rods are shown in Fig. 17. Section 7.3 provides a detailed description of the sampled versus modeled fuel rods. The irradiation histories of the samples are presented in Tables 23 and 24, which were calculated from Eq. (5.1) using the reported assembly average burnup values.[17,18]

The nominal mass flow rate and reactor power were obtained from directories of nuclear reactors.[21] Gundremmingen reports point out that the average void fraction at the sample elevation was 50%. Therefore, no void fraction calculations were performed, and a 50% void fraction was used to calculate the moderator density for the samples cut at 268 cm. Saturated water density was used for the remaining two samples, which were cut at 44 cm. The calculated densities are presented in Table 25.

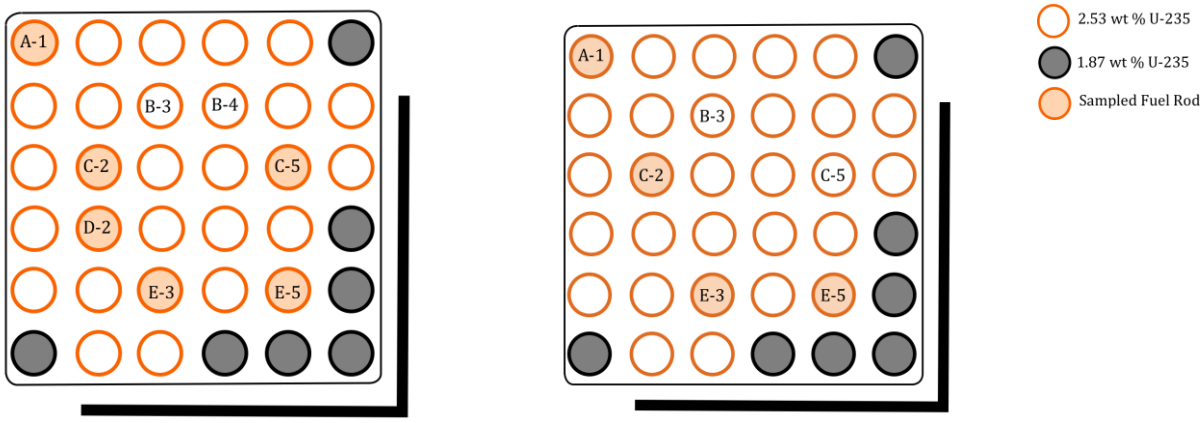


**Fig. 17. Radial loading diagram of B23 and C16 assemblies.** Source: Reference 17.

**Table 23. Irradiation histories of the Gundremmingen-A B23 samples**

| Cycle length days | Shutdown (days) | Power (MW/MTU) | | | | | | |
|---|---|---|---|---|---|---|---|---|
| | | B23 | | | | | | |
| | | A1-1 | A1-2 | B3 | E3 | B4 | C5 | E5 |
| 279 | 56 | 23.798 | 25.343 | 19.645 | 21.745 | 20.626 | 21.273 | 23.299 |
| 323 | 33 | 21.584 | 22.985 | 17.818 | 19.722 | 18.707 | 19.294 | 21.131 |
| 290 | 61 | 21.500 | 22.895 | 17.748 | 19.645 | 18.634 | 19.219 | 21.049 |
| 309 | 0 | 19.041 | 20.276 | 15.718 | 17.398 | 16.502 | 17.020 | 18.641 |

Source: Reference 17 and Gundremmingen_B23_data_V4.xlsx.

**Table 24. Irradiation histories of the Gundremmingen-A C16 samples**

| Cycle length days | Shutdown (days) | Power (MW/MTU) | | | | |
|---|---|---|---|---|---|---|
| | | C16 | | | | |
| | | A1-1 | A1-2 | B3 | C5 | E5 |
| 279 | 56 | 23.798 | 25.343 | 19.645 | - | - |
| 323 | 33 | 21.584 | 22.985 | 17.818 | 17.122 | 18.905 |
| 290 | 61 | 21.500 | 22.895 | 17.748 | 16.267 | 16.442 |
| 309 | 0 | 19.041 | 20.276 | 15.718 | 18.099 | 19.984 |

Source: Reference 17 and Gundremmingen_C16_data_V5.xlsx.

**Table 25. Calculated moderator densities for Gundremmingen-A samples**

| Bundle | Sample | Void fraction % | Density ($kg/m^3$) |
|---|---|---|---|
| B23 | A1-1 | 0.0 | 740 |
| B23 | A1-2 | 50.0 | 388 |
| B23 | B3 | 50.0 | 388 |
| B23 | C5 | 50.0 | 388 |
| B23 | E5 | 50.0 | 388 |
| C16 | A1-1 | 0.0 | 740 |
| C16 | A1-2 | 50.0 | 388 |
| C16 | B3 | 50.0 | 388 |
| C16 | C5 | 50.0 | 388 |
| C16 | E5 | 50.0 | 388 |

Source: Gundremmingen_Void_Calculation_B23.xlsx, Gundremmingen_Void_Calculation_C16.xlsx.

# 6. COMPUTATIONAL MODELING AND METHODOLOGY

## 6.1 CODES AND NUCLEAR DATA

Computational analysis of the spent fuel isotopic composition was carried out using the T_DEPL 2-D depletion sequence in version 5.1 of the SCALE computer code system, released publicly in 2006.

### 6.1.1 TRITON/NEWT

The T-DEPL sequence of TRITON[1] couples the 2-D arbitrary polygonal mesh transport code NEWT[1] with the point depletion and decay code ORIGEN-S[1] to perform burnup simulations. At each depletion step, the neutron transport flux solution from NEWT is used to generate cross sections for the ORIGEN-S calculation; the isotopic composition data resulting from each isotopic depletion step are used in the subsequent transport calculation to obtain updated cross sections for the next depletion step in an iterative manner throughout the irradiation history.

NEWT is a 2-D discrete ordinates ($S_N$) multigroup transport code that uses an Extended Step Characteristics method solver. This method allows cells to be defined in the form of arbitrary polygons and has an automatic fine grid generation feature. The SN method in NEWT allows arbitrary-order angular scattering ($P_N$ approximation) and arbitrary quadrature order. NEWT has a coarse-mesh finite difference accelerator that uses a low order solution for homogenized cells in a coarse spatial grid to substantially reduce the number of iterations needed for flux and eigenvalue convergence.

TRITON can simulate the depletion of multiple mixtures and regions in a fuel assembly model. This is a powerful feature for nuclide inventory analysis of measured fuel rods as it allows an accurate representation of the local flux distribution and environmental effects on a specific fuel rod in the assembly.

### 6.1.2 Cross-Section Libraries

Neutron transport calculations were performed using the SCALE 44-group cross-section library that contains 22 thermal upscatter groups. The 44-group library is collapsed from the ENDF/B-V SCALE 238-group library using light water reactor (LWR) fuel flux spectrum from a fuel cell spectrum in a 17 × 17 assembly.

### 6.1.3 Resonance Processing

The NITAWL[1] module, which is based on the Nordheim Integral Treatment, was used in this study for self-shielding of the resolved resonance cross sections. Selection of the NITAWL module was based on its demonstrated performance for LWR fuel analyses. NITAWL, however, cannot be used with the ENDF/B–VI and –VII cross-section libraries, and it does not allow fuel rod subdivision (i.e., fuel rods must be treated as a single region with one radial zone).

### 6.1.4 Isotopic Depletion Calculations

Isotope transmutation and decay calculations were performed with the ORIGEN-S code. Cross sections used in the ORIGEN-S calculations are generated automatically during the TRITON depletion analysis using region- and time-dependent cross sections calculated by NEWT. Burnup-dependent cross sections for 232 isotopes defined in the 44-group library are generated by the transport calculation solution (addnux = 3-input option). This procedure ensures that cross sections are updated for many of the key isotopes of interest to spent fuel safety applications and their capture and/or decay precursors.

## 6.2 MODELING ASSUMPTIONS

The SCALE depletion simulation models in this report include several assumptions due to missing operation and design data of the benchmark samples.

### 6.2.1 General Assumptions

The general assumptions that apply to all models are as follows.

a. The samples are assumed to be located away from any control blades or the bundle is exposed to the control blade early in cycle such that the control blade effect on the isotopic content is negligible. It is very likely that some of the samples are actually exposed to control blades during their lifetimes. However, the control blade histories are not available for any samples in this report.

b. In-channel radial void fraction distribution data are not available. Therefore it is assumed that the in-channel radial void fraction is uniform across the sample axial node. Although high or low power fuel rods will exhibit gradients from the average, this approximation is necessary in lieu of detailed pin power data.

c. It is assumed that the void fraction is constant with burnup. The basis for this assumption is that the void history is averaged over irradiation time and normalized to the sample measured burnup. During reactor operations local assembly conditions can change over time, but the average effects are being modeled. Uncertainties from this modeling approximation are inherent in the methodology and will be propagated as a bias to the results.

d. It is assumed that the sample characteristics are uniform across the assembly axial node, and that there was no significant power tilt across the bundle. The basis for this assumption is that assemblies are typically relocated within the reactor core between cycles to minimize the effects of radial flux variations which can occur due to leakage at the core periphery, due to reactivity control components, and the neutronic effects of surrounding assemblies. The uncertainty associated with this assumption is greater for lower burnup assemblies.

e. The clad temperature is set to be equal to the moderator temperature. In normal reactor operations, the clad temperature is at a temperature between the fuel pin outside temperature and the coolant temperature. However, the sensitivity of the clad neutron absorption to the clad temperature is negligible.

f. The fuel pellet radius is assumed to be equal to the clad inner diameter. The basis for this assumption is that the external operating pressure is always greater than the fuel pin internal pressure.

g. The fuel temperature is assumed to be uniform across the fuel assembly and constant over the irradiation of the assembly. The basis for this assumption is that the effect of fuel temperature history on fuel isotopics diminishes over long assembly exposures. A study by JAERI[8] also shows that this assumption is valid for modeling fuel isotopics.

h. It is assumed that representing the fuel channel as a square has a negligible impact on the results. The basis for this assumption is that although the fuel channel corners are round and that can affect the moderation and reflection around the corner pins, this is a geometrical approximation and an inherent modeling bias only on the corner fuel pins.

### 6.2.2 Initial Uranium Isotopic Content

Uranium isotopes $^{234}U$ and $^{236}U$ are usually measured in burnt fuel, but their concentration in fresh fuel is not usually available. $^{234}U$ depletes through neutron capture to form additional $^{235}U$ and is a long-lived isotope unaffected by reactor downtime and discharge from the reactor. Over long periods of time, minute quantities of $^{234}U$ are produced through alpha emissions in $^{238}Pu$ ($T_{1/2}$ = 87.7 years). $^{236}U$ is a

long-lived isotope that depletes through neutron capture to form additional $^{237}U$. However, the $^{236}U$ thermal capture cross section is small compared to that of $^{235}U$. As a result, more $^{236}U$ is produced than is lost during reactor operation.

The fresh fuel uranium isotopic concentrations are assumed to have the dependence on *X* weight percent of $^{235}U$ enrichment shown in Table 15 (Ref. 25). The isotopic ratio factors shown in the table were derived from mass spectrometric analyses of initial fuel for the Yankee Reactor Core V. Therefore, it is assumed that the isotopic ratio factors are applicable to all fresh $UO_2$.

### 6.3 SCALE MODELS

Analysis of the fuel samples was carried out by developing individual models for each of the considered samples. Each SCALE input model was prepared by using the geometry, material, and burnup data listed in Tables 10 through 14 and 16 through 25. Because no information regarding the adjacent fuel assemblies is provided in any of the publicly available reports, each modeled fuel assembly was assumed to be surrounded by identical fuel assemblies. In modeling fuel pins, a separate mixture number was used for pins with different uranium enrichments. Furthermore, sampled fuel pins were assigned a different mixture number regardless of their enrichments. This approach allows the pin powers to be normalized to the sample pin power so that the input power history produces the targeted depletion for each sample.

The enrichment distribution and the sample locations were taken from the assembly diagrams in Sect. 5. For consistency with a previous isotopic validation report on Gundremmingen measurements,[15] the sample locations were modeled at the symmetric positions with respect to the diagonal axis (e.g., C-2 and D-2 samples are modeled at B-3 and B-4 locations, respectively, in Fig. 17). Because the fuel assembly enrichment distribution and the geometry are diagonally symmetric, this modeling approach is accurate. The geometrical and material layouts of the SCALE models for the sampled fuel assemblies are plotted in Fig. 18 through Fig. 20. Detailed SCALE input file samples for each reactor are included in Appendix C.

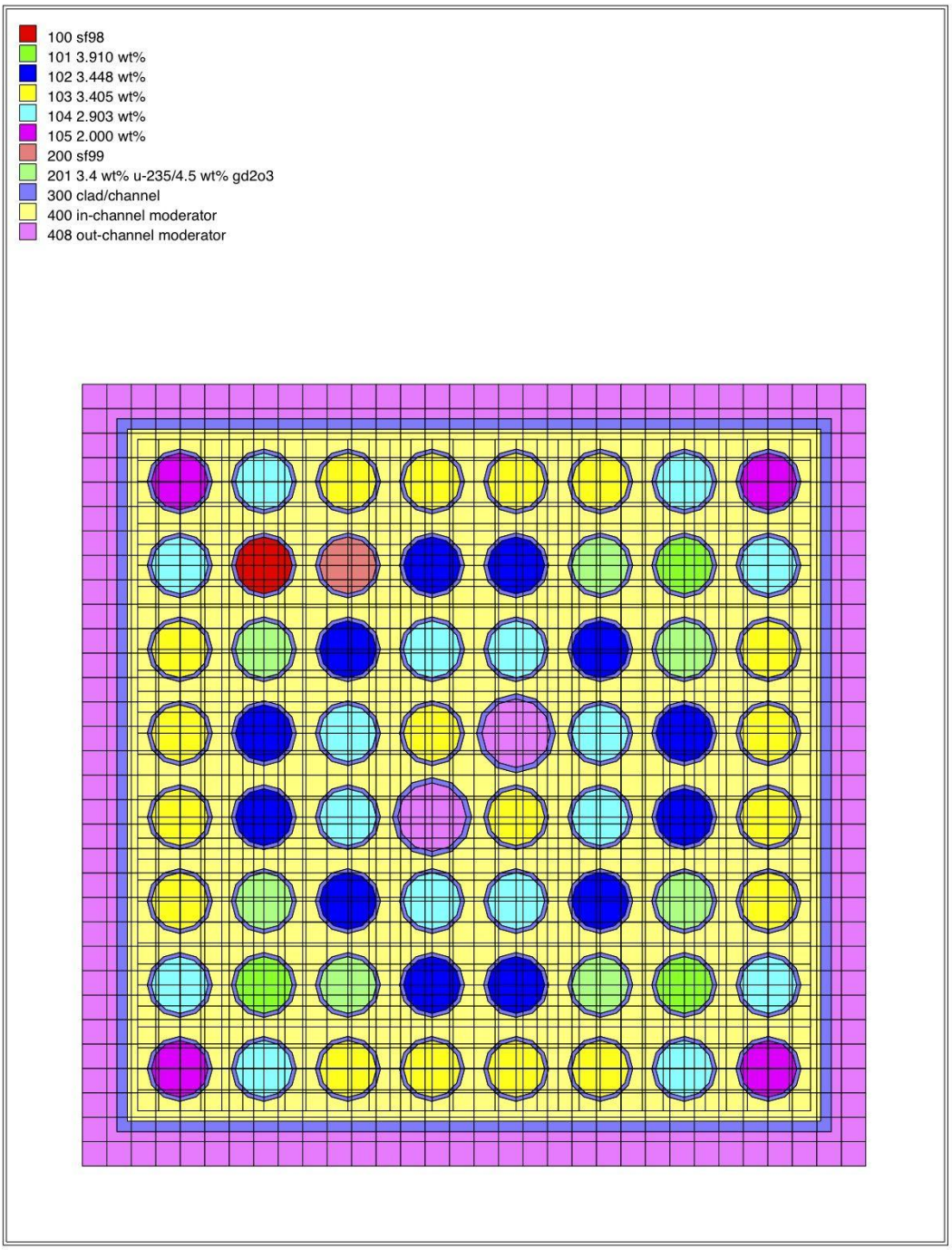


**Fig. 18. Geometrical model of Fukushima Daini-2 8 × 8 BWR fuel assembly.**

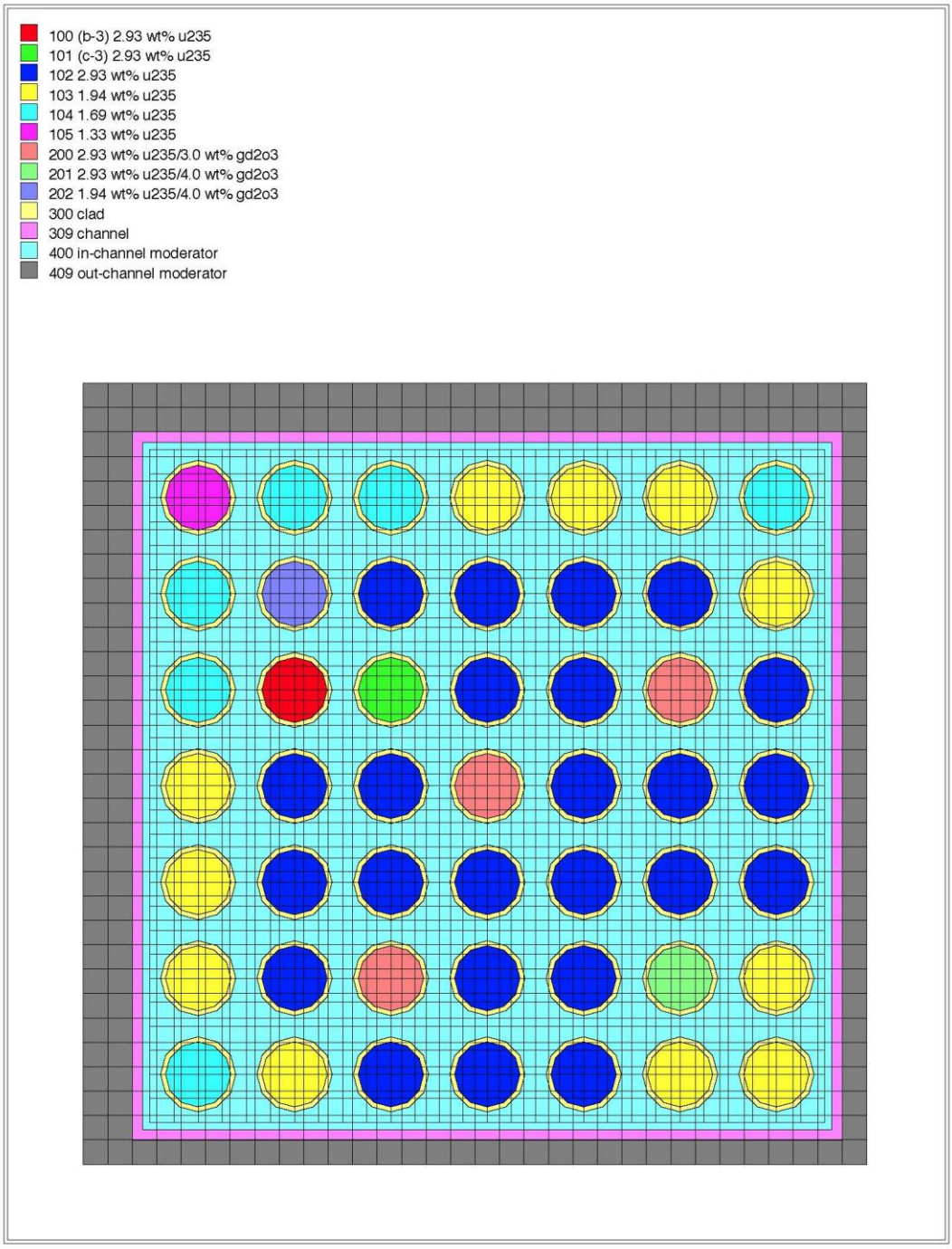


**Fig. 19. Geometrical model of Cooper 7 × 7 BWR fuel assembly.**

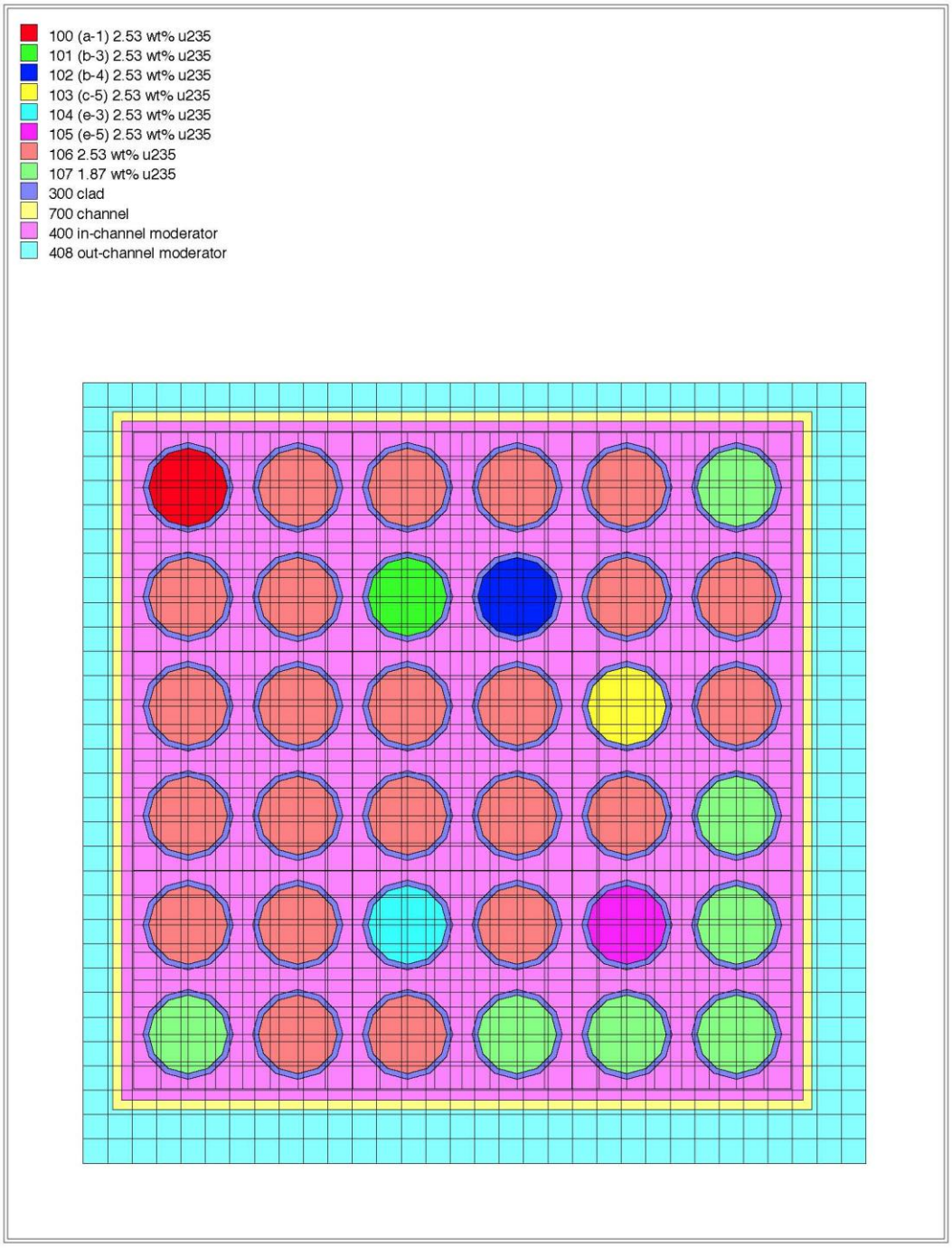


**Fig. 20. Geometrical model of Gundremmingen-A 6 × 6 BWR fuel assembly.**

# 7. RESULTS AND DISCUSSIONS

## 7.1 FUKUSHIMA DAINI Unit 2

The isotopic concentrations of the SF98 and SF99 samples were calculated using fuel assembly depletion simulations. Tables 26 and 27 present the ratios of the calculated isotopic concentrations to the measured isotopic concentrations (C/Es), and the results are plotted for actinides and FPs in Fig. 21 through Fig. 24. SF98-1, SF98-2, SF99-1, and SF99-10 samples were not modeled because these samples were taken either from the natural blanket region (from 0 to about 155 mm)[19] or very close to the blanket region at the bottom and top of the two fuel rods. Because of the large flux gradient in that region, a 2-D model is not valid and a detailed three-dimensional assembly model would be required to capture the different spectral effects.

Tables 26 and 27 show the excellent agreement between the calculated and the measured isotopic concentrations for the uranium and the plutonium isotopes. The $^{242}$Cm, $^{243}$Cm, $^{245}$Cm, $^{246}$Cm, $^{243}$Am, $^{106}$Ru, $^{147}$Sm, $^{148}$Sm, $^{149}$Sm, $^{150}$Sm, $^{152}$Sm, and$^{154}$Sm isotopes show larger differences compared with the other isotopic ratios. Although, measurement uncertainties are as large as 10% for some of the isotopes, these uncertainties still cannot explain the large discrepancies in the results as seen in Fig. 25 and Fig. 26. Similar underpredictions and overpredictions of the mentioned isotopes were also observed in other benchmark studies.[19] The large discrepancies between the measured and the calculated concentrations could be to the result of the suspected uncertainties in the nuclear data or more systematic errors like solubility of isotopes in the measured solution as in case of $^{106}$Ru. The $^{125}$Sb and $^{247}$Cm isotopes were omitted in comparisons because no measurement data were available for most of the samples.

The SF99 results in Table 27 show slightly larger C/E ratios for uranium and plutonium isotopes. SF98 and SF99 are adjacent to each other, and the main difference between the two fuel rods is SF99 contains gadolinium poison and slightly lower $^{235}$U enrichment compared to the SF98 fuel rod. As a common practice in deterministic lattice physics, the gadolinium loaded fuel rods are modeled differently than the other fuel pins because of the strong shelf shielding effects of gadolinium. The single region fuel rod model fails to capture the strong gradient in the neutron flux inside a gadolinium fuel rod, resulting in depletion of the gadolinium content at an excessive rate. One of the solutions to this problem is to increase the spatial resolution of the fuel rod by modeling the gadolinium fuel pin as a set of equal volume concentric rings. Because gadolinium is depleted early in the cycle and the fuel samples analyzed in this study were irradiated for more than three cycles, gadolinium depletion effects were assumed to be negligible, and the SF99 rod model was similar to the SF98 rod. However, to justify this assumption, sample SF99-4 was also modeled with concentric rings. As mentioned in Sect. 6.1.3, the NITAWL cross-section processing module was used for the fuel assembly depletion simulations in this report. Unfortunately, the NITAWL module is not capable of modeling concentric fuel rings. Therefore a more sophisticated cross-section processing module in the SCALE package, CENTRM,[1] was used for this special fuel pin model. The fuel lattice geometry and the SF99-4 fuel rings are shown in Fig. 27.

To separate the effect of using a different cross-section module and the effect of modeling the fuel in rings, a solid SF99-4 fuel pin simulation was also run using the CENTRM module. The results are presented in Fig. 28. As expected, the fuel rings model does not change the isotopics significantly after long depletion periods. However, there is a small reduction in the overestimated calculated $^{235}$U, Pu, and Am isotopic concentrations.

**Table 26. Calculated-to-measured isotopic inventory ratios for SF98 samples**

| Nuclide | C/E | | | | | | | |
|---|---|---|---|---|---|---|---|---|
| | SF98-3 | SF98-4 | SF98-5 | SF98-6 | SF98-7 | SF98-8 | Average | Standard deviation |
| $^{234}$U | 1.012 | 1.007 | 1.000 | 1.076 | 1.010 | 1.024 | 1.02 | 0.03 |
| $^{235}$U | 1.005 | 1.003 | 0.960 | 0.948 | 1.005 | 1.014 | 0.99 | 0.03 |
| $^{236}$U | 1.001 | 0.999 | 1.003 | 0.998 | 0.994 | 0.980 | 1.00 | 0.01 |
| $^{238}$U | 0.999 | 0.999 | 1.000 | 1.000 | 1.000 | 0.997 | 1.00 | 0.00 |
| $^{237}$Np | 1.082 | 1.022 | 1.287 | 0.944 | 1.111 | 1.106 | 1.09 | 0.11 |
| $^{238}$Pu | 0.950 | 0.933 | 0.985 | 1.068 | 0.937 | 0.911 | 0.96 | 0.06 |
| $^{239}$Pu | 1.003 | 0.996 | 0.991 | 0.940 | 0.989 | 1.006 | 0.99 | 0.02 |
| $^{240}$Pu | 1.013 | 0.991 | 0.991 | 0.963 | 0.978 | 0.998 | 0.99 | 0.02 |
| $^{241}$Pu | 0.996 | 0.989 | 0.991 | 0.953 | 0.972 | 0.984 | 0.98 | 0.02 |
| $^{242}$Pu | 1.018 | 1.003 | 1.040 | 1.049 | 0.995 | 1.008 | 1.02 | 0.02 |
| $^{241}$Am | 0.936 | 0.915 | 0.955 | 1.044 | 1.068 | 1.144 | 1.01 | 0.09 |
| $^{242m}$ Am | 1.025 | 1.003 | 1.002 | 0.971 | 1.085 | 1.093 | 1.03 | 0.05 |
| $^{243}$Am | 1.152 | 1.136 | 1.246 | 1.142 | 1.186 | 1.204 | 1.18 | 0.04 |
| $^{242}$Cm | 0.663 | 0.658 | 0.492 | 0.265 | 0.555 | 0.651 | 0.55 | 0.15 |
| $^{243}$Cm | 0.770 | 0.891 | 0.972 | 0.831 | 0.816 | 0.778 | 0.84 | 0.08 |
| $^{244}$Cm | 1.013 | 1.004 | 1.023 | 0.921 | 0.950 | 0.953 | 0.98 | 0.04 |
| $^{245}$Cm | 0.765 | 0.765 | 0.734 | 0.601 | 0.658 | 0.669 | 0.70 | 0.07 |
| $^{246}$Cm | 0.634 | 0.646 | 0.637 | 0.553 | 0.597 | 0.917 | 0.66 | 0.13 |
| $^{143}$Nd | 1.017 | 1.026 | 1.005 | 0.996 | 1.012 | 1.014 | 1.01 | 0.01 |
| $^{144}$Nd | 0.985 | 1.003 | 1.034 | 1.009 | 1.031 | 1.058 | 1.02 | 0.03 |
| $^{145}$Nd | 1.027 | 1.031 | 1.022 | 1.025 | 1.019 | 1.022 | 1.02 | 0.00 |
| $^{146}$Nd | 1.026 | 1.023 | 1.021 | 1.015 | 1.016 | 1.019 | 1.02 | 0.00 |
| $^{148}$Nd | 1.013 | 1.009 | 1.007 | 1.007 | 1.005 | 1.011 | 1.01 | 0.00 |
| $^{150}$Nd | 1.026 | 1.018 | 1.022 | 1.013 | 1.013 | 1.015 | 1.02 | 0.01 |
| $^{137}$Cs | 1.021 | 0.986 | 1.015 | 0.970 | 0.925 | 1.047 | 0.99 | 0.04 |
| $^{134}$Cs | 1.000 | 0.971 | 0.984 | 0.875 | 0.829 | 0.951 | 0.94 | 0.07 |
| $^{154}$Eu | 0.973 | 0.949 | 1.031 | 0.902 | 0.980 | 0.897 | 0.96 | 0.05 |
| $^{144}$Ce | 1.131 | 1.070 | 0.946 | 1.011 | 0.924 | 0.879 | 0.99 | 0.09 |
| $^{106}$Ru | 1.245 | 1.400 | 1.417 | 1.474 | 1.249 | 1.224 | 1.33 | 0.11 |
| $^{147}$Sm | 0.877 | 0.866 | 0.919 | 0.920 | 0.909 | 0.884 | 0.90 | 0.02 |
| $^{148}$Sm | 0.844 | 0.825 | 0.873 | 0.859 | 0.871 | 0.874 | 0.86 | 0.02 |
| $^{149}$Sm | 1.109 | 1.251 | 0.929 | 1.076 | 0.897 | 0.790 | 1.01 | 0.17 |
| $^{150}$Sm | 0.964 | 0.973 | 1.041 | 1.003 | 0.995 | 0.943 | 0.99 | 0.03 |
| $^{151}$Sm | 1.161 | 1.183 | 1.267 | 1.175 | 1.276 | 1.192 | 1.21 | 0.05 |
| $^{152}$Sm | 1.066 | 1.095 | 1.203 | 1.248 | 1.222 | 1.096 | 1.16 | 0.08 |
| $^{154}$Sm | 0.897 | 0.898 | 0.948 | 0.948 | 0.925 | 0.860 | 0.91 | 0.03 |

Source: FukushimaDaini2 SF98 Validation Results-V6.xlsx.

**Table 27. Calculated-to-measured isotopic inventory ratios for SF99 samples**

| Nuclide | C/E | | | | | | | | | |
|---|---|---|---|---|---|---|---|---|---|---|
| | SF99-2 | SF99-3 | SF99-4 | SF99-5 | SF99-6 | SF99-7 | SF99-8 | SF99-9 | Average | Standard deviation |
| $^{234}$U | 1.093 | 1.055 | 1.069 | 1.060 | 1.090 | 1.080 | 1.082 | 1.040 | 1.070 | 0.02 |
| $^{235}$U | 1.057 | 1.051 | 1.122 | 1.024 | 1.037 | 1.047 | 1.065 | 1.045 | 1.056 | 0.03 |
| $^{236}$U | 0.981 | 1.000 | 0.990 | 1.001 | 0.981 | 0.990 | 0.987 | 0.985 | 0.990 | 0.01 |
| $^{238}$U | 0.999 | 1.000 | 0.999 | 1.000 | 1.001 | 1.000 | 1.013 | 0.999 | 1.001 | 0.00 |
| $^{237}$Np | 0.897 | 0.876 | 0.985 | 0.890 | 0.938 | 0.914 | 0.949 | 0.925 | 0.924 | 0.03 |
| $^{238}$Pu | 1.069 | 0.991 | 1.039 | 1.190 | 0.957 | 1.036 | 1.008 | 1.048 | 1.048 | 0.07 |
| $^{239}$Pu | 1.007 | 1.008 | 1.055 | 0.982 | 0.966 | 0.994 | 1.054 | 1.101 | 1.014 | 0.04 |
| $^{240}$Pu | 1.023 | 1.019 | 1.021 | 0.988 | 0.972 | 0.981 | 1.022 | 1.044 | 1.009 | 0.02 |
| $^{241}$Pu | 0.944 | 0.985 | 1.008 | 0.964 | 0.951 | 0.970 | 1.015 | 1.090 | 0.983 | 0.04 |
| $^{242}$Pu | 0.947 | 0.998 | 0.963 | 0.998 | 1.005 | 0.998 | 1.021 | 1.088 | 0.998 | 0.04 |
| $^{241}$Am | 1.432 | 0.938 | 1.123 | 0.976 | 1.103 | 1.114 | 1.113 | 1.028 | 1.042 | 0.19 |
| $^{242m}$ Am | 1.188 | 1.169 | 1.228 | 1.124 | 1.089 | 1.241 | 1.220 | 1.419 | 1.292 | 0.26 |
| $^{243}$Am | 1.040 | 1.083 | 1.065 | 1.090 | 1.050 | 1.091 | 1.105 | 1.231 | 1.088 | 0.05 |
| $^{242}$Cm | 0.323 | 0.503 | 0.392 | 0.259 | 0.353 | 0.343 | 0.401 | 0.619 | 0.397 | 0.10 |
| $^{243}$Cm | 0.799 | 0.859 | 0.850 | 0.859 | 0.781 | 0.791 | 0.764 | 0.712 | 0.801 | 0.05 |
| $^{244}$Cm | 0.826 | 0.910 | 0.872 | 0.889 | 0.783 | 0.862 | 0.859 | 1.043 | 0.881 | 0.07 |
| $^{245}$Cm | 0.565 | 0.662 | 0.637 | 0.624 | 0.487 | 0.570 | 0.577 | 0.446 | 0.576 | 0.07 |
| $^{246}$Cm | No Data | 0.551 | 0.500 | 0.541 | 0.438 | 0.509 | 0.504 | 0.101 | 0.454 | 0.15 |
| $^{143}$Nd | 1.001 | 0.999 | 1.018 | 0.987 | 0.994 | 0.988 | 1.006 | 0.978 | 0.996 | 0.01 |
| $^{144}$Nd | 0.974 | 0.761 | 0.932 | 1.009 | 1.003 | 1.111 | 1.068 | 0.968 | 0.978 | 0.10 |
| $^{145}$Nd | 1.007 | 1.006 | 1.009 | 1.003 | 1.011 | 0.998 | 1.015 | 0.987 | 1.004 | 0.01 |
| $^{146}$Nd | 0.997 | 0.997 | 0.994 | 0.993 | 0.988 | 0.986 | 1.008 | 0.993 | 0.995 | 0.01 |
| $^{148}$Nd | 0.991 | 0.992 | 0.991 | 0.989 | 0.987 | 0.985 | 1.007 | 0.992 | 0.992 | 0.01 |
| $^{150}$Nd | 0.996 | 1.006 | 1.008 | 1.003 | 0.988 | 0.993 | 1.012 | 1.008 | 1.002 | 0.01 |
| $^{137}$Cs | 0.952 | 0.950 | 0.949 | 0.944 | 0.930 | 0.909 | 0.952 | 0.940 | 0.940 | 0.01 |
| $^{134}$Cs | 0.803 | 0.870 | 0.852 | 0.848 | 0.782 | 0.764 | 0.806 | 0.834 | 0.822 | 0.03 |
| $^{154}$Eu | 0.791 | 0.874 | 0.931 | 0.894 | 0.814 | 0.847 | 0.845 | 0.856 | 0.858 | 0.04 |
| $^{144}$Ce | 0.992 | No Data | 1.087 | 0.858 | 0.908 | 0.670 | 0.801 | 0.943 | 0.894 | 0.12 |
| $^{106}$Ru | 2.147 | 1.526 | 1.814 | 2.256 | 1.898 | 2.645 | 1.755 | 1.024 | 1.880 | 0.46 |
| $^{147}$Sm | No Data | 0.982 | No Data | 0.954 | No Data | 0.956 | 0.961 | 0.955 | 0.960 | 0.01 |
| $^{148}$Sm | No Data | 0.899 | No Data | 0.863 | No Data | 0.885 | 0.920 | 1.000 | 0.915 | 0.05 |
| $^{149}$Sm | No Data | 1.088 | No Data | 1.149 | No Data | 1.019 | 1.043 | 1.078 | 1.074 | 0.05 |
| $^{150}$Sm | No Data | 1.016 | No Data | 1.001 | No Data | 0.982 | 0.977 | 0.987 | 0.993 | 0.01 |
| $^{151}$Sm | No Data | 1.237 | No Data | 1.213 | No Data | 1.250 | 1.257 | 1.309 | 1.249 | 0.03 |
| $^{152}$Sm | No Data | 1.145 | No Data | 1.179 | No Data | 1.223 | 1.152 | 1.091 | 1.156 | 0.04 |
| $^{154}$Sm | No Data | 0.958 | No Data | 0.943 | No Data | 0.948 | 0.952 | 0.967 | 0.952 | 0.01 |

Source: FukushimaDaini2 SF99 Validation Results-V6.xls.

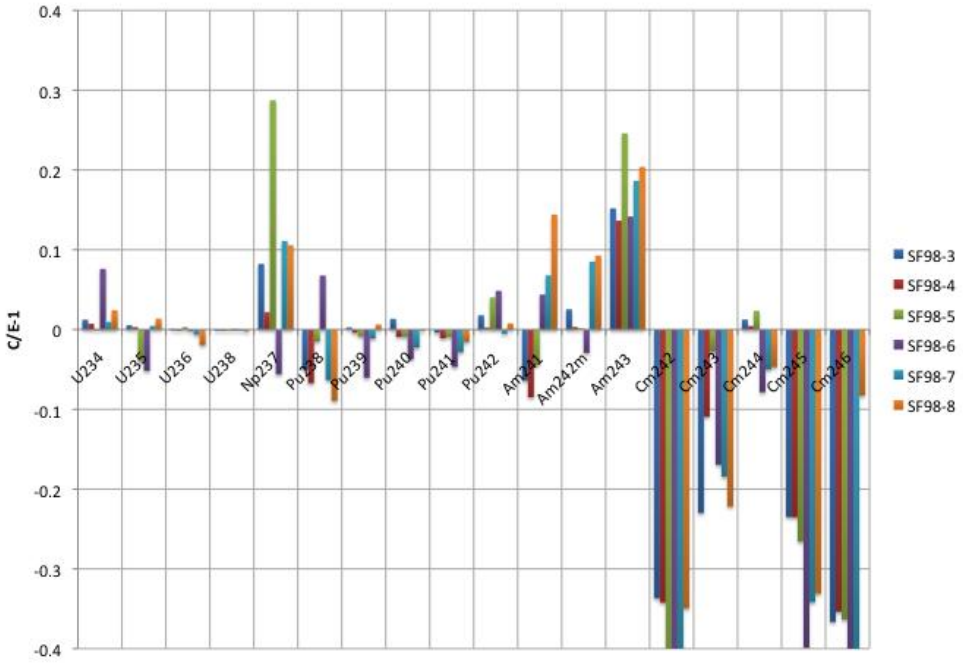


**Fig. 21. Calculated-to-measured actinide concentration ratios for SF98 samples.** Source: FukushimaDaini2 SF98 Validation Results-V6.xlsx.

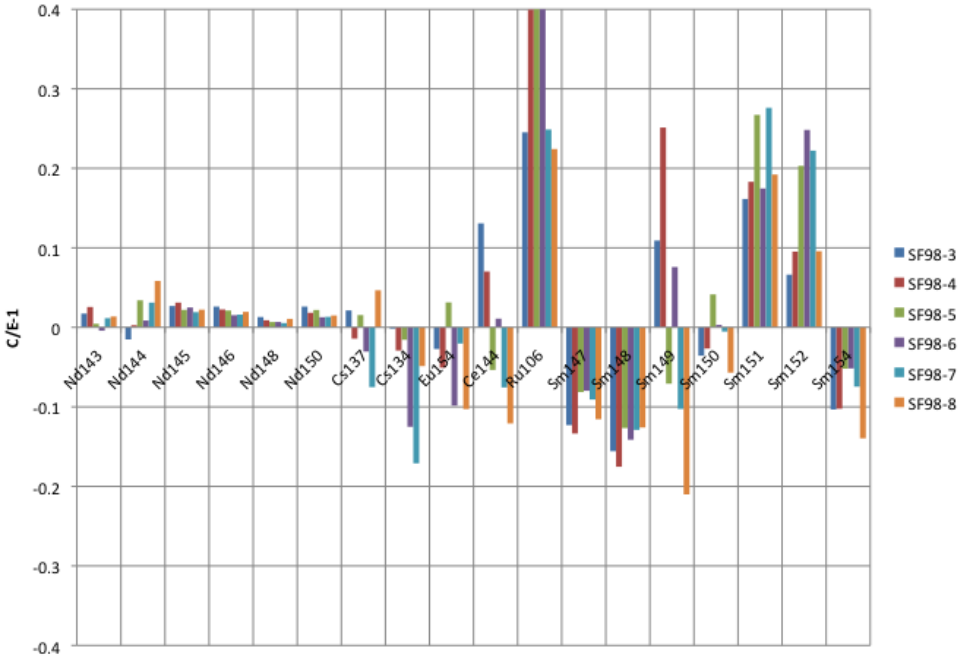


**Fig. 22. Calculated-to-measured fission product concentration ratios for SF98 samples.** Source: FukushimaDaini2 SF98 Validation Results-V6.xlsx.

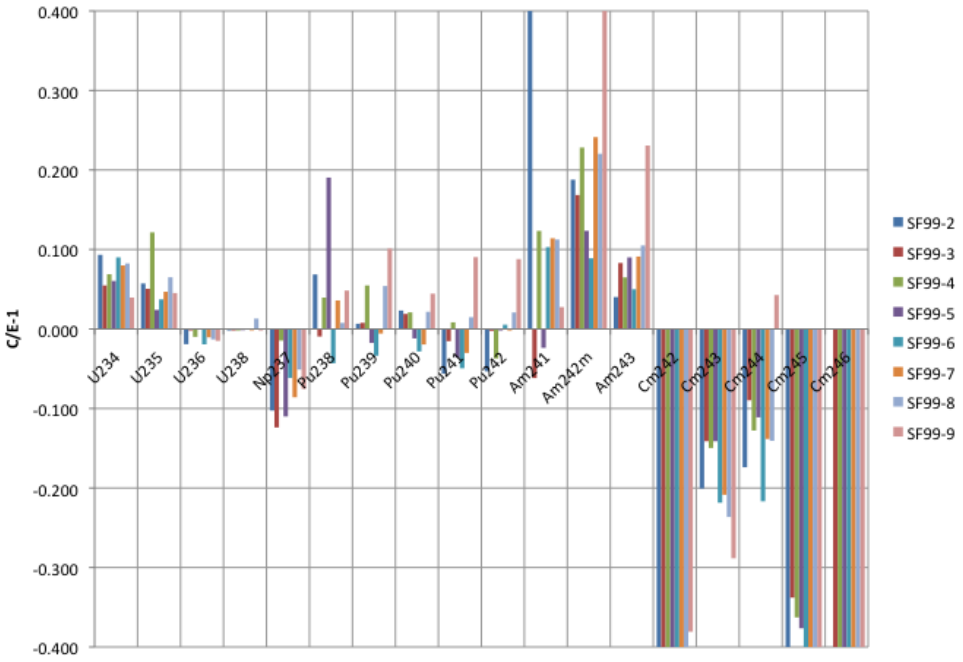


**Fig. 23. Calculated-to-measured actinide concentration ratios for SF99 samples.** Source: FukushimaDaini2 SF99 Validation Results-V6.xls.

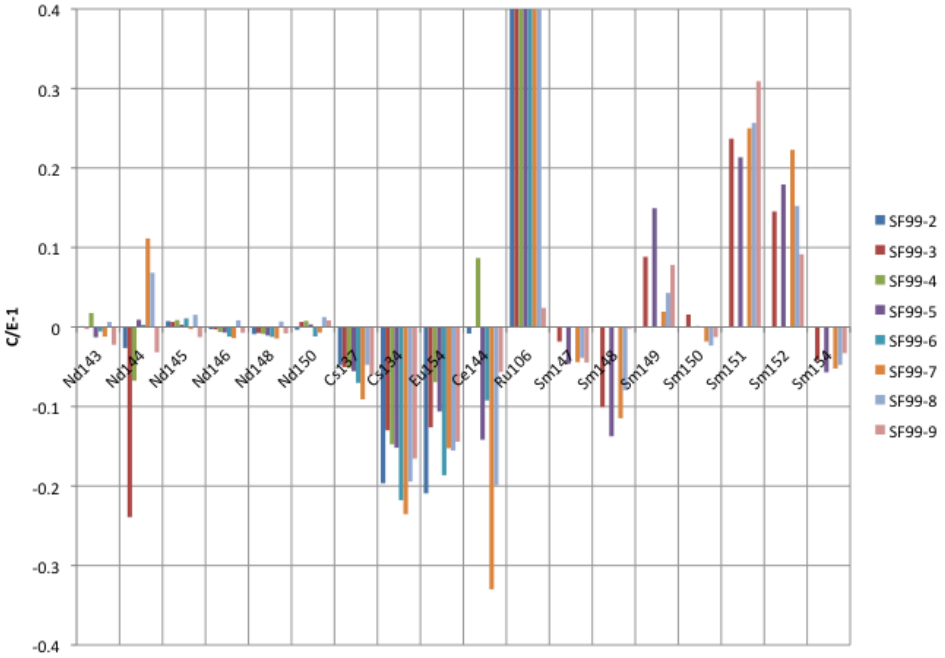


**Fig. 24. Calculated-to-measured fission product concentration ratios for SF99 samples.** Source: FukushimaDaini2 SF99 Validation Results-V6.xls.

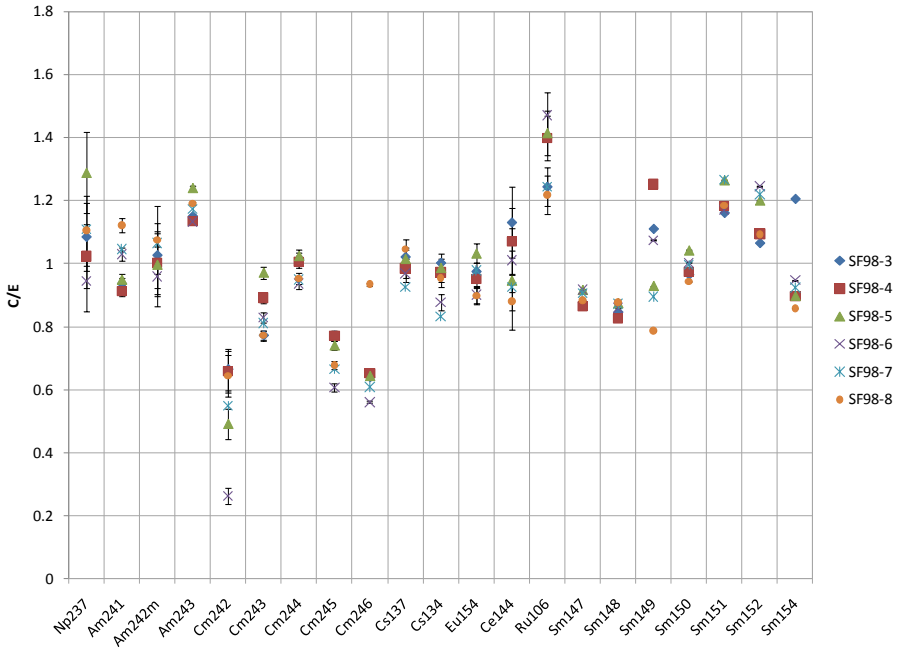


**Fig. 25. Effect of the measurement uncertainties for SF98 samples.**
Source: FukushimaDaini2 SF98 Validation Results-V6.xlsx.

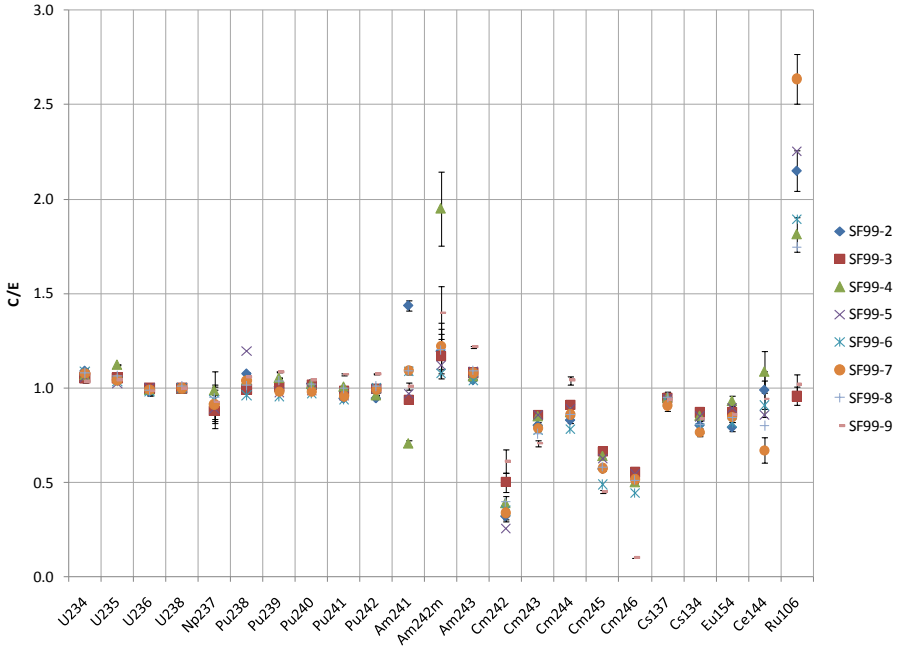


**Fig. 26. Effect of the measurement uncertainties for SF99 samples.**
Source: FukushimaDaini2 SF99 Validation Results-V6.xls.

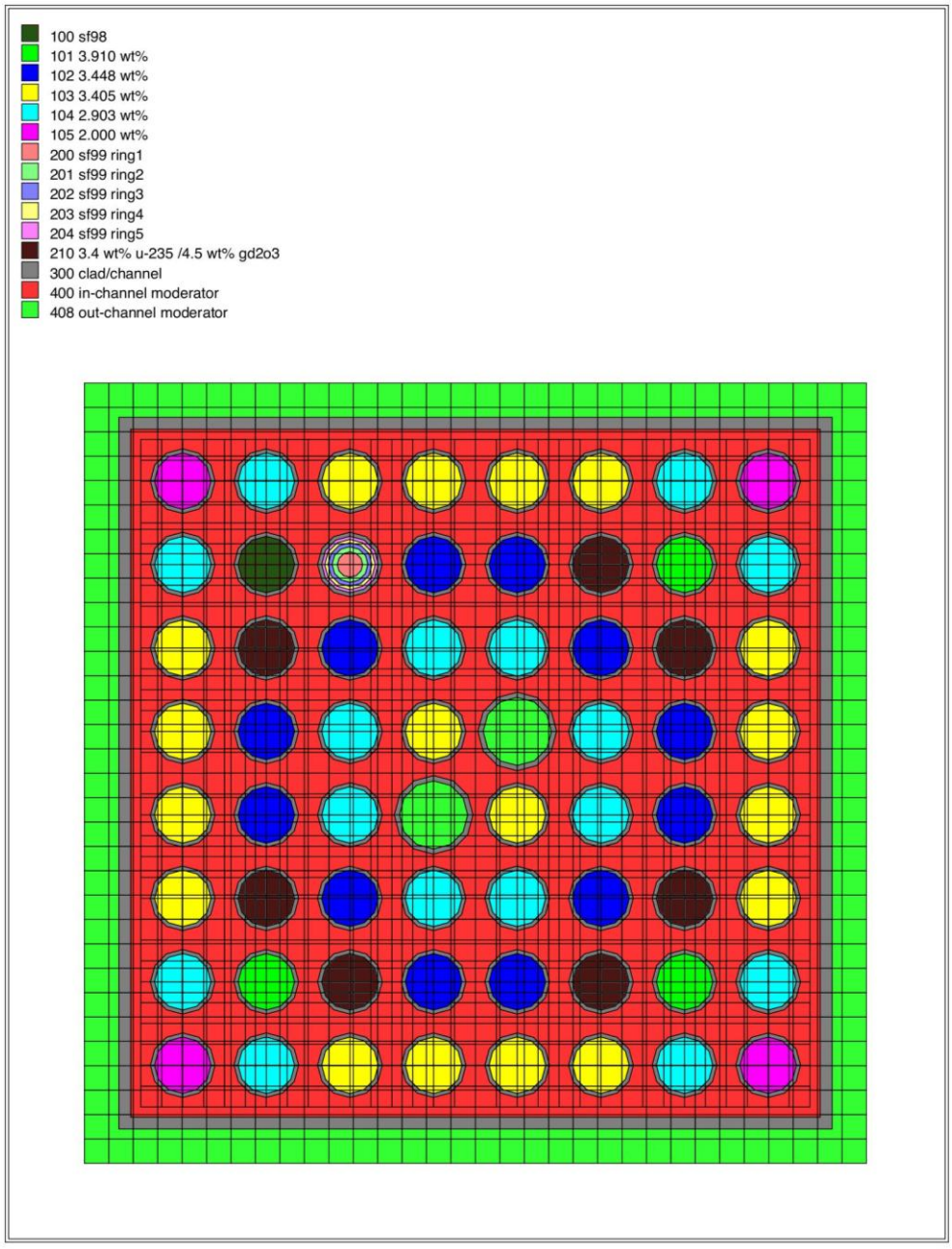


**Fig. 27. Geometrical model of Fukushima Daini-2 8 × 8 BWR fuel assembly with gadolinium rod rings.**

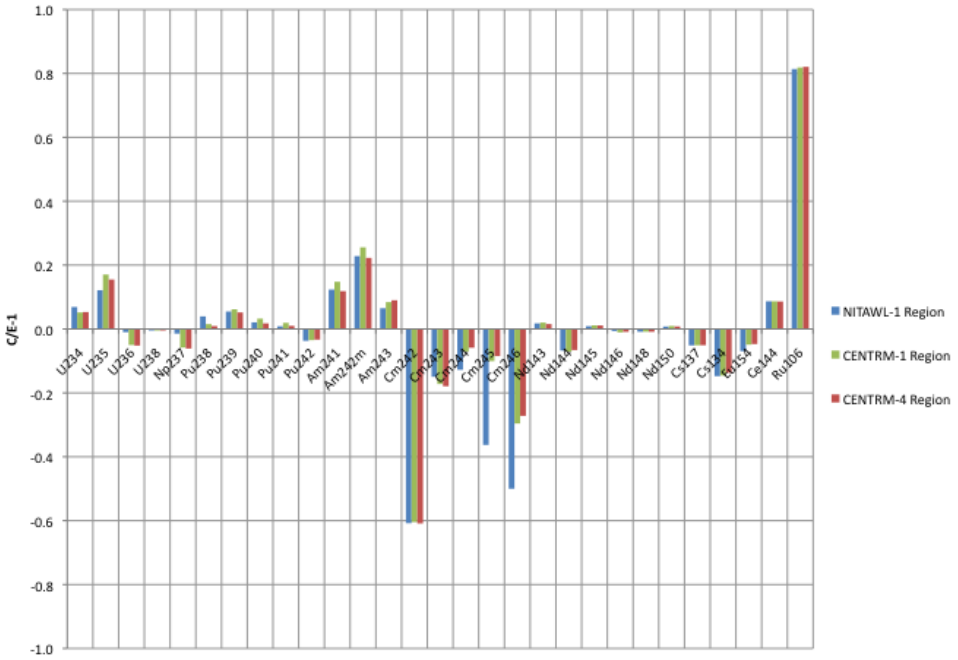


**Fig. 28. Effect of modeling gadolinium rings for SF99-4 sample.** Source: FukushimaDaini2 SF99 Validation Results-V6.xls.

## 7.2 COOPER

The results of the depletion simulations for the ADD2966 and ADD2974 samples in terms of the C/E ratios are presented in Table 28 and plotted in Fig. 29 and Fig. 30. The two measured rods are at adjacent locations, and the C/E ratios for the samples that were cut at the same elevations show consistent agreement across all measured isotopes. While on average $^{235}$U is underpredicted by 5% to 7%, plutonium isotopes except $^{238}$Pu and $^{240}$Pu are all overpredicted by 3% to 6%. $^{241}$Am is overpredicted by 12% to 14%. The largest discrepancies between the measured and the calculated isotopic concentrations were seen in $^{79}$Se and $^{126}$Sn concentrations. The calculated concentrations were much larger than the reported measurement uncertainties for all samples. The consistent bias and small standard deviation suggest a systematic problem either in the measurement or in the modeling of the samples.

In addition to uncertainties in the sample operating history, Cooper depletion simulations have additional uncertainties due to calculated moderator densities. Because no void fraction profiles were reported, a profile was generated using the developed semianalytical profile fit void fraction model. Although there are uncertainties in the void fraction models, there are also uncertainties in the results due to uncertainties in the reported axial sample locations as discussed in Sect. 4.2. To illustrate the effect of the void fraction uncertainties in the calculated isotopic concentrations, the calculated void fraction of each ADD2966 sample was perturbed by ±10% (i.e., $\alpha$=0.50 ±0.10), and the corresponding isotopic concentrations were calculated. The results for the uranium and plutonium isotopes are depicted in Fig. 31. Although the effects of the perturbations were minimal at high void fractions, there were significant changes in $^{235}$U, $^{238}$Pu, $^{239}$Pu, and $^{241}$Pu concentrations at low- and mid-void fractions. The consistent improvement in Cut T isotopic concentrations with increase in void fraction could be an indication that the sample was actually located at a higher elevation and or the void fraction was underpredicted for that sample. Lower than expected $^{235}$U and $^{238}$Pu C/E ratios for Cut T and Cut U samples, which are located near the bottom of the ADD2966 and ADD2974 rods, may be attributable to moderator density uncertainties.

**Table 28. Calculated-to-measured isotopic inventory ratios for ADD2966 (B3) and ADD2974 (C3) samples**

| Nuclide | C/E | | | | | | | | | |
|---|---|---|---|---|---|---|---|---|---|---|
| | Cut T | Cut K | Cut B | Average | Standard deviation | Cut U | Cut J | Cut B | Average | Standard deviation |
| $^{234}$U | 0.969 | 1.044 | 1.008 | 1.007 | 0.037 | 0.949 | 1.008 | 0.992 | 0.983 | 0.031 |
| $^{235}$U | 0.888 | 0.939 | 0.978 | 0.935 | 0.045 | 0.902 | 0.975 | 0.977 | 0.952 | 0.043 |
| $^{236}$U | 0.978 | 0.988 | 0.995 | 0.987 | 0.009 | 0.977 | 0.975 | 1.009 | 0.987 | 0.019 |
| $^{238}$U | 0.996 | 1.000 | 1.000 | 0.999 | 0.003 | 0.990 | 0.983 | 0.987 | 0.987 | 0.003 |
| $^{238}$Pu | 0.836 | 0.845 | 0.926 | 0.869 | 0.050 | 0.911 | 0.861 | 0.940 | 0.904 | 0.040 |
| $^{239}$Pu | 1.011 | 1.044 | 1.052 | 1.036 | 0.022 | 0.993 | 1.079 | 1.075 | 1.049 | 0.048 |
| $^{240}$Pu | 0.955 | 0.951 | 1.025 | 0.977 | 0.042 | 0.954 | 0.940 | 1.016 | 0.970 | 0.040 |
| $^{241}$Pu | 0.973 | 1.002 | 1.100 | 1.025 | 0.067 | 0.972 | 1.048 | 1.126 | 1.049 | 0.077 |
| $^{242}$Pu | 1.015 | 1.016 | 1.159 | 1.064 | 0.083 | 1.020 | 1.011 | 1.160 | 1.064 | 0.084 |
| $^{237}$Np | 0.903 | 0.905 | 1.132 | 0.980 | 0.132 | 0.895 | 0.994 | 1.175 | 1.021 | 0.142 |
| $^{241}$Am | 1.079 | 1.112 | 1.205 | 1.132 | 0.066 | 1.054 | 1.168 | 1.228 | 1.150 | 0.089 |
| $^{244}$Cm | 0.974 | 1.018 | 1.257 | 1.083 | 0.152 | 0.954 | 1.037 | 1.121 | 1.037 | 0.084 |
| $^{79}$Se | 1.327 | 1.397 | 1.381 | 1.368 | 0.036 | 1.348 | 1.333 | 1.327 | 1.336 | 0.011 |
| $^{90}$Sr | 1.083 | 1.100 | 1.052 | 1.079 | 0.024 | 1.061 | 1.076 | 1.079 | 1.072 | 0.010 |
| $^{99}$Tc | 1.175 | 1.177 | 1.169 | 1.174 | 0.004 | 1.151 | 1.092 | 1.115 | 1.119 | 0.030 |
| $^{126}$Sn | 2.971 | 3.054 | 3.059 | 3.028 | 0.049 | 2.935 | 2.900 | 3.064 | 2.966 | 0.086 |
| $^{135}$Cs | 1.036 | 1.048 | 1.096 | 1.060 | 0.032 | 1.062 | 0.995 | 1.088 | 1.048 | 0.048 |
| $^{137}$Cs | 1.022 | 1.024 | 1.029 | 1.025 | 0.004 | 1.052 | 0.933 | 1.020 | 1.002 | 0.061 |

Source: Cooper_B3_V6.xlsx, Cooper_C3_V4.xlsx.

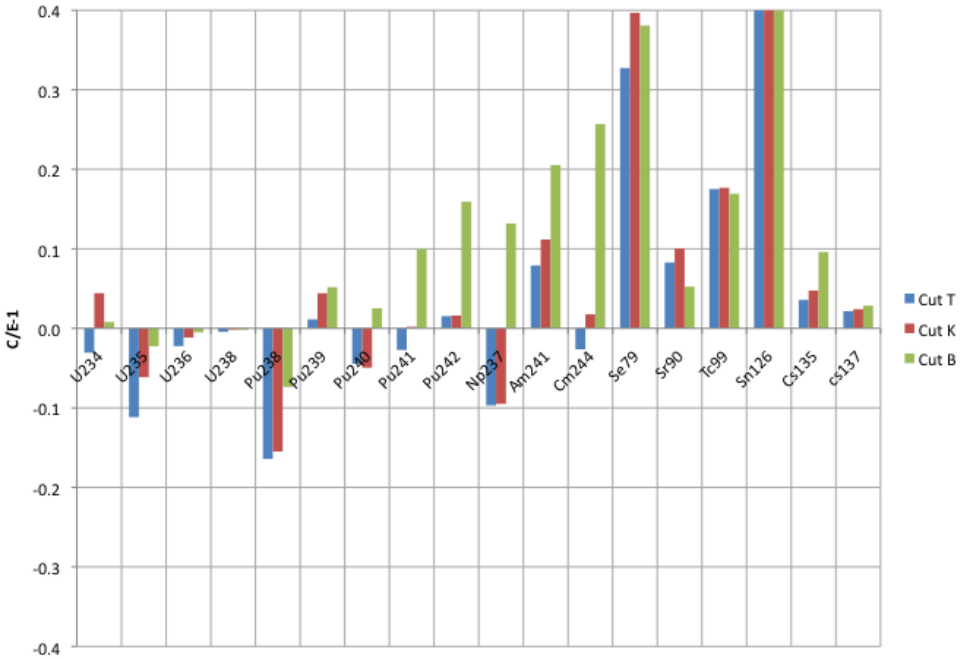


**Fig. 29. Calculated-to-measured fission product concentration ratios for ADD2966 samples.** Source: Cooper_B3_V6.xlsx.

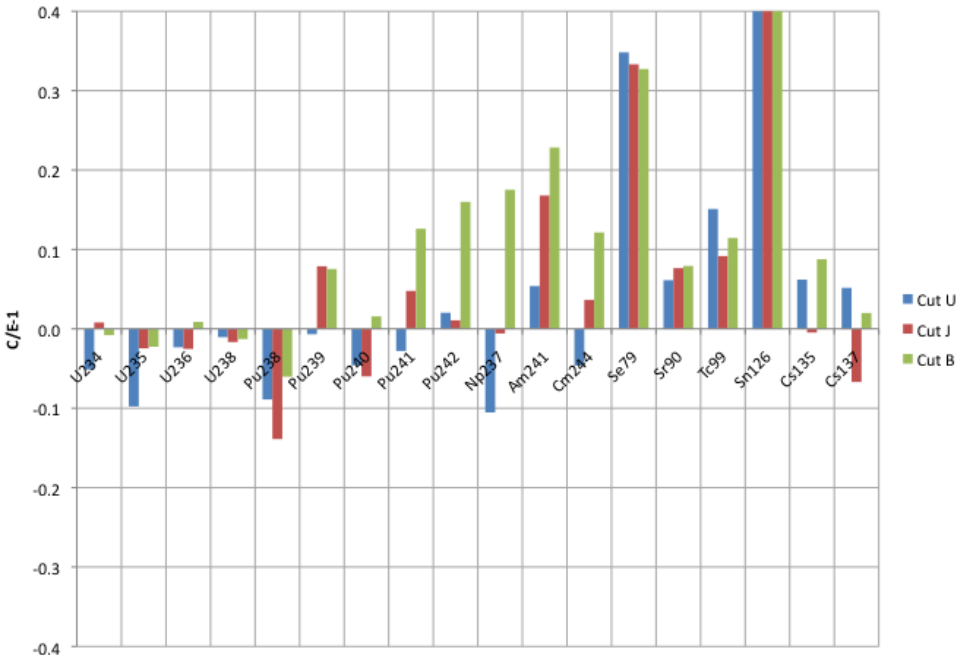


**Fig. 30. Calculated-to-measured fission product concentration ratios for ADD2974 samples.** Source: Cooper_C3_V4.xlsx.

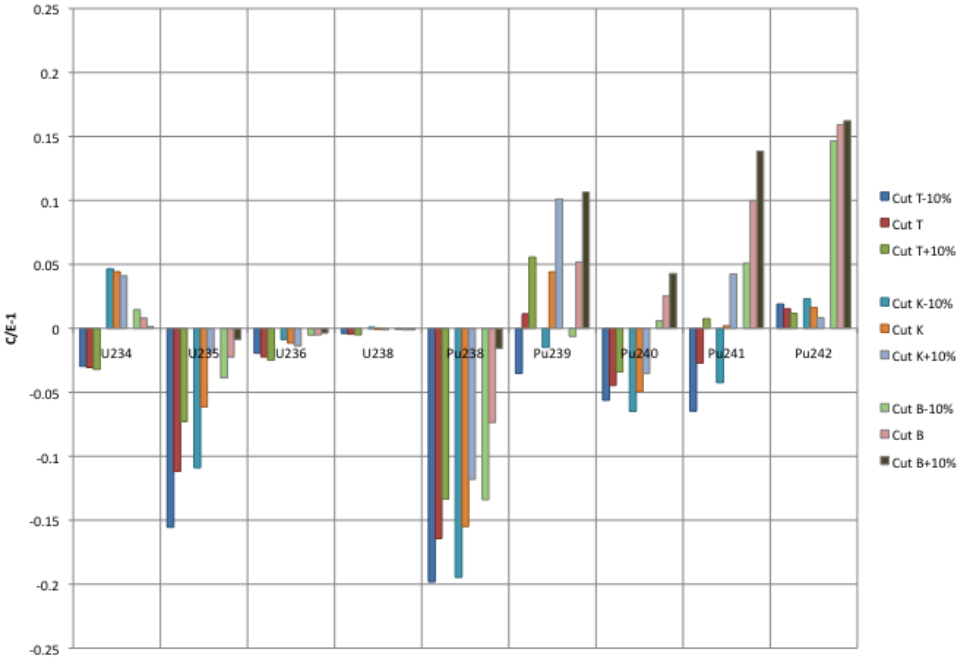


**Fig. 31. Effect of void fraction perturbations on the calculated isotopics for ADD2966 samples.** Source: Cooper_B3_V6.xlsx.

### 7.3 GUNDREMMINGEN-A

The isotopic concentrations of Gundremmingen-A fuel samples from 10 different fuel rods from two different fuel bundles were compared with the calculated isotopic concentrations from depletion simulations, and the results are presented in Tables 29 and 30 and plotted in Figs. 32 and 33. The reported $^{241}$Am data are not included in the comparisons because of the large uncertainty in the measured data (discussed in Sect. 4.3.1). The $^{236}$Pu data were also excluded from the comparisons because the measured concentration is around $10^{-6}$ g/TIHM, and such a trace amount is at the lower limits of detection.

Except for the two samples from the bottom portion of the A1 rods, all the samples were cut at the same axial elevation in the high void region. With the exception of cesium isotopes, the general consistency in the isotopic ratios of the samples at the same axial locations can be seen in Fig. 32 and Fig. 33. While $^{137}$Cs and $^{134}$Cs concentrations in the A1-2 sample from the B23 bundle were calculated to be 20% higher than the measurements, the same isotopic concentrations were calculated to be 20% less than the measurements for the A1-2 sample from the C16 bundle. Although, the reported uncertainty in $^{137}$Cs measurements is around 3.5%, as seen in Fig. 6, the measurements at the two laboratories can be different by as much as 20% for the same sample. This inconsistency in the measurements indicates additional undocumented uncertainties in the measurements. The inconsistency in the cesium isotopic concentrations could be due to such uncertainties. Another large discrepancy in the calculated versus measured values was observed for the curium isotopes. The predicted $^{242}$Cm concentrations are about 30% lower than the measured concentrations for all samples. On the other hand, the $^{244}$Cm C/E ratio shows large variations ranging from 10% higher to 30% lower than the predictions. Considering a variation up to 20% between the two laboratory measurements for the same sample (Fig. 6) and the consistency in the C/E ratios for the same sample locations in the two different bundles in Fig. 32 and Fig. 33, the large deviations in the predicted curium isotopes could be due both to measurements and/or to nuclear data uncertainties.

**Table 29. Calculated-to-measured isotopic inventory ratios for B23 samples**

| Nuclide | C/E | | | | | | | | |
|---|---|---|---|---|---|---|---|---|---|
| | A1-1 | A1-2 | B3 | B4 | C5 | E3 | E5 | Average | Standard deviation |
| $^{235}$U | 0.901 | 0.914 | 1.001 | 1.032 | 1.005 | 0.972 | 1.042 | 0.981 | 0.055 |
| $^{236}$U | 0.988 | 0.997 | 0.963 | 0.974 | 0.944 | 0.960 | 0.954 | 0.969 | 0.019 |
| $^{238}$U | 1.000 | 1.001 | 0.999 | 0.999 | 1.000 | 1.000 | 1.001 | 1.000 | 0.001 |
| $^{238}$Pu | 1.017 | 0.965 | 0.874 | 0.850 | 0.877 | 0.973 | 0.857 | 0.916 | 0.067 |
| $^{239}$Pu | 0.957 | 0.969 | 1.038 | 1.089 | 1.038 | 1.066 | 1.008 | 1.023 | 0.049 |
| $^{240}$Pu | 1.075 | 1.025 | 0.978 | 1.021 | 0.979 | 1.067 | 0.973 | 1.017 | 0.042 |
| $^{241}$Pu | 0.950 | 0.869 | 0.999 | 1.043 | 0.993 | 1.059 | 0.964 | 0.982 | 0.064 |
| $^{242}$Pu | 1.062 | 0.900 | 0.981 | 1.035 | 0.977 | 1.117 | 0.953 | 1.004 | 0.073 |
| $^{242}$Cm | 0.782 | 0.711 | 0.713 | 0.785 | 0.742 | 0.813 | 0.763 | 0.758 | 0.038 |
| $^{244}$Cm | 1.131 | 1.009 | 0.919 | 1.005 | 0.915 | 1.191 | 0.851 | 1.003 | 0.122 |
| $^{148}$Nd | 0.982 | 0.981 | 0.987 | 0.989 | 0.988 | 0.962 | 0.958 | 0.978 | 0.013 |
| $^{137}$Cs | 0.858 | 1.159 | 0.975 | 1.001 | 0.910 | 1.039 | 0.972 | 0.988 | 0.096 |
| $^{134}$Cs | 0.883 | 1.187 | 0.745 | 0.895 | No Data | 0.946 | 0.965 | 0.937 | 0.145 |
| $^{154}$Eu | 0.696 | 0.987 | 0.839 | 0.929 | No Data | 0.937 | 0.883 | 0.878 | 0.103 |

Source: Gundremmingen_B23_data_V4.xlsx.

**Table 30. Calculated-to-measured isotopic inventory ratios for C16 samples**

| Nuclide | C/E | | | | | | |
|---|---|---|---|---|---|---|---|
| | A1-1 | A1-2 | B3 | C5 | E5 | Average | Standard deviation |
| $^{235}$U | 0.965 | 0.965 | 1.021 | 0.947 | 1.032 | 0.986 | 0.038 |
| $^{236}$U | 0.939 | 0.969 | 0.926 | 0.975 | 0.946 | 0.951 | 0.021 |
| $^{238}$U | 1.000 | 1.000 | 1.000 | 1.001 | 1.000 | 1.000 | 0.000 |
| $^{238}$Pu | 1.037 | 0.996 | 0.882 | 0.794 | 0.853 | 0.912 | 0.101 |
| $^{239}$Pu | 0.960 | 0.987 | 1.023 | 0.906 | 1.000 | 0.975 | 0.045 |
| $^{240}$Pu | 1.042 | 1.052 | 0.991 | 0.987 | 0.956 | 1.006 | 0.040 |
| $^{241}$Pu | 0.951 | 0.911 | 0.974 | 0.909 | 0.947 | 0.938 | 0.028 |
| $^{242}$Pu | 1.042 | 0.935 | 0.964 | 1.021 | 0.879 | 0.968 | 0.066 |
| $^{242}$Cm | 0.802 | 0.702 | 0.672 | 0.697 | 0.678 | 0.710 | 0.053 |
| $^{244}$Cm | 1.153 | 0.998 | 0.864 | 0.731 | 0.826 | 0.914 | 0.164 |
| $^{148}$Nd | 0.995 | 0.996 | 0.986 | 1.001 | 0.981 | 0.992 | 0.008 |
| $^{137}$Cs | 0.978 | 0.905 | 0.936 | 0.879 | 1.009 | 0.941 | 0.053 |
| $^{134}$Cs | 0.925 | 0.802 | 0.885 | No Data | 1.038 | 0.912 | 0.098 |
| $^{154}$Eu | 0.908 | 0.907 | 0.820 | No Data | 0.885 | 0.880 | 0.041 |

Source: Gundremmingen_C16_data_V5.xlsx.

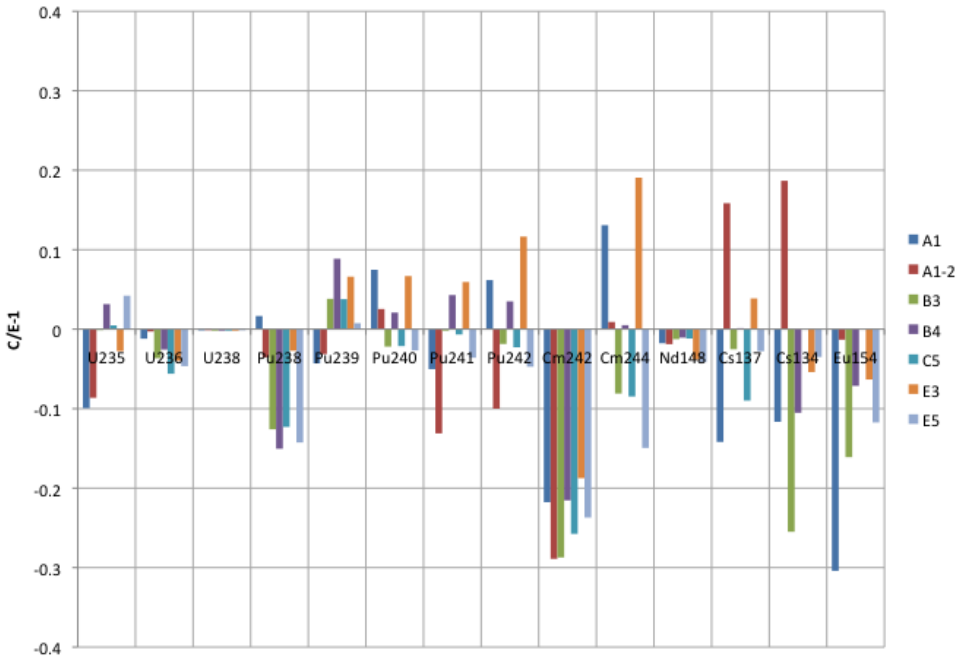


**Fig. 32. Ratios of calculated-to-measured isotopic concentrations for B23 samples.** Source: Gundremmingen_B23_data_V4.xlsx.

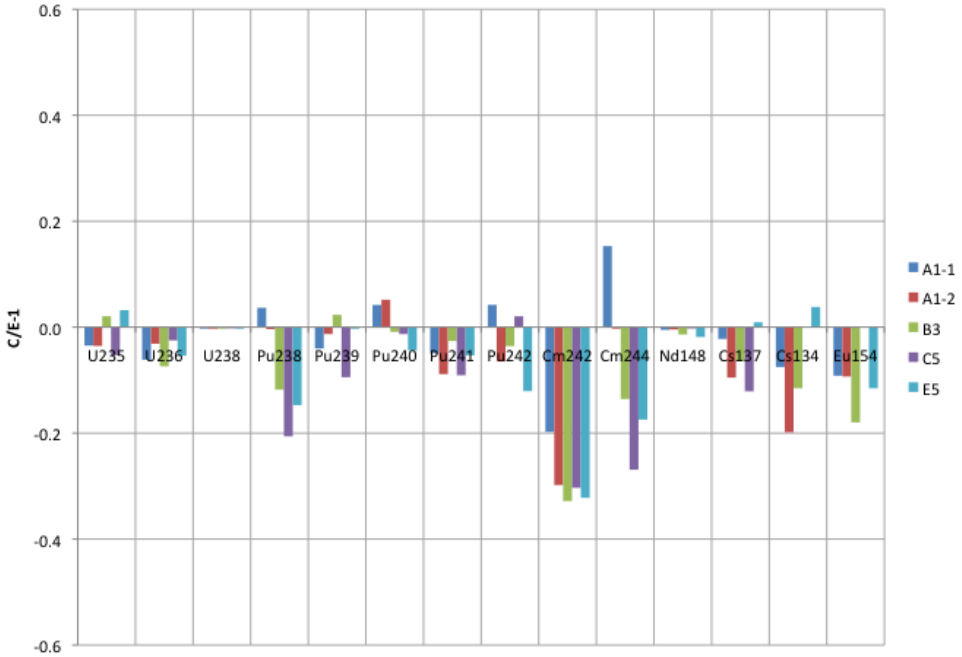


**Fig. 33. Ratios of calculated-to-measured isotopic concentrations for C16 samples.** Source: Gundremmingen_C16_data_V5.xlsx.

# 8. SUMMARY

The results of SCALE 5.1 simulations of 32 samples from 14 fuel rods in four fuel assemblies are presented in this report. The measured and the calculated isotopic compositions of the 34 samples were compared for 38 isotopes. Depletion simulations of BWR assemblies are more challenging than those for pressurized water reactor assemblies because of the greater complexities associated with the BWR spent nuclear fuel characteristics. Some of the isotopic measurements included in this report were made 35 years ago and therefore present challenges in obtaining any missing core operating history information. Because some key design/operating data are missing or unavailable, the SCALE5 isotopic results in this report include uncertainties (described in Sect. 6.2). The void fraction uncertainties are one of the most prominent uncertainties observed in this report. All modeled fuel samples demonstrated high sensitivity to the void fraction, especially the $^{235}$U and Pu isotopes.

A summary of the isotopic comparisons for all samples is given in Appendix D. Even with the mentioned uncertainties, the results show good agreement with the measurements for all uranium and plutonium isotopes. The $^{235}$U C/E ratios are in the ±10% range for all samples. The $^{236}$U results are within ±0.5% of the measurements. The slight bias in the Gundremmingen $^{236}$U results are suspected to be due to underestimated initial $^{236}$U concentration of the fresh fuel. Comparisons of plutonium isotopes show different degrees of deviation. While $^{240}$Pu shows the smallest standard deviation, $^{238}$Pu results are the most scattered ones with a couple C/E ratios reaching up to 20%.

In general, the Fukushima results show the smallest standard deviation and the smallest variation from the measurements compared to the other samples. The unexpectedly large deviations and a very low average C/E ratio compared to the Gundremmingen results for $^{242}$Cm isotope could be a sign of a systematic error in the measurements. There is a clear trend with the increasing sample number in the Fukushima results across most isotopes. This oscillating trend in the results corresponds to the increasing elevation of the samples in the first rod and then the second rod. Since void fraction increases with increasing elevation, the observed behavior with the sample number is actually a trend in the void fractions. These trends indicate that in reality the effective average void fractions, which take the historical void effects into account, can be higher than the reported generic void fractions for the samples located in the middle section of the rods. In fact, the void mispredictions may not necessarily be localized to the middle section; however, as discussed in Sect. 7.3, the isotopics are more sensitive to the errors in the mid-void regions, hence more observable. A similar void trend can be seen in the Cooper results, since all Cooper samples were also obtained from different axial locations.

The Gundremmingen-A isotopic comparisons demonstrate the largest standard deviations for isotopes. As no trend was observed in the results, the large standard deviations suggest higher than reported uncertainties in the Gundremmingen measurements.

## 9. REFERENCES


1. *SCALE: A Modular Code System for Performing Standardized Computer Analyses for Licensing Evaluations*, ORNL/TM-2005/39, Version 5.1, Vols. I–III, November 2006. Available from Radiation Safety Information Computational Center at Oak Ridge National Laboratory as CCC-732.
2. *Test Plan for: Isotopic Validation for Postclosure Criticality of Commercial Spent Nuclear Fuel*, TP-OCRWM-LL-ORNL-02 Rev. 00, CN 01.
3. *Calculation Packages*, ORNL-OCRW-19.1, Rev. 03, CN 00.
4. *Scientific Investigations*, ORNL-OCRW-21.0, Rev. 03, CN 00.
5. *Control of the Electronic Management of Data*, ORNL-OCRW-23.0, Rev. 01, CN 01.
6. *Software Control*, ORNL-OCRW-19.0, Rev. 06, CN 00.
7. SCALE-YMP Software Verification Report for Linux_2, ORNL OCRW-SQA-011, Revision 03, CN 00.
8. Y. Nakahara, K. Suyama, T. Suzaki, *Technical Development on Burm-up Credit for Spent LWR Fuels*, JAERI-Tech 2000-071, ORNL/TR-2001/01.
9. SFCOMPO - Spent Fuel Isotopic Composition Database, http://www.nea.fr/sfcompo/.
10. Y. Nakahara, K. Suyama, J. Inagawa *et al.*, "Nuclide Composition Benchmark Data Set for Verifying Burnup Codes on Spent Light Water Reactor Fuel," *Nucl. Technol.* **137**, 111 (2002).
11. "Atom Percent Fission of Uranium and Plutonium (Nd-148 Method)," *Annual Book of ASTM Standards* **E321**(12.02), 172, American Society for Testing and Materials (1984).
12. M. T. Hutchings, "High-Temperature Studies of $UO_2$ and $ThO_2$ Using Neutron Scattering Techniques," *J. Chem. Soc. Faraday Trans. II* **83,** 1083–1103 (1987), http://www.insc.anl.gov/matprop/uo2/density/solid/soldens.php.
13. IAEA TECDOC-849, *In Core Fuel Management Code Package Validation for BWRs*, 1995.
14. *Characterization of Spent Fuel Approved Testing Material-ATM-105*, PNL-5109-105/UC-802.
15. O. W. Hermann and M. D. DeHart, *Validation of SCALE (SAS2H) Isotopic Predictions for BWR Spent Fuel*," ORNL/TM-13315, Oak Ridge National Laboratory, Oak Ridge, Tenn., September 1998.
16. T. Yamamoto, "Compilation of Measurement and Analysis Results of Isotopic Inventories of Spent BWR Fuels" *JNES*, http://www.nea.fr/science/wpncs/ADSNF.
17. Post-Irradiation Analysis of the Gudremmingen BWR Spent Fuel," Nucl. Sci. and Tech., Commission of the European Communities, ISBN 92-825-1099-9, 1979.
18. S. Guardini and G. Guzzi, "BENCHMARK Reference Data on Post Irradiation Analysis of Light Water Reactor Fuel Samples," Nucl. Sci. and Tech. Commission of the European Communities, 1983, ISBN 92-825-1099-9.
19. T. Yamamoto and M. Yamamoto, "Nuclear Analysis of PIE Data of Irradiated BWR 8×8-2 and 8×8-4 $UO_2$ Fuel Assemblies," *Nucl. Sci Techol.* **45**(11), November 2008.
20. S. E. Fisher and F. C. Difilippo, *Neutronics Benchmark for the Quad Cities-1 (Cycle 2) Mixed-Oxide Assembly Irradiation*, ORNL/TM-13567, Oak Ridge National Laboratory, Oak Ridge, Tenn., April 1998.

21. H. Fijii, *Directory of Nuclear Power Plants in the World*, Japan Nuclear-Energy Information Center, 1985.

22. *Nuclear Engineering International, World Nuclear Industry Handbook 2007*, Reed Business Publishing, London, 2006.

23. *Directory of Nuclear Reactors*, International Atomic Energy Agency, Vienna, 1976.

24. "Method for Increasing the Burn-up Capability of Boiling Water Nuclear Reactors Containing Plutonium-bearing Fuel Assemblies," United States Patent 3910818, http://www.freepatentsonline.com/3910818.html.

25. O. W. Hermann, C. V. Parks, and J. P. Renier, *Technical Support for a Proposed Decay Heat Guide Using SAS2H/ORIGEN-S Data*," NUREG/CR-5625 (ORNL/6698), prepared for the U.S. Nuclear Regulatory Commission by Oak Ridge National Laboratory, Oak Ridge, Tenn., July 1994.

## 10. ATTACHMENTS

A list of the Excel files which are referenced in the report is given below. These files are included in the CD under "Excel Files" directory as described in Appendix B.

1. Gundremmingen_Experimental_Data.xls
2. FukushimaDaini2 Void Calculation_V2.xlsx
3. Cooper Void Calculation_Version2.xlsx
4. Cooper Void Calculation_average_channelV1.xlsx
5. Gundremmingen_Void_Calculation_B23.xlsx
6. Gundremmingen_Void_Calculation_C16.xlsx
7. FukushimaDaini2 SF98 Validation Results-V6.xlsx
8. FukushimaDaini2 SF99 Validation Results-V6.xls
9. Cooper_B3_V6.xlsx
10. Cooper_C3_V4.xlsx
11. Gundremmingen_B23_data_V4.xlsx
12. Gundremmingen_C16_data_V5.xlsx
13. Summary.xlsx
14. Void_validation.xlsx

## APPENDIX A. MODERATOR DENSITY PROFILE

Moderator density is an important parameter in reactor calculations, particularly for boiling water reactors (BWRs). Because a moderator's ability to slow down neutrons is a direct function of its density, moderator density becomes a crucial factor in determining reactivity and isotope generation in a fuel assembly. The moderator density is a function of system pressure and temperature in single phase flow in pressurized water reactors. However, because of the existence of steam flow in two phase flow in BWRs, the average density is a volume weighted average of liquid and vapor in the fuel channel.[1] If the void fraction, $\alpha(z)$, is the ratio of vapor to liquid volume at axial location *z*, then the average static water density is given as

$$\rho(z) = \alpha(z)\rho_g + (1-\alpha(z))\rho_f , \tag{A.1}$$

where $\rho_g$ and $\rho_f$ are the saturated vapor and liquid densities, respectively. Because the coolant is saturated for most of the flow through the fuel assembly, the coolant density becomes a function of the void fraction only.

The void distribution and corollary, the moderator density, are not constant throughout the lifetime of a fuel assembly. As the void fraction changes axially and radially with changing power distribution, it also changes during the regular reactor operation due to changes in the control blade positions, coolant flow rate, and feed water temperature as a part of the plant reactor operation. Although detailed void fraction distribution history is needed for an accurate simulation of a fuel assembly, usually radial void distribution is not available and radially averaged axial void distribution is used for the reactor simulations.

Void fraction history data were not disclosed for any fuel samples in this report. Only core average cycle generic void fraction values were reported for the Fukushima Daini-2 and Gundremmingen-A fuel samples. However, there were no reported void fraction data for the fuel samples from the Cooper reactor. Therefore, two void fraction models were developed as part of this study to calculate the moderator density for the Cooper samples. The first approach uses simplified energy and mass conservation equations along with empirical correlations to calculate the void fraction from the flow quality. The second method uses actual reported void fraction distributions from various assemblies at different average assembly powers; a void fraction distribution is then generated from these trends.

### A.1 FLOW QUALITY PROFILE FIT MODEL

In state-of-the-art thermal hydraulic codes, void fraction distribution can be calculated from mass energy and momentum equations with approximations ranging from complicated separate fluid models to simple mixture models. As the coolant flow rate through the fuel samples and the axial power profile are not known, using a more detailed thermal hydraulic model is questionable for accuracy.
Starting with a simple energy balance along the channel gives the following:

$$\dot{m}(h_{mix}(z) - h_{inlet}) = \int_0^z q''(z)dz , \tag{A.2}$$

where $q''$ is axially changing heat flux in the channel, *z* is the axial distance from channel inlet, $\dot{m}$ is the channel coolant mass flow rate, and $h_{mix}$ (*z*) and $h_{inlet}$ are axial liquid-vapor mixture and inlet enthalpies, respectively. The mixture enthalpy is a mass flow rate weighted average of the saturated liquid ($h_f$) and vapor ($h_g$) enthalpies[1] as follows:

$$h_{mix}(z) = h_f + x_e(z)(h_g - h_f) \ , \tag{A.3}$$

where $x_e$ is the equilibrium vapor quality defined as the ratio of the saturated vapor mass flow rate to the total flow rate as

$$x_e(z) = \frac{\dot{m}_g}{\dot{m}} \ . \tag{A.4}$$

Using the enthalpy relation in Eq. (A.3), the flow quality can be obtained from Eq. (A.2):

$$x_e(z) = \frac{h_{inlet} - h_f}{h_g - h_f} + \frac{1}{\dot{m}(h_g - h_f)} \int_0^z q''(z)dz \ . \tag{A.5}$$

As no axial power shape is reported and it is assumed that there is no control blade in the vicinity of the sample fuel assembly, a cosine shape can be assumed for the axial heat flux in Eq. (A.5):

$$x_e(z) = \frac{h_{inlet} - h_f}{h_g - h_f} + \frac{1}{\dot{m}(h_g - h_f)} \int_0^z q_o'' \cos(\pi \frac{z}{L} - \frac{\pi}{2})dz \ , \tag{A.6}$$

and it simplifies to

$$x_e(z) = \frac{h_{inlet} - h_f}{h_g - h_f} + \frac{\dot{q}}{2\dot{m}(h_g - h_f)} \left( \sin(\pi \frac{z}{L} - \frac{\pi}{2}) + 1 \right) \ , \tag{A.7}$$

where $\dot{q}$ is the channel power.

The equilibrium quality does not account for subcooled boiling and bubbles formed before the saturation point. Therefore the actual flow quality is higher than the equilibrium quality in Eq. (A.7). A popular empirical model to calculate the flow quality is Levy's profile fit model[2] given below:

$$x(z) = x_e(z) - x_e(Z_{sc}) \exp\left[ \frac{x_e(z)}{x_e(Z_{sc})} - 1 \right] . \tag{A.8}$$

The equilibrium flow quality, $x_e(Z_{sc})$, at subcooled boiling point is given by

$$x_e(Z_{sc}) = -\left( \frac{c_{pf}(\Delta T_{sub})_{SC}}{h_g - h_f} \right), \tag{A.9}$$

where $c_{pf}$ is the average specific enthalpy. $(\Delta T_{sub})_{SC}$ is the difference between the saturation temperature and the mean temperature at the start of the subcooled boiling, and it is calculated from an empirical correlation based on Peclet number (*Pe*) by Saha and Zuber:[3]

$$(\Delta T_{sub})_{SC} = 0.0022\left(\frac{q''D_e}{k_l}\right) \text{ for } Pe \le 70{,}000$$
$$(\Delta T_{sub})_{SC} = 153.8\left(\frac{q''D_e}{G_m c_{pf}}\right) \text{ for } Pe \ge 70{,}000 \quad , \tag{A.10}$$

where, $G_m$ is the total mass flux and $D_e$ is equivalent hydraulic diameter. The Peclet number is defined as $Pe = G_m D_e c_{pf}/k_l$ where $k_l$ is thermal conductivity.

Once the flow quality is known, it is possible to relate the area-averaged volume ratios (void fraction) to mass ratios (quality) via vapor ($\rho_g$) and liquid ($\rho_f$) densities as follows:

$$\alpha(z) = \frac{1}{1+\left(\frac{1-x(z)}{x(z)}\right)\frac{\rho_g}{\rho_f}\frac{v_g}{v_f}} \quad . \tag{A.11}$$

The ratio of vapor to liquid velocity $v_g/v_f$ in Eq. (A.11) is commonly referred to as the slip ratio, and it is flow regime dependent. The slip ratio can be calculated from the solution of the momentum and mass balance equations. However, as explained previously, a simpler approach was taken for this report. Based on comparison of the profile fit model to the void fraction distributions in eight fuel assemblies from four Swedish BWRs,[4] a channel average value of 1.3 (Ref. Void_validation.xlsx) was used for the slip ratio in this report.

## A.2 ASSEMBLY POWER TRENDS FIT MODEL

Although the void fraction model developed in the previous section includes several assumptions to eliminate the requirement for some of the operating condition data, it still requires knowledge of thermal hydraulic data such as fuel bundle coolant flow rate and active fuel coolant inlet temperature which are not generally publicly available. Therefore, an empirical void fraction model was developed using the reported void profiles from 11 fuel bundles at different power levels in three Swedish BWRs.[4] The void fraction distribution data in Table A.1 is used in linear regression analysis to generate an axial void fraction correlation as a function of bundle average power level for each axial node location. The distribution of the data and the correlations are presented in Fig. A.1.

**Table A.1. Axial void distribution data for the assembly power trends void fraction fit model**

| **Power (MWd/MTU)** | 9.002 | 9.46 | 10.53 | 15.17 | 15.5 | 18.03 | 18.71 | 20.02 | 21.48 | 23.05 | 25.08 |
|---|---|---|---|---|---|---|---|---|---|---|---|
| **Power Plant** | Oskarshamn 2 | Oskarshamn 2 | Oskarshamn 2 | Ringhals 1 | Oskarshamn 2 | Ringhals 1 | Oskarshamn 2 | Forsmark 1 | Forsmark 1 | Oskarshamn 2 | Forsmark 1 |
| **Assembly ID** | 1389 | 1696 | 1704 | 1186 | 1546 | 1177 | 2995 | KU0278 | KU0282 | 12684 | KU0269 |
| **Axial Node** | | | | | | | | | | | |
| 1 | 0 | 0 | 0 | 0 | 0 | 0 | 0 | 0 | 0 | 0 | 0 |
| 2 | 0 | 0.001 | 0 | 0.001 | 0.004 | 0 | 0.005 | 0 | 0 | 0 | 0 |
| 3 | 0.002 | 0.011 | 0.006 | 0.022 | 0.027 | 0.017 | 0.028 | 0 | 0 | 0.014 | 0 |
| 4 | 0.018 | 0.038 | 0.029 | 0.06 | 0.068 | 0.055 | 0.073 | 0.022 | 0.037 | 0.085 | 0.047 |
| 5 | 0.045 | 0.078 | 0.068 | 0.105 | 0.114 | 0.104 | 0.129 | 0.083 | 0.105 | 0.167 | 0.128 |
| 6 | 0.077 | 0.118 | 0.111 | 0.155 | 0.172 | 0.159 | 0.192 | 0.147 | 0.170 | 0.245 | 0.208 |
| 7 | 0.113 | 0.162 | 0.162 | 0.204 | 0.232 | 0.217 | 0.253 | 0.208 | 0.236 | 0.313 | 0.283 |
| 8 | 0.155 | 0.208 | 0.218 | 0.253 | 0.283 | 0.272 | 0.311 | 0.265 | 0.298 | 0.371 | 0.349 |
| 9 | 0.198 | 0.250 | 0.272 | 0.297 | 0.334 | 0.324 | 0.363 | 0.320 | 0.354 | 0.423 | 0.408 |
| 10 | 0.238 | 0.285 | 0.320 | 0.337 | 0.383 | 0.371 | 0.410 | 0.371 | 0.405 | 0.471 | 0.461 |
| 11 | 0.278 | 0.318 | 0.364 | 0.373 | 0.426 | 0.415 | 0.452 | 0.418 | 0.450 | 0.514 | 0.507 |
| 12 | 0.316 | 0.351 | 0.406 | 0.406 | 0.463 | 0.453 | 0.488 | 0.461 | 0.491 | 0.551 | 0.548 |
| 13 | 0.353 | 0.380 | 0.440 | 0.434 | 0.497 | 0.487 | 0.520 | 0.500 | 0.529 | 0.584 | 0.583 |
| 14 | 0.387 | 0.409 | 0.472 | 0.461 | 0.529 | 0.516 | 0.548 | 0.537 | 0.563 | 0.614 | 0.615 |
| 15 | 0.419 | 0.437 | 0.501 | 0.487 | 0.557 | 0.544 | 0.575 | 0.569 | 0.594 | 0.640 | 0.643 |
| 16 | 0.448 | 0.462 | 0.526 | 0.511 | 0.582 | 0.569 | 0.598 | 0.597 | 0.621 | 0.662 | 0.668 |
| 17 | 0.473 | 0.485 | 0.548 | 0.533 | 0.604 | 0.591 | 0.618 | 0.622 | 0.645 | 0.683 | 0.689 |
| 18 | 0.496 | 0.507 | 0.568 | 0.554 | 0.625 | 0.611 | 0.638 | 0.645 | 0.666 | 0.701 | 0.708 |
| 19 | 0.517 | 0.527 | 0.588 | 0.573 | 0.644 | 0.630 | 0.654 | 0.664 | 0.684 | 0.718 | 0.725 |
| 20 | 0.535 | 0.543 | 0.603 | 0.589 | 0.661 | 0.646 | 0.669 | 0.681 | 0.700 | 0.732 | 0.739 |
| 21 | 0.551 | 0.558 | 0.617 | 0.604 | 0.675 | 0.661 | 0.683 | 0.697 | 0.713 | 0.744 | 0.752 |
| 22 | 0.564 | 0.572 | 0.630 | 0.617 | 0.687 | 0.674 | 0.694 | 0.710 | 0.725 | 0.754 | 0.763 |
| 23 | 0.575 | 0.582 | 0.639 | 0.627 | 0.697 | 0.684 | 0.703 | 0.720 | 0.733 | 0.763 | 0.771 |
| 24 | 0.583 | 0.589 | 0.647 | 0.635 | 0.704 | 0.693 | 0.710 | 0.729 | 0.740 | 0.768 | 0.776 |
| 25 | 0.590 | 0.597 | 0.654 | 0.638 | 0.711 | 0.698 | 0.716 | 0.728 | 0.738 | 0.773 | 0.776 |

Source: Reference A.4.

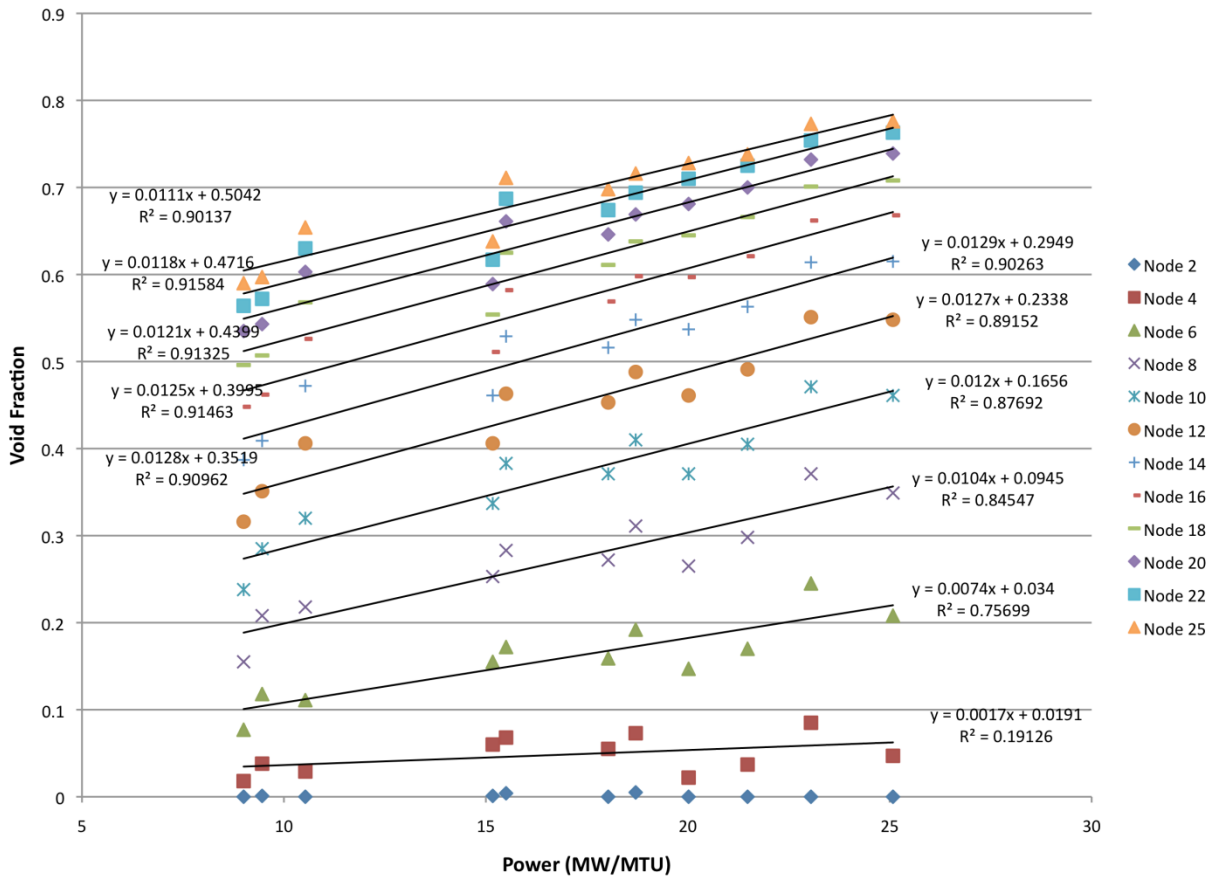


**Fig. A.1. Power trend fit void fraction model.**

## A. REFERENCES


A.1. N. Todreas, M. Kazimi, *Nuclear Systems I*, T*hermal Hydraulic Fundamentals*, Taylor & Francis, 1993.

A.2. S. Levy, "Forced Convection Subcooled Boiling Prediction of Vapor Volumetric Fraction," *Int. J. Heat Mass Transfer* **10**, 247, 1967.

A.3. P. Saha and N. N. Zuber, "Point of Net Vapor Generation and Vapor Void Fraction in Subcooled Boiling," Paper B4.7, *Proceedings of the 5th International Heat Transfer Conference*, Tokyo, 1974.

A.4. B. D. Murphy and I. C. Gauld, *Spent Fuel Decay Heat Measurements Performed at the Swedish Central Interim Storage Facility*, ORNL/TM-2008/016, Oak Ridge National Laboratory, Oak Ridge, Tenn., February 2010.

## APPENDIX B. ELECTRONIC DATA SPECIFICATIONS

This appendix contains a listing and description of the files contained in the CD attached to the calculation report *SCALE 5 Analysis of BWR Spent Nuclear Fuel Isotopic Compositions for Safety Studies*. The operating system used to create the electronic data on the CD was Microsoft Windows 7 Ultimate. The zip archives were created using standard Windows 7 compress capabilities. The following process controls for storage and protection of electronic data apply.

| | |
|---|---|
| Medium: | CD |
| Conditions: | Fireproof cabinet kept at ambient temperature |
| Location: | OCRWM QA Records, currently stored in Building 5700, Room H330 |
| Retention Time: | Lifetime |
| Security: | Fireproof cabinet is locked |
| Access: | Project manager and records custodian only |

The attributes of the electronic files are as follows.

| File/folder name | Size (bytes) (on disk) | Number of files | File date | File time | Description |
|---|---|---|---|---|---|
| | | | [a] | | |
| References | 79,609,856 | 1 | 12/28/2010 | 12:07 pm | Folder containing archive reports and publications referenced in this report |
| Input_Output_PLT | 344,035,328 | 18 | 12/28/2010 | 12:07 pm | Folder containing archive SCALE/TRITON input and output files for depletion calculations |
| Excel Files | 1,138,688 | 10 | 12/28/2010 | 12:07 pm | Folder containing all Excel files used in this calculation |

[a]The CD was created on December 28, 2010, by U. Mertyurek.

# APPENDIX C. SCALE INPUT EXAMPLES

## Fukushima Daini-2 SF99-4

```
=t-depl  parm=(nitawl,addnux=3)
BWR Validation sample5
44groupndf
read comp
' 3.910 wt% U-235 tested
uo2 100 den=9.943 1 900 92234 0.036 92235 3.910 92238 96.054  end
'
' 3.910 wt% U-235 not tested
uo2 101 den=9.943 1 900 92234 0.036 92235 3.910 92238 96.054   end
'
' 3.448 wt% U-235 not tested
uo2 102 den=9.943 1 900 92234 0.031 92235 3.448  92238 96.521   end
'
' 3.405 wt% U-235 not tested
uo2 103 den=9.943 1 900 92234 0.03 92235 3.405  92238 96.565   end
'
' 2.903 wt% U-235 not tested
uo2 104 den=9.943 1 900 92234 0.026 92235 2.903  92238 97.071   end
'
' 2.000 wt% U-235 not tested
uo2 105 den=9.943 1 900 92234 0.018 92235 2.000  92238 97.982   end
'
' ba rod with 3.4 wt% U-235 /4.5 wt% Gd2O3 tested
uo2         200 den=9.943  0.955  900 92234 0.03 92235 3.410  92238 96.56   end
atom-gd2o3  200 9.943 2 64000 2 8016 3  0.045  900 end
'
' ba rod with 3.4 wt% U-235 /4.5 wt% Gd2O3 not tested
uo2         201 den=9.943  0.955  900 92234 0.03 92235 3.410  92238 96.56   end
atom-gd2o3  201 9.943 2 64000 2 8016 3  0.045  900 end
'
' zirc2 clad
zirc2 300 1 559 end
zirc2 301 1 559 end
zirc2 302 1 559 end
zirc2 303 1 559 end
zirc2 304 1 559 end
zirc2 305 1 559 end
zirc2 306 1 559 end
zirc2 307 1 559 end
'
' h2o
h2o 400 den=0.6627 1 559 end
h2o 401 den=0.6627 1 559 end
h2o 402 den=0.6627 1 559 end
h2o 403 den=0.6627 1 559 end
h2o 404 den=0.6627 1 559 end
h2o 405 den=0.6627 1 559 end
h2o 406 den=0.6627 1 559 end
h2o 407 den=0.6627 1 559 end
h2o 408 den=0.7401 1 559 end
end comp
read celldata
latticecell squarepitch   pitch=1.6300 400 fuelr=0.527 100 cladr=0.615 300  end
latticecell squarepitch   pitch=1.6300 401 fuelr=0.527 101 cladr=0.615 301  end
latticecell squarepitch   pitch=1.6300 402 fuelr=0.527 102 cladr=0.615 302  end
latticecell squarepitch   pitch=1.6300 403 fuelr=0.527 103 cladr=0.615 303  end
latticecell squarepitch   pitch=1.6300 404 fuelr=0.527 104 cladr=0.615 304  end
latticecell squarepitch   pitch=1.6300 405 fuelr=0.527 105 cladr=0.615 305  end
latticecell squarepitch   pitch=1.6300 406 fuelr=0.527 200 cladr=0.615 306  end
latticecell squarepitch   pitch=1.6300 407 fuelr=0.527 201 cladr=0.615 307  end
end celldata
read burndata
power=12.95 burn=6    down=0   nlib=1 end
power=32.68 burn=3    down=0   nlib=1 end
power=40.29 burn=132  down=21  nlib=2 end
power=14.59 burn=5    down=0   nlib=1 end
power=35.15 burn=244  down=0   nlib=2 end
power=40.70 burn=8    down=117 nlib=1 end
power=14.59 burn=5    down=0   nlib=1 end
power=35.15 burn=317  down=9   nlib=2 end
power=15.21 burn=4    down=0   nlib=1 end
power=35.76 burn=72   down=0   nlib=1 end
power=40.29 burn=10   down=81  nlib=1 end
```

```
power=16.65 burn=3    down=0   nlib=1 end
power=37.20 burn=365  down=2005   nlib=2 end
end burndata
read depletion
-100 101 102 103 104 105 200 201
end depletion
read opus
units=grams
' nrank=37 sort=no
symnuc=u-234 u-235 u-236 u-238 np-237 pu-238 pu-239
       pu-240 pu-241 pu-242 am-241 am-242m am-243 cm-242
       cm-243 cm-244 cm-245 cm-246 nd-143 nd-144 nd-145
       nd-146 nd-148 nd-150 cs-137 cs-134 eu-154 ce-144
       ru-106 sm-147 sm-148 sm-149 sm-150 sm-151 sm-152
       sm-154 o end
matl=100 end
end opus
read model
BWR Fuel Bundle
read parm
 run=yes sn=4 inners=10 epsinner=1e-4 epsouter=1e-4
 epseigen=1e-4 echo=yes drawit=yes combine=no
 cmfd=yes xycmfd=2
end parm
read materials
100 1 'fuel tested' end
101 1 'fuel' end
102 1 'fuel' end
103 1 'fuel' end
104 1 'fuel' end
105 1 'fuel' end
200 1 'Gad tested' end
201 1 'Gad' end
300 1 'clad' end
400 1 'mod' end
408 1 'mod2' end
end materials
read geom
unit 1
cylinder 1 0.527
cylinder 2 0.615
cuboid   3 0.815 -0.815 0.815 -0.815
media 100 00 1
media 300 00 2 -1
media 400 00 3 -2
boundary 3 4 4
unit 2
cylinder 1 0.527
cylinder 2 0.615
cuboid   3 0.815 -0.815 0.815 -0.815
media 101 00 1
media 300 00 2 -1
media 400 00 3 -2
boundary 3 4 4
unit 3
cylinder 1 0.527
cylinder 2 0.615
cuboid   3 0.815 -0.815 0.815 -0.815
media 102 00 1
media 300 00 2 -1
media 400 00 3 -2
boundary 3 4 4
unit 4
cylinder 1 0.527
cylinder 2 0.615
cuboid   3 0.815 -0.815 0.815 -0.815
media 103 00 1
media 300 00 2 -1
media 400 00 3 -2
boundary 3 4 4
unit 5
cylinder 1 0.527
cylinder 2 0.615
cuboid   3 0.815 -0.815 0.815 -0.815
media 104 00 1
media 300 00 2 -1
media 400 00 3 -2
boundary 3 4 4
unit 6
cylinder 1 0.527
cylinder 2 0.615
```

```
cuboid   3 0.815 -0.815 0.815 -0.815
media 105 00 1
media 300 00 2 -1
media 400 00 3 -2
boundary 3 4 4
unit 7
cylinder 1 0.527
cylinder 2 0.615
cuboid   3 0.815 -0.815 0.815 -0.815
media 200 00 1
media 300 00 2 -1
media 400 00 3 -2
boundary 3 4 4
unit 8
cylinder 1 0.527
cylinder 2 0.615
cuboid   3 0.815 -0.815 0.815 -0.815
media 201 00 1
media 300 00 2 -1
media 400 00 3 -2
boundary 3 4 4
unit 9
cylinder 1 0.675
cylinder 2 0.75
cuboid   3 0.815 -0.815 0.815 -0.815
media 408 00 1
media 300 00 2 -1
media 400 00 3 -2
boundary 3 4 4
global unit 10
cuboid 10 13.04   0.0   13.04   0.0
cuboid 11 13.24  -0.2   13.24  -0.2
cuboid 12 13.47  -0.43  13.47  -0.43
cuboid 13 14.14 -1.1 14.14 -1.1
array 1 10 place 1 1 0.815 0.815
media 400 00 10
media 400 00 11 -10
media 300 00 12 -11
media 408 00 13 -12
boundary 13 32 32
end geom
read array
ara=1 typ=cuboidal
nux=8 nuy=8
fill
6 5 4 4 4 4 5 6
5 2 8 3 3 8 2 5
4 8 3 5 5 3 8 4
4 3 5 9 4 5 3 4
4 3 5 4 9 5 3 4
4 8 3 5 5 3 8 4
5 1 7 3 3 8 2 5
6 5 4 4 4 4 5 6
end fill
end array
read bounds
all=refl
end bounds
end model
end
```

## Cooper C3J

```
=t-depl  parm=(nitawl,addnux=3)
BWR Validation C3j
44groupndf
read comp
' 2.93 wt% U-235 tested
uo2 100 den=9.795 1 833 92234 0.026 92235 2.939 92236 0.014 92238 97.021  end
'
' 2.93 wt% U-235 tested
uo2 101 den=9.795 1 833 92234 0.026 92235 2.939 92236 0.014 92238 97.021  end
'
' 2.93 wt% U-235 not tested
uo2 102 den=9.795 1 833 92234 0.026 92235 2.939 92236 0.014 92238 97.021  end
'
' 1.94 wt% U-235 not tested
uo2 103 den=9.795 1 833 92234 0.017 92235 1.94 92236 0.009 92238 98.034   end
'
' 1.69 wt% U-235 not tested
uo2 104 den=9.795 1 833 92234 0.015 92235 1.69 92236 0.008 92238 98.287   end
'
' 1.33 wt% U-235 not tested
uo2 105 den=9.795 1 833 92234 0.012 92235 1.33 92236 0.006 92238 98.652   end
'
' ba rod with 2.93 wt% U-235 /3.0 wt% Gd2O3 tested
uo2         200 den=9.795  0.970  833 92234 0.026 92235 2.93 92236 0.014 92238 97.021   end
atom-gd2o3  200 9.795 2 64000 2 8016 3  0.03  833 end
'
' ba rod with 2.93 wt% U-235 /4.0 wt% Gd2O3 tested
uo2         201 den=9.795  0.960  833 92234 0.026 92235 2.93 92236 0.014 92238 97.021   end
atom-gd2o3  201 9.795 2 64000 2 8016 3  0.04  833 end
'
' ba rod with 1.94 wt% U-235 /4.0 wt% Gd2O3 tested
uo2         202 den=9.795  0.960  833 92234 0.017 92235 1.94 92236 0.009 92238 98.034   end
atom-gd2o3  202 9.795 2 64000 2 8016 3  0.04  833 end
'
' zirc clad
zirc2 300 1 558 end
zirc2 301 1 558 end
zirc2 302 1 558 end
zirc2 303 1 558 end
zirc2 304 1 558 end
zirc2 305 1 558 end
zirc2 306 1 558 end
zirc2 307 1 558 end
zirc2 308 1 558 end
zirc4 309 1 558 end
'
' h2o
h2o 400 den=0.349 1 558 end
h2o 401 den=0.349 1 558 end
h2o 402 den=0.349 1 558 end
h2o 403 den=0.349 1 558 end
h2o 404 den=0.349 1 558 end
h2o 405 den=0.349 1 558 end
h2o 406 den=0.349 1 558 end
h2o 407 den=0.349 1 558 end
h2o 408 den=0.349 1 558 end
h2o 409 den=0.7401 1 558 end
end comp
read celldata
latticecell squarepitch   pitch=1.8750 400 fuelr=0.621 100 cladr=0.715 300  end
latticecell squarepitch   pitch=1.8750 401 fuelr=0.621 101 cladr=0.715 301  end
latticecell squarepitch   pitch=1.8750 402 fuelr=0.621 102 cladr=0.715 302  end
latticecell squarepitch   pitch=1.8750 403 fuelr=0.621 103 cladr=0.715 303  end
latticecell squarepitch   pitch=1.8750 404 fuelr=0.621 104 cladr=0.715 304  end
latticecell squarepitch   pitch=1.8750 405 fuelr=0.621 105 cladr=0.715 305  end
latticecell squarepitch   pitch=1.8750 406 fuelr=0.621 200 cladr=0.715 306  end
latticecell squarepitch   pitch=1.8750 407 fuelr=0.621 201 cladr=0.715 307  end
latticecell squarepitch   pitch=1.8750 408 fuelr=0.621 202 cladr=0.715 308  end
end celldata
read burndata
power=17.97 burn=806 down=60  nlib=6 end
power=17.84 burn=306 down=31  nlib=3 end
power=17.56 burn=165 down=800 nlib=3 end
power=10.78 burn=317 down=49  nlib=3 end
power= 8.56 burn=347 down=1929 nlib=3 end
end burndata
read depletion
```

```
100 -101 102 103 104 105 200 201 202
end depletion
read opus
units=grams
'nrank=10 sort=no
symnuc=u-234 u-235 u-236 u-238 pu-238 pu-239
       pu-240 pu-241 pu-242 o end
matl=101 end
end opus
read keep_output
 origen opus newt
end keep_output
read model
BWR Fuel Bundle
read parm
 run=yes sn=4 inners=10 epsinner=1e-4 epsouter=1e-4
 epseigen=1e-4 echo=yes drawit=no combine=no
 cmfd=yes xycmfd=2
end parm
read materials
100 1 'fuel tested' end
101 1 'fuel tested2' end
102 1 'fuel' end
103 1 'fuel' end
104 1 'fuel' end
105 1 'fuel' end
200 1 'Gad' end
201 1 'Gad' end
202 1 'Gad' end
300 1 'zirc2' end
309 1 'zirc4' end
400 1 'mod' end
409 1 'channel' end
end materials
read geom
unit 1
cylinder 1 0.621
cylinder 2 0.715
cuboid   3 0.9375 -0.9375 0.9375 -0.9375
media 100 00 1
media 300 00 2 -1
media 400 00 3 -2
boundary 3 4 4
unit 2
cylinder 1 0.621
cylinder 2 0.715
cuboid   3 0.9375 -0.9375 0.9375 -0.9375
media 101 00 1
media 300 00 2 -1
media 400 00 3 -2
boundary 3 4 4
unit 3
cylinder 1 0.621
cylinder 2 0.715
cuboid   3 0.9375 -0.9375 0.9375 -0.9375
media 102 00 1
media 300 00 2 -1
media 400 00 3 -2
boundary 3 4 4
unit 4
cylinder 1 0.621
cylinder 2 0.715
cuboid   3 0.9375 -0.9375 0.9375 -0.9375
media 103 00 1
media 300 00 2 -1
media 400 00 3 -2
boundary 3 4 4
unit 5
cylinder 1 0.621
cylinder 2 0.715
cuboid   3 0.9375 -0.9375 0.9375 -0.9375
media 104 00 1
media 300 00 2 -1
media 400 00 3 -2
boundary 3 4 4
unit 6
cylinder 1 0.621
cylinder 2 0.715
cuboid   3 0.9375 -0.9375 0.9375 -0.9375
media 105 00 1
media 300 00 2 -1
```

```
media 400 00 3 -2
boundary 3 4 4
unit 7
cylinder 1 0.621
cylinder 2 0.715
cuboid   3 0.9375 -0.9375 0.9375 -0.9375
media 200 00 1
media 300 00 2 -1
media 400 00 3 -2
boundary 3 4 4
unit 8
cylinder 1 0.621
cylinder 2 0.715
cuboid   3 0.9375 -0.9375 0.9375 -0.9375
media 201 00 1
media 300 00 2 -1
media 400 00 3 -2
boundary 3 4 4
unit 9
cylinder 1 0.621
cylinder 2 0.715
cuboid   3 0.9375 -0.9375 0.9375 -0.9375
media 202 00 1
media 300 00 2 -1
media 400 00 3 -2
boundary 3 4 4
global unit 10
cuboid 10 13.125   0.00   13.125   0.00
cuboid 11 13.266  -0.141   13.266  -0.141
cuboid 12 13.469 -0.344 13.469 -0.344
cuboid 13 13.944 -1.2965 14.4215 -0.819
array 1 10 place 1 1 0.9375 0.9375
media 400 00 10
media 400 00 11 -10
media 309 00 12 -11
media 409 00 13 -12
boundary 13 32 32
end geom
read array
ara=1 typ=cuboidal
nux=7 nuy=7
fill
5 4 3 3 3 4 4
4 3 7 3 3 8 4
4 3 3 3 3 3 3
4 3 3 7 3 3 3
5 1 2 3 3 7 3
5 9 3 3 3 3 4
6 5 5 4 4 4 5
end fill
end array
read bounds
all=refl
end bounds
end model
end
```

## Gundremmingen-A B23-B3

```
=t-depl  parm=(nitawl,addnux=3)
Gundremmingen B23 B3 268 cm
44groupndf
read comp
'2.53 wt% U-235 A1
uo2 100 den=10.07 1 923 92234 0.023 92235 2.530 92236 0.012 92238 97.435 end
'
'2.53 wt% U-235 B3
uo2 101 den=10.07 1 923 92234 0.023 92235 2.530 92236 0.012 92238 97.435 end
'
'2.53 wt% U-235 B4
uo2 102 den=10.07 1 923 92234 0.023 92235 2.530 92236 0.012 92238 97.435 end
'
'2.53 wt% U-235 C5
uo2 103 den=10.07 1 923 92234 0.023 92235 2.530 92236 0.012 92238 97.435 end
'
'2.53 wt% U-235 E3
uo2 104 den=10.07 1 923 92234 0.023 92235 2.530 92236 0.012 92238 97.435 end
'
'2.53 wt% U-235 E5
uo2 105 den=10.07 1 923 92234 0.023 92235 2.530 92236 0.012 92238 97.435 end
'
'2.53 wt% U-235 not tested
uo2 106 den=10.07 1 923 92234 0.023 92235 2.530 92236 0.012 92238 97.435 end
'
'1.87 wt% U-235 not tested
uo2 107 den=10.07 1 923 92234 0.023 92235 1.870 92236 0.012 92238 98.095 end
'
'zirc2 clad
zirc2 300 1 559 end
zirc2 301 1 559 end
zirc2 302 1 559 end
zirc2 303 1 559 end
zirc2 304 1 559 end
zirc2 305 1 559 end
zirc2 306 1 559 end
zirc2 307 1 559 end
'
'zirc4 channel
zirc4 700 1 559 end
'
' h2o
h2o 400 den=0.388 1 559 end
h2o 401 den=0.388 1 559 end
h2o 402 den=0.388 1 559 end
h2o 403 den=0.388 1 559 end
h2o 404 den=0.388 1 559 end
h2o 405 den=0.388 1 559 end
h2o 406 den=0.388 1 559 end
h2o 407 den=0.388 1 559 end
h2o 408 den=0.7401 1 559 end
end comp
read celldata
latticecell squarepitch  pitch=1.780 400 fuelr=0.625 100 cladr=0.714 300 end
latticecell squarepitch  pitch=1.780 401 fuelr=0.625 101 cladr=0.714 301 end
latticecell squarepitch  pitch=1.780 402 fuelr=0.625 102 cladr=0.714 302 end
latticecell squarepitch  pitch=1.780 403 fuelr=0.625 103 cladr=0.714 303 end
latticecell squarepitch  pitch=1.780 404 fuelr=0.625 104 cladr=0.714 304 end
latticecell squarepitch  pitch=1.780 405 fuelr=0.625 105 cladr=0.714 305 end
latticecell squarepitch  pitch=1.780 406 fuelr=0.625 106 cladr=0.714 306 end
latticecell squarepitch  pitch=1.780 407 fuelr=0.625 107 cladr=0.714 307 end
end celldata
read burndata
power=19.645 burn=279 down=56   nlib=4 end
power=17.818 burn=323 down=33   nlib=4 end
power=17.748 burn=290 down=61   nlib=4 end
power=15.718 burn=309 down=1010 nlib=4 end
end burndata
read depletion
100 -101 102 103 104 105 106 107
end depletion
read opus
units=grams
'nrank=18 sort=no
symnuc= cs-137 cs-134 eu-154 u-235 u-236 u-238 pu-236 pu-238 pu-239 pu-240 pu-241
        pu-242 am-241 cm-242 cm-244 nd-148 u-234 o end
matl=101 end
```

```
end opus
read keep_output
 origen opus newt
end keep_output
read model
BWR Fuel Bundle
read parm
 run=yes sn=4 inners=10 epsinner=1e-4 epsouter=1e-4
 epseigen=1e-4 echo=yes drawit=no combine=no cmfd=yes xycmfd=2
end parm
read materials
100 1 'fuel tested' end
101 1 'fuel' end
102 1 'fuel' end
103 1 'fuel' end
104 1 'fuel' end
105 1 'fuel' end
106 1 'fuel' end
107 1 'fuel' end
300 1 'clad' end
700 1 'channel' end
400 1 'mod' end
408 1 'mod2' end
end materials
read geom
unit 1
cylinder 1 0.625
cylinder 2 0.714
cuboid 3 0.890 -0.890 0.890 -0.890
media 100 00 1
media 300 00 2 -1
media 400 00 3 -2
boundary 3 4 4
unit 2
cylinder 1 0.625
cylinder 2 0.714
cuboid 3 0.890 -0.890 0.890 -0.890
media 101 00 1
media 300 00 2 -1
media 400 00 3 -2
boundary 3 4 4
unit 3
cylinder 1 0.625
cylinder 2 0.714
cuboid 3 0.890 -0.890 0.890 -0.890
media 102 00 1
media 300 00 2 -1
media 400 00 3 -2
boundary 3 4 4
unit 4
cylinder 1 0.625
cylinder 2 0.714
cuboid 3 0.890 -0.890 0.890 -0.890
media 103 00 1
media 300 00 2 -1
media 400 00 3 -2
boundary 3 4 4
unit 5
cylinder 1 0.625
cylinder 2 0.714
cuboid 3 0.890 -0.890 0.890 -0.890
media 104 00 1
media 300 00 2 -1
media 400 00 3 -2
boundary 3 4 4
unit 6
cylinder 1 0.625
cylinder 2 0.714
cuboid 3 0.890 -0.890 0.890 -0.890
media 105 00 1
media 300 00 2 -1
media 400 00 3 -2
boundary 3 4 4
unit 7
cylinder 1 0.625
cylinder 2 0.714
cuboid 3 0.890 -0.890 0.890 -0.890
media 106 00 1
media 300 00 2 -1
media 400 00 3 -2
boundary 3 4 4
```

```
unit 8
cylinder 1 0.625
cylinder 2 0.714
cuboid 3 0.890 -0.890 0.890 -0.890
media 107 00 1
media 300 00 2 -1
media 400 00 3 -2
boundary 3 4 4
global unit 9
cuboid 10 10.68   0.0   10.68   0.0
cuboid 11 10.866 -0.186 10.866 -0.186
cuboid 12 11.016 -0.336 11.016 -0.336
cuboid 13 11.889 -0.811 11.491 -1.209
array 1 10 place 1 1 0.890 0.890
media 400 00 10
media 400 00 11 -10
media 700 00 12 -11
media 408 00 13 -12
boundary 13 32 32
end geom
read array
ara=1 typ=cuboidal  pinpow=yes
nux=6 nuy=6
fill
8 7 7 8 8 8
7 7 5 7 6 8
7 7 7 7 7 8
7 7 7 7 4 7
7 7 2 3 7 7
1 7 7 7 7 8
end fill
end array
read bounds
all=refl
end bounds
end model
end
```

# APPENDIX D. ISOTOPICS COMPARISONS SUMMARY

**Table D.1. Summary statistics of calculated-to-measured isotopic inventory ratios for all samples**

| Nuclide | Fukushima | | Cooper | | Gundremmingen | | All samples | | Number of samples |
|---|---|---|---|---|---|---|---|---|---|
| | Average | Standard deviation | Average | Standard deviation | Average | Standard deviation | Average | Standard deviation | |
| $^{234}$U | 1.050 | 0.034 | 0.995 | 0.033 | No Data | No Data | 1.034 | 0.042 | 20 |
| $^{235}$U | 1.027 | 0.044 | 0.943 | 0.040 | 0.983 | 0.047 | 0.995 | 0.054 | 32 |
| $^{236}$U | 0.992 | 0.008 | 0.987 | 0.013 | 0.961 | 0.021 | 0.980 | 0.021 | 32 |
| $^{238}$U | 1.001 | 0.004 | 0.993 | 0.007 | 1.000 | 0.001 | 0.999 | 0.005 | 32 |
| $^{237}$Np | 0.995 | 0.116 | 1.001 | 0.125 | No Data | No Data | 0.997 | 0.115 | 20 |
| $^{238}$Pu | 1.009 | 0.074 | 0.887 | 0.045 | 0.915 | 0.079 | 0.950 | 0.087 | 32 |
| $^{239}$Pu | 1.007 | 0.040 | 1.042 | 0.034 | 1.003 | 0.051 | 1.012 | 0.045 | 32 |
| $^{240}$Pu | 1.000 | 0.024 | 0.974 | 0.037 | 1.012 | 0.040 | 1.000 | 0.035 | 32 |
| $^{241}$Pu | 0.987 | 0.037 | 1.037 | 0.066 | 0.964 | 0.055 | 0.988 | 0.055 | 32 |
| $^{242}$Pu | 1.009 | 0.035 | 1.064 | 0.074 | 0.989 | 0.069 | 1.012 | 0.062 | 32 |
| $^{241}$Am | 1.064 | 0.132 | 1.141 | 0.070 | No Data | No Data | 1.087 | 0.121 | 20 |
| $^{242m}$ Am | 1.133 | 0.122 | No Data | No Data | No Data | No Data | 1.133 | 0.122 | 14 |
| $^{243}$Am | 1.130 | 0.067 | No Data | No Data | No Data | No Data | 1.130 | 0.067 | 14 |
| $^{242}$Cm | 0.463 | 0.148 | No Data | No Data | 0.738 | 0.049 | 0.590 | 0.179 | 26 |
| $^{243}$Cm | 0.820 | 0.065 | No Data | No Data | No Data | No Data | 0.820 | 0.065 | 14 |
| $^{244}$Cm | 0.922 | 0.079 | 1.060 | 0.113 | 0.966 | 0.142 | 0.964 | 0.120 | 32 |
| $^{245}$Cm | 0.626 | 0.095 | No Data | No Data | No Data | No Data | 0.626 | 0.095 | 14 |
| $^{246}$Cm | 0.548 | 0.178 | No Data | No Data | No Data | No Data | 0.548 | 0.178 | 13 |
| $^{143}$Nd | 1.003 | 0.014 | No Data | No Data | No Data | No Data | 1.003 | 0.014 | 14 |
| $^{144}$Nd | 0.996 | 0.081 | No Data | No Data | No Data | No Data | 0.996 | 0.081 | 14 |
| $^{145}$Nd | 1.013 | 0.012 | No Data | No Data | No Data | No Data | 1.013 | 0.012 | 14 |
| $^{146}$Nd | 1.005 | 0.014 | No Data | No Data | No Data | No Data | 1.005 | 0.014 | 14 |
| $^{148}$Nd | 0.999 | 0.010 | No Data | No Data | 0.984 | 0.013 | 0.992 | 0.013 | 26 |
| $^{150}$Nd | 1.009 | 0.011 | No Data | No Data | No Data | No Data | 1.009 | 0.011 | 14 |
| $^{137}$Cs | 0.964 | 0.040 | 1.013 | 0.041 | 0.968 | 0.081 | 0.975 | 0.060 | 32 |
| $^{135}$Cs | No Data | No Data | 1.054 | 0.037 | No Data | No Data | 1.054 | 0.037 | 6 |
| $^{134}$Cs | 0.869 | 0.077 | No Data | No Data | 0.927 | 0.123 | 0.893 | 0.101 | 24 |
| $^{154}$Eu | 0.899 | 0.068 | No Data | No Data | 0.879 | 0.080 | 0.890 | 0.072 | 24 |
| $^{144}$Ce | 0.940 | 0.125 | No Data | No Data | No Data | No Data | 0.940 | 0.125 | 13 |
| $^{147}$Sm | 0.926 | 0.039 | No Data | No Data | No Data | No Data | 0.926 | 0.039 | 11 |
| $^{148}$Sm | 0.883 | 0.046 | No Data | No Data | No Data | No Data | 0.883 | 0.046 | 11 |
| $^{149}$Sm | 1.039 | 0.127 | No Data | No Data | No Data | No Data | 1.039 | 0.127 | 11 |
| $^{150}$Sm | 0.989 | 0.026 | No Data | No Data | No Data | No Data | 0.989 | 0.026 | 11 |
| $^{151}$Sm | 1.229 | 0.048 | No Data | No Data | No Data | No Data | 1.229 | 0.048 | 11 |
| $^{152}$Sm | 1.157 | 0.063 | No Data | No Data | No Data | No Data | 1.157 | 0.063 | 11 |
| $^{154}$Sm | 0.931 | 0.033 | No Data | No Data | No Data | No Data | 0.931 | 0.033 | 11 |
| $^{79}$Se | No Data | No Data | 1.352 | 0.030 | No Data | No Data | 1.352 | 0.030 | 6 |
| $^{90}$Sr | No Data | No Data | 1.075 | 0.017 | No Data | No Data | 1.075 | 0.017 | 6 |
| $^{99}$Tc | No Data | No Data | 1.146 | 0.036 | No Data | No Data | 1.146 | 0.036 | 6 |
| $^{126}$Sn | No Data | No Data | 2.997 | 0.072 | No Data | No Data | 2.997 | 0.072 | 6 |

Source: Summary.xlsx.

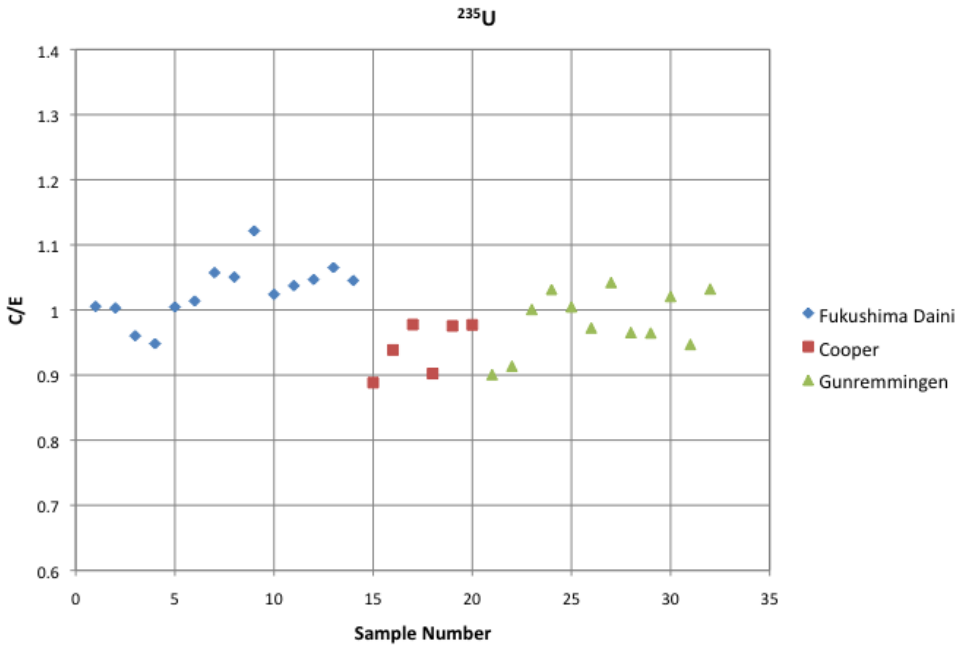


**Fig. D.1. Calculated-to-measured $^{235}$U concentration ratio for all samples.**
Source: Summary.xlsx**.**

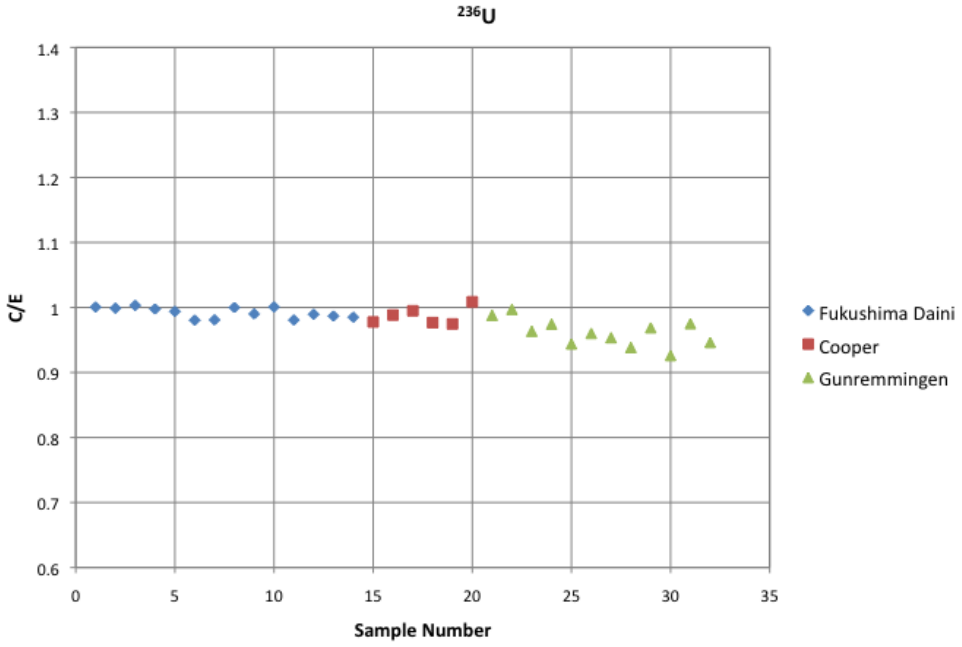


**Fig. D.2. Calculated-to-measured $^{236}$U concentration ratio for all samples.**

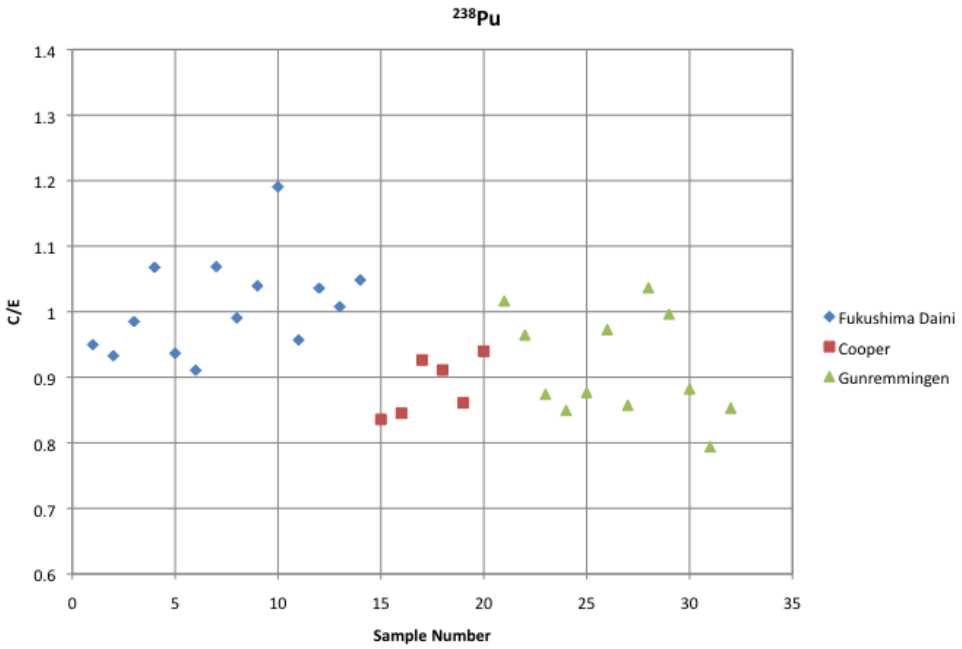


**Fig. D.3. Calculated-to-measured $^{238}$Pu concentration ratio for all samples.**

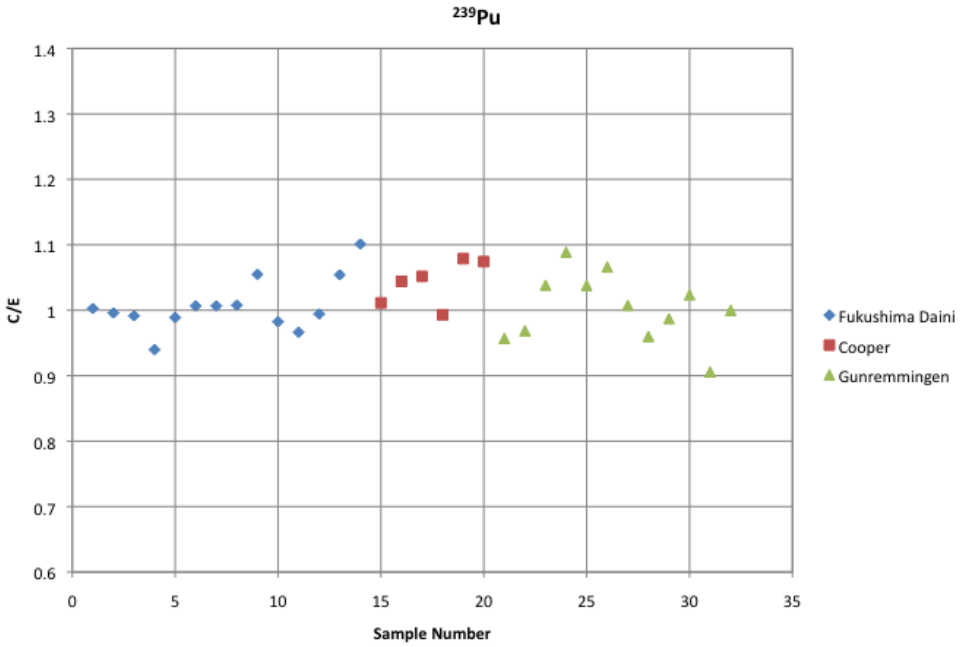


**Fig. D.4. Calculated-to-measured $^{239}$Pu concentration ratio for all samples.**

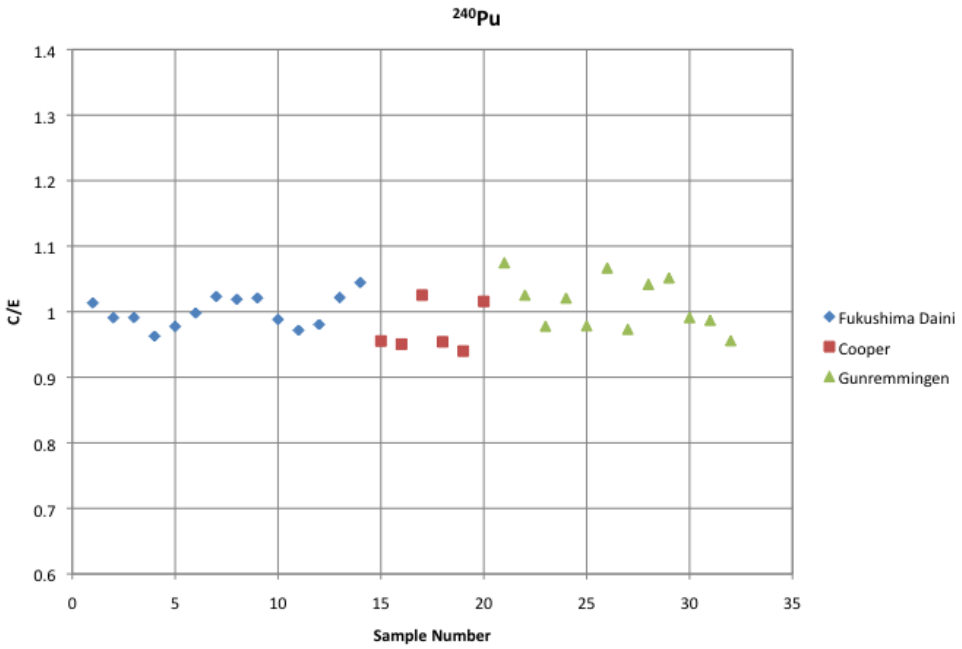


**Fig. D.5. Calculated-to-measured $^{240}$Pu concentration ratio for all samples.**

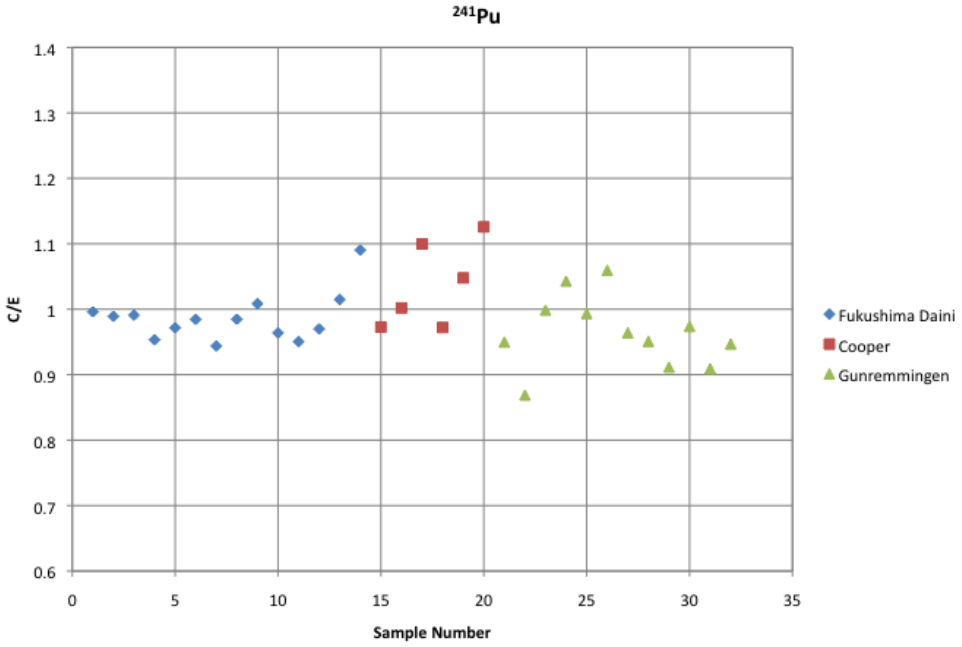


**Fig. D.6. Calculated-to-measured $^{241}$Pu concentration ratio for all samples.**

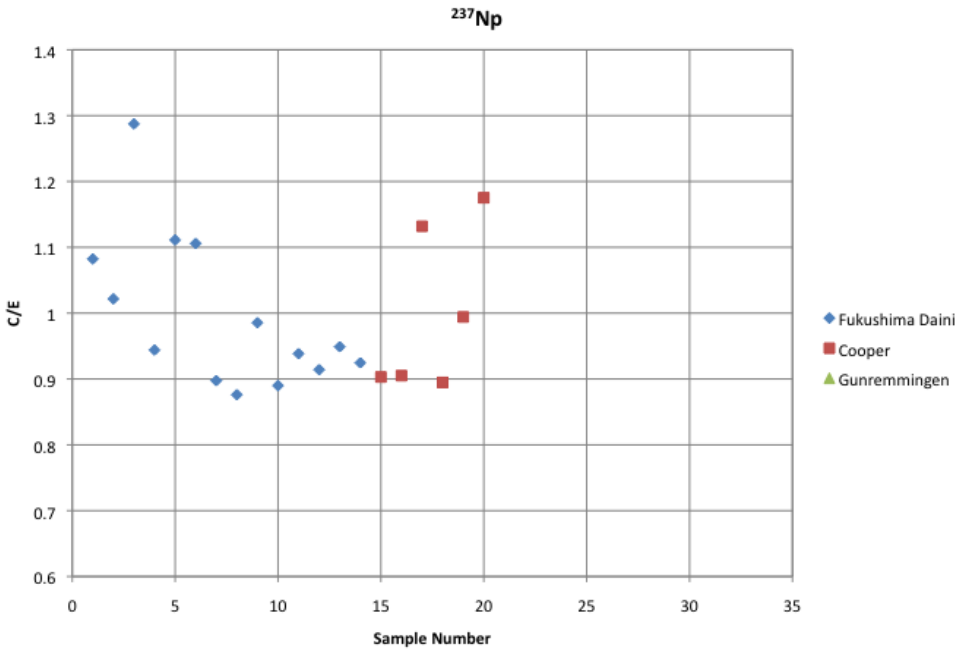


**Fig. D.7. Calculated-to-measured $^{237}$Np concentration ratio for all samples.**

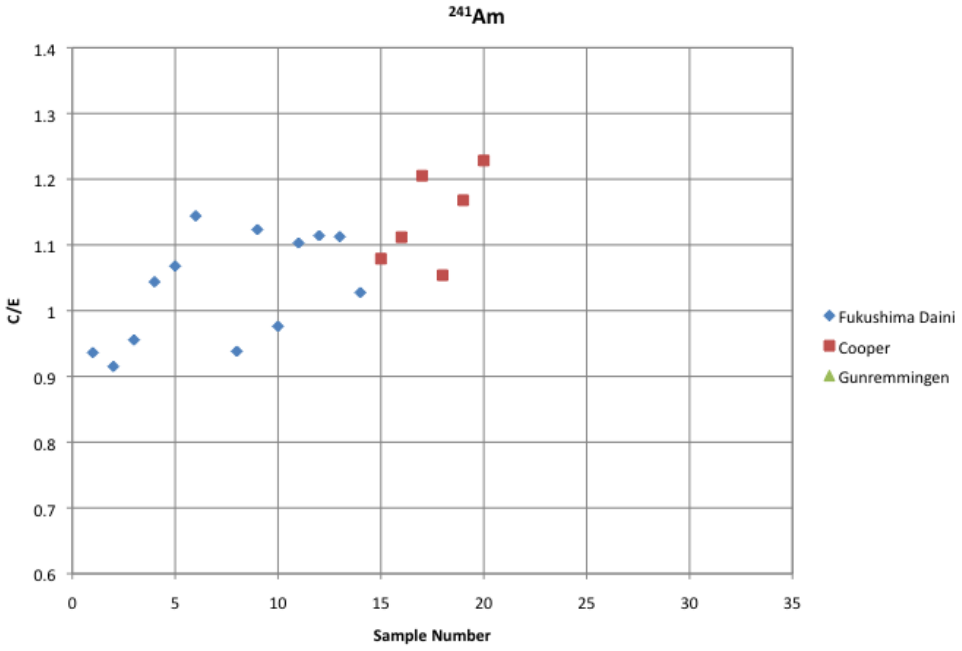


**Fig. D.8. Calculated-to-measured $^{241}$Am concentration ratio for all samples.**

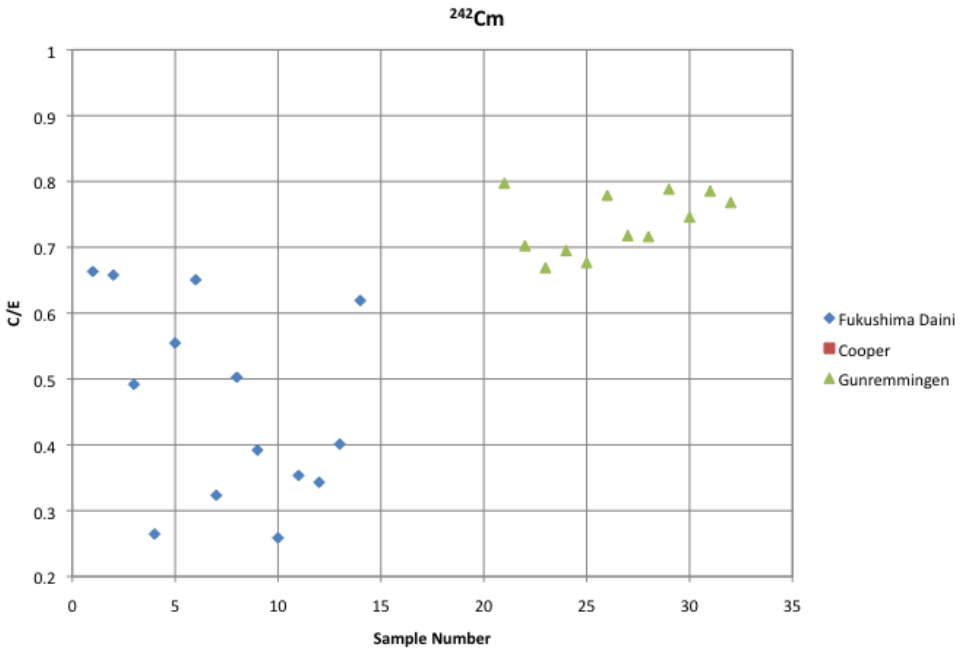


**Fig. D.9. Calculated-to-measured $^{242}$Cm concentration ratio for all samples.**

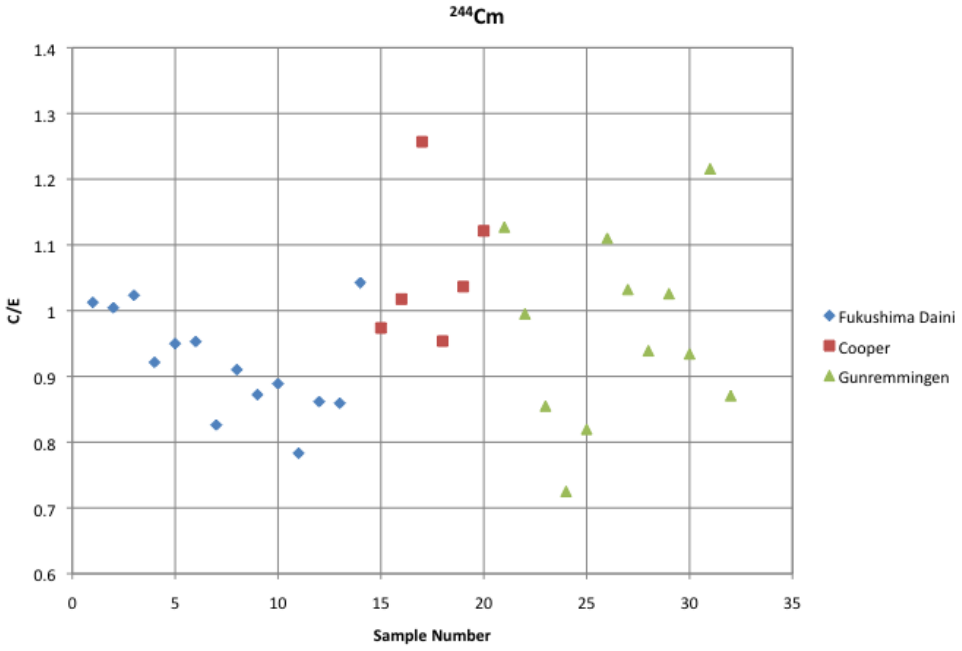


**Fig. D.10. Calculated-to-measured $^{244}$Cm concentration ratio for all samples.**

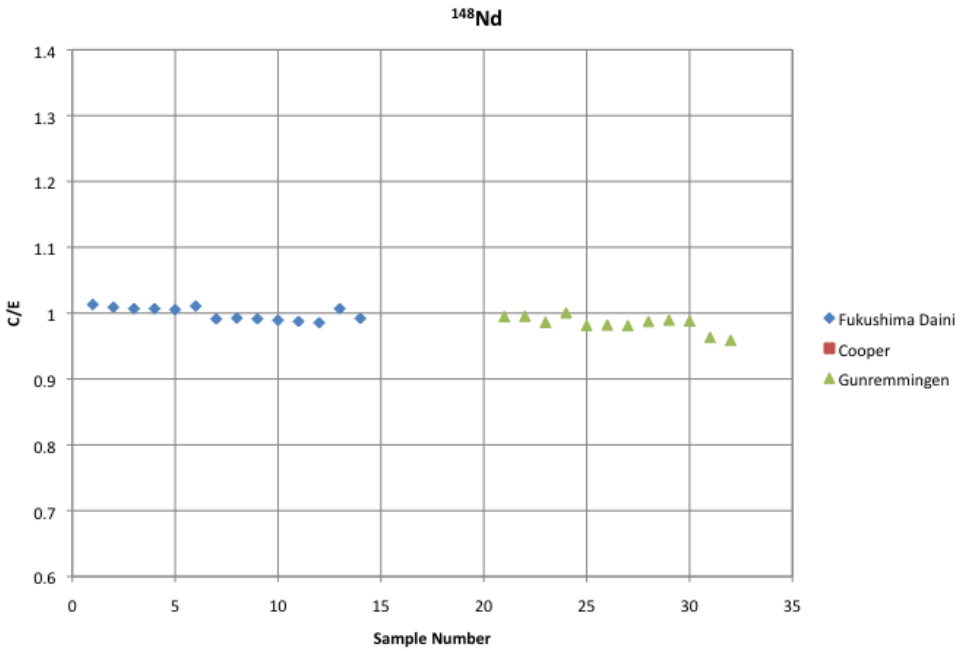


**Fig. D.11. Calculated-to-measured $^{148}$Nd concentration ratio for all samples.**

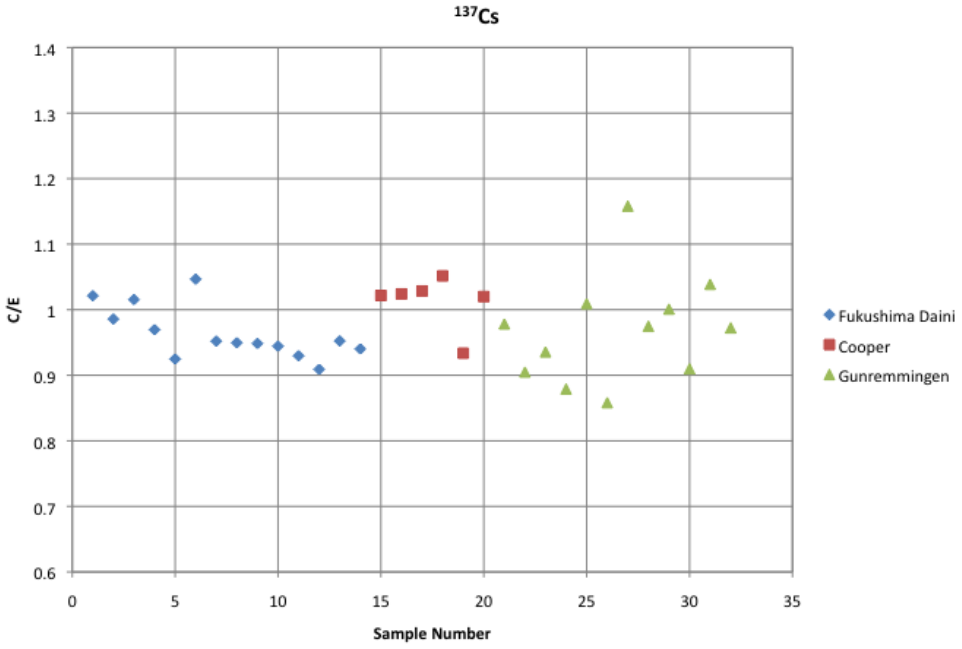


**Fig. D.12. Calculated-to-measured $^{137}$Cs concentration ratio for all samples.**

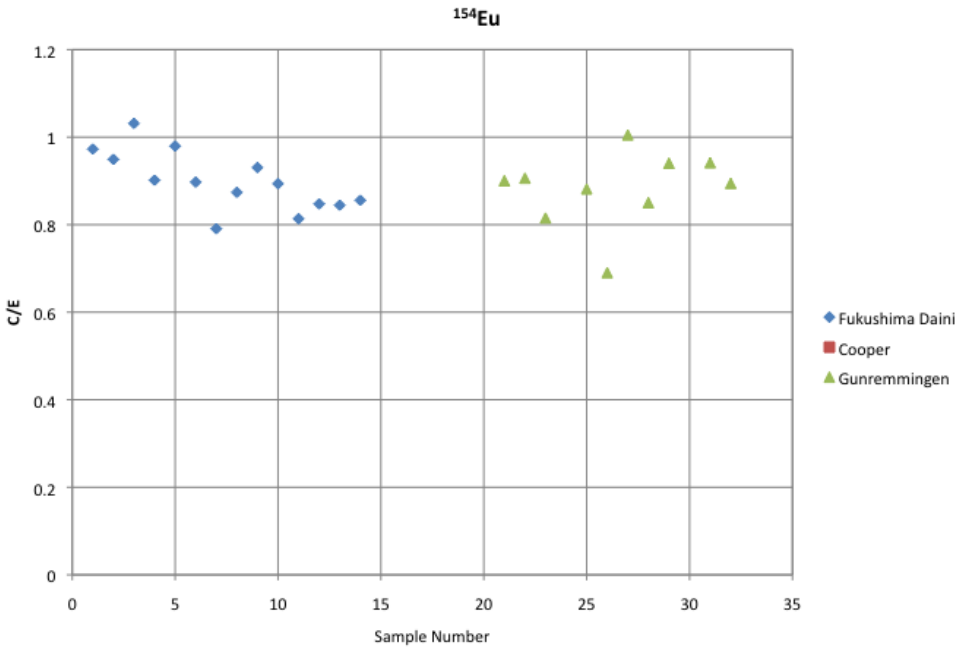


**Fig. D.13. Calculated-to-measured $^{154}$Eu concentration ratio for all samples.**